GIEDRIUS SMALAKYS

PECULIARITIES OF TOBERMORITE AND XONOTLITE SYNTHESIS FROM NATURAL ROCKS, THEIR PROPERTIES AND APPLICATION

DOCTORAL DISSERTATION

Kaunas
2021

KAUNAS UNIVERSITY OF TECHNOLOGY

GIEDRIUS SMALAKYS

PECULIARITIES OF TOBERMORITE AND XONOTLITE SYNTHESIS FROM NATURAL ROCKS, THEIR PROPERTIES AND APPLICATION

Doctoral Dissertation
Technological Sciences, Chemical Engineering (T 005)

2021, Kaunas

This doctoral dissertation was prepared at Kaunas University of Technology, Faculty of Chemical Technology, Department of Silicate Technology, during the period of 2016–2020.

Scientific supervisor:

Prof. dr. Raimundas Šiaučiūnas (Kaunas University of Technology, Technological Sciences, Chemical Engineering, T 005).

This doctoral dissertation has been published in:
http://ktu.edu

Editor:

Armandas Rumšas (Publishing House "Technologija")

KAUNO TECHNOLOGIJOS UNIVERSITETAS

GIEDRIUS SMALAKYS

TOBERMORITO IR KSONOTLITO SINTEZĖS IŠ GAMTINIŲ ŽALIAVŲ YPATYBĖS, JŲ SAVYBĖS IR PANAUDOJIMAS

Daktaro disertacija
Technologijos mokslai, Chemijos inžinerija (T 005)

2021, Kaunas

Disertacija rengta 2016–2020 metais Kauno technologijos universiteto Cheminės technologijos fakultete, Silikatų technologijos katedroje. Mokslinius tyrimus rėmė Lietuvos mokslo taryba.

Mokslinis vadovas:

Prof. dr. Raimundas Šiaučiūnas (Kauno technologijos universitetas, technologijos mokslai, chemijos inžinerija, T005).

Interneto svetainės, kurioje skelbiama disertacija, adresas:
http://ktu.edu

Redagavo:

Armandas Rumšas (leidykla "Technologija")

Table of contents

Abbreviations

A – annite
Ac – actionolite
Al – albite
An – anorthite
C – calcite
CSH – calcium silicate hydrate
C-S-H – semicrystalline type compound C-S-H(I) and C-S-H(II)
D – dolomite
DSC – differential scanning calorimetry
FT-IR – Fourier-transform infrared spectroscopy
Ge – gehlenite
G – gyrolite
Kr – cristobalite
L – calcium oxide
Lr – larnite
M – microcline
Mu – muscovite
P – portlandite
Q – quartz
S_{BET} – specific surface area of a sample calculated with BET equation
SEM – scanning electron microscopy
STA – simultaneous thermal analysis
T – 1.13 nm tobermorite
TG – thermogravimetry
Tr – tridymite
W – wollastonite
X – xonotlite
XRD – X-ray power diffraction
Z – Z-phase
α-C_2SH – α-dicalcium silicate hydrate ($2CaO \cdot SiO_2 \cdot H_2O$)

Introduction

Relevance of the work

The main measure to reduce energy losses is the usage of insulating materials. Organic insulating materials (e.g., polyurethane, polystyrene) are denoted by excellent technical properties, but they are thermo-labile. When the temperature exceeds 500 °C, silicate and ceramic materials must be used. Due to this reason, fiberglass is widely used to produce high-temperature thermal insulation materials. However, glass powder in the product can damage the eyes, lungs, and even the skin. Stone wool is a great alternative, which is non-flammable, but it has to be covered with expensive additives so that it can be used at temperatures above 600 °C. Cellulose is one of the most environmentally friendly and fire-resistant types of insulation. However, this material only works in the temperature range of 50–550 °C, and, on top of that, it can cause allergic diseases. The new type material – aerogel – is one of the most effective types of industrial insulation in the world. Its thickness is 50–80% lower than other insulation materials and resistant to high temperatures (1100 °C). However, it is expensive and has so far only been used for special purposes.

One of the most efficient types of energy-saving products with an operating temperature of 1050 °C is calcium silicate insulation materials. The raw materials for the production of calcium silicate insulation products are readily available (lime, SiO_2, fibers). The molar ratio of CaO to SiO_2 in the initial mixture is usually 0.8–1.0. The most important performance characteristics are as follows: low density; low thermal conductivity; high mechanical strength; good heat resistance; low shrinkage up to 1050 °C; durability and resistance to chemical corrosion. The thermal stability of calcium silicates is limited by the recrystallization of its main minerals: xonotlite, tobermorite and others to wollastonite at 800–900 °C, as well as the impurities which lower the melting point. To improve thermal stability, it is necessary to reduce the amount of amorphous or semi-amorphous phases, which results in high shrinkage values. Another advantage of xonotlite is the structure of the crystal lattice, which is very close to wollastonite, so that it hardly shrinks when undergoing thermal transformation.

Moreover, xonotlite features the lowest content of crystalline water, is the most heat-resistant and the most thermally stable (its decomposition temperature is 1050–1100 ℃) of all calcium silicate hydrates. It, as well as all other compounds of this group, due to their thermal stability, biological activity and environmental friendliness, is widely used in the manufacture of insulation panels, refractory materials, ceiling and wall boards, microporous materials, architectural and light-weight panels, etc. The properties of calcium silicate products used for thermal insulation of buildings are regulated by EN 16977:2020.

Xonotlite and 1.13 nm tobermorite are industrially produced as the main component of thermal insulation materials because they are stable at high temperatures. Moreover, these materials can be easily formed via hydrothermal synthesis from a suspension of SiO_2 and $Ca(OH)_2$. The mechanism of formation of

xonotlite and 1.13 nm tobermorite crystals is complex and highly dependent on the reactivity of the raw materials as various reaction intermediates are formed. The synthesis of calcium silicate hydrates is also significantly influenced by the conditions of hydrothermal treatment. Thus, the properties of the raw materials and the autoclave mode are the main parameters that need to be controlled or modified. Given that modification of one of the various conditions can unpredictably affect the whole process of compound formation, when using natural raw materials, it is always necessary to carry out systematic studies of specific parameters.

The aim of this work is to synthesize 1.13 nm tobermorite and xonotlite from natural raw materials with a controlled structure and properties, to compare the course of processes with the sequence of reactions in reagent systems and to evaluate the suitability of the obtained products for the production of heat-resistant thermal insulation materials.

The goals of this work are:

1) to determine the chemical and mineralogical composition, purity and dispersity of natural raw materials (limestone, carbonate opoka, granite sawing waste) and to prepare them for the synthesis of the target compounds;
2) to study and compare with CaO and SiO_2 reagent mixtures the influence of the nature of raw materials, mixture composition and hydrothermal synthesis parameters on the formation of the controlled structure and properties of 1.13 nm tobermorite and xonothlite, to determine their structure, crystallite size, thermal stability and the process of the formation of intermediates;
3) to compare the suitability of materials with various modifications of SiO_2 (quartz; a mixture of cristobalite, tridymite, quartz and an amorphous part; silicic acid) for the fast and economically attractive xonotlite synthesis and to determine the intervals for the formation and stable existence of intermediates;
4) to determine the most important characteristics of the xonotlite microstructure: its specific surface area, pore diameter and volume, the model of predominant pores, and to assess whether they meet the requirements for heat-insulating materials;
5) to evaluate the suitability of carbonate opoka for the production of xonotlite-based heat-resistant (up to 1000 °C) thermal insulation products.

Statements presented for defense:

1) the processes of hydrothermal synthesis of 1.13 nm tobermorite and xonotlite, the formation of intermediates and their stability are more influenced not by the modification of SiO_2 in raw materials, but by the nature and amount of Al^{3+} and alkali metal ions containing impurities in them;
2) as the amount and crystallinity of the xonotlite increases in the synthesis products, the shrinkage of the samples made from them decreases during recrystallization to wollastonite.

Scientific novelty of the research:

1) it has been shown that in the mixtures with an aluminum additive, 1.13 nm tobermorite with a stoichiometric composition after a long synthesis duration (72 h) or at a high temperature (200–220 °C) can not only recrystallize to a thermodynamically stable compound, xonotlite, as previously thought, but can also decompose together with the above mentioned mineral to form calcium silicate hydrate with a lower basicity – gyrolite;
2) it has been found that the small amounts of potassium and sodium compounds in the raw materials (up to 1%, calculated as K_2O+Na_2O), in the xonotlite-based heat-resistant products up to 1000 °C, do not promote liquid phase sintering processes and do not increase their shrinkage.

Practical significance of the scientific research

1) the influence of the chemical and mineralogical composition of natural raw materials (limestone, carbonate opoka, granite sawing waste), the composition of the initial mixture and the hydrothermal treatment conditions on the synthesis processes of 1.13 nm tobermorite and xonotlite, as well as the duration of the formation of intermediates have been determined. The optimal values of these parameters have been proposed, which allows reducing significantly the time for obtaining the target compounds;
2) it has been found that opoka calcined at 775 °C is perfectly suited for the synthesis of 1.13 nm tobermorite and xonotlite. The high reactivity of opoka under hydrothermal conditions is due to its chemical composition, especially due to the presence of 2.53% Al_2O_3 and 0.83% K_2O. Al^{3+} ions stimulate the reactions of amorphous SiO_2 and CaO; thus the formation of 1.13 nm tobermorite occurs rapidly at the beginning of the hydrothermal treatment. K^+ ions accelerate the dissolution of SiO_2 crystalline modifications (quartz, tridymite and cristobalite) by eroding the surface of the particles and by increasing the concentration of SiO_4^{4-} ions;
3) it has been proven that heat-resistant (up to 1000 °C), low-density (up to 200 kg/m^3) thermal insulation products on the basis of xonotlite can be made from lime and Stoniskiai-Zemaitkiemis deposit opoka mixtures.

Approval and publication of the research results:

The results of the dissertation were published in 3 scientific publications included in the *Clarivate Analytics Web of Science* database: 2 of them were published in the *Journal of Thermal Analysis and Calorimetry*; 1 was published in *Ceramics-Silikáty*.

The results were presented in 6 international conferences: "Chemistry and Chemical Technology", (2017, Lithuania), "4th Central and Eastern European Conference on Thermal Analysis and Calorimetry (CEEC-TAC4)", (2017, Moldova), "The 8th International Conference on Silicate Materials BaltSilica" (2018, Latvia), "12th European Symposium on Thermal Analysis and Calorimetry (ESTAC12)", (2018 Romania), "Chemistry and Chemical Technology", (2019,

Lithuania), "15th International Congress on the Chemistry of Cement (ICCC 2019)", (2019, the Czech Republic).

Structure and contents of the dissertation:

The dissertation consists of an introduction, literature overview, materials and methods, results and discussion, conclusion, a list of references and publications on the dissertation topic as well as in the appendices. The list of references includes 183 bibliographic sources. The main results are discussed on 128 pages and illustrated with 8 tables and 87 figures.

The contribution of the author and co-authors:

The author synthesized and described the calcium silicate hydrates which are mentioned in the thesis, examined the peculiarities of hydrothermal synthesis and presented the applications for the obtained compounds. Raimundas Šiaučiūnas advised on the progress of the experiment and the preparation of the manuscript.

1. Literature Review

1.1 Description of calcium silicate hydrates and their structure

The group of compounds named calcium silicate hydrates (C-S-H) consists of approximately 40 different semi-amorphous and crystalline, natural and synthetic minerals formed in the system of CaO-SiO_2-H_2O [1–4]. The diversity of these compounds is determined by the molar ratio of CaO/SiO_2 which varies from 0.44 to 3.0 [5–8]. The most favorable and eco-friendly way to artificially obtain these compounds is by treatment of mixtures in a high-pressure autoclave [9, 10].

The formula of calcium silicate hydrates (C-S-H) is expressed by the molar ratio of $nCaO$-$mSiO_2$-pH_2O (where indexes n, m, p stand for the number of moles) [11]. In the nature, calcium silicate hydrates form as alteration minerals in metamorphosed limestone and vesicle filings in basalts [12, 13]. Other calcium silicate hydrates can be found in concrete after silicate phase hydration (abundance of these minerals determines the strength of concrete) or hydrothermally by high pressure steam curing silicate-lime mixtures in an autoclave [14, 15]. The formation of calcium silicate hydrates largely depends on the stoichiometric composition of the initial mixture expressed by the molar ratio of calcium oxides and silica (CaO/SiO_2) [13, 16]. The mixture of the molar ration can be divided into two groups: low-base (CaO/SiO_2 = 0.6–1.5) and high-base (CaO/SiO_2 = 1.5–3). Low-base calcium silicate hydrates are commonly suitable as fillers for the production of plastic, rubber, paper, paint, or as low-cost absorbents for treatment of water contaminated with heavy metal ions and organic and/or inorganic effluents [17]. Meanwhile, high-base calcium silicate hydrates are more favorable for the production of hydraulic cementitious materials and products hardened under supercritical CO_2 [18].

The composition and properties of calcium silicate hydrates are significantly different, but the structure models of these minerals have certain similarities [19, 20]. Moreover, the crystalline structure of calcium silicate hydrates is the field of research of many scientists and is constantly supplemented with new results [21–26]. However, it is generally agreed that the main mineral element of the compound of C-S-H is based on a layered structure [20].

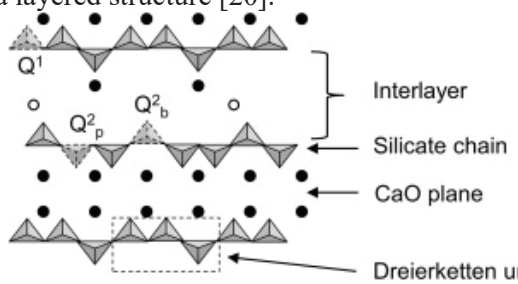

Fig. 1.1. Structure model of calcium silicate hydrate [27]. The triangles are silica tetrahedra; the black circles are calcium atoms/ions in CaO planes and calcium ions; the empty circles are species in the interlayer (water); in Qn, n represents the number of SiO_4^{4-} units attached to an individual silicate tetrahedron; p are pairing units; b are bridging sites

The recurring main element of the layers is a silicate chain which is linked to another chain with calcium ions. The central part of this structure is coordinated within oxygen atoms of calcium oxide and silicate tetrahedrals. The silicate chains consist of the repetition of three-tetrahedra, and, in these structure models, it is called the dreierket chain. The main silicate tetrahedra (which is called the bridging tetrahedron) forms the link between two adjacent pairs of silicate tetrahedra, thus forming a dreierket chain. In the adjacent pairs of silicate tetrahedra, there are two oxygen atoms which can be co-stored with the silicate neighbor or a calcium ion in the interlayer. Yet, it can also form a bond with a proton thus creating the silanol group. In silicon chemistry, the function group is called *silanol* when a silicon atom is connected with hydrogen via an oxygen atom. The length of a silica chain in a structure of calcium silicate hydrates is variable and depends on the molar ratio of the compound. Therefore, it has been established that the molar ratio CaO/SiO_2 varies from 0.66 to 3, and that the calcium hydroxide concertation equilibrium varies from less than 1 to 30 $mmol \cdot l^{-1}$ [28]. Only when the stoichiometric molar ratio of C-S-H is $CaO/SiO_2 = 0.66$, or equilibration with low calcium hydroxide concentration is less than 1 $mmol \cdot l^{-1}$, the chains of silicate are infinite [29]. However, the model and the mechanism of the incorporation of other ions into the calcium silicate hydrate structure is an area of work for many scientists who are constantly improving the scope of knowledge [30, 31].

1.2 Classification of calcium silicate hydrates

H.F.W. Taylor along with colleagues formed the basis for the classification of calcium silicate hydrates. Due to the variable composition and the abundance of extraneous ions capable to get into the crystal lattice of calcium silicate hydrates, the study of their structure and properties is complicated. For this reason, separate research by recognized scientists is constantly supplementing the classification of calcium silicate hydrates with newly synthesized or discovered compounds. Therefore, in the overview of calcium silicate hydrates, the classification by I.G. Richardson serves to summarize the main characters of crystalline minerals and poorly ordered phases which are divided into the following groups: wollastonite, tobermorite, jennite, gyrolite, γ-C_2S, other C-S-H [11].

The following minerals were included into the wollastonite group: nekoite, okenite, xonotlite, foshagite, hellebrandite, wollastonite and pectolite. The main mineral of this group is wollastonite (calcium metasilicate) $CaSiO_3$ with the stoichiometric molar ratio CaO/SiO_2=1.0. Moreover, this compound has several polymorphs that are divided into two groups: low temperature (β-wollastonite) and high temperature (α-wollastonite). The more common are the low temperature representatives: triclinic (1T) and monoclinic (2M) [32, 33]. Calcium silicate hydrates recrystallize into the low temperature phase β-wollastonite during thermal treatment at 800 °C.

The crystal structure of the compounds features similarities between triclinic and monoclinic wollastonite which are both referred to monoclinic morphological axes [34]. The high temperature polymorphs recrystallize from triclinic wollastonite

to the high temperature: cyclo-wollastonite or pseudo-wollastonite. The transition of β-wollastonite into the α-wollastonite starts at temperatures above 1200 °C when the triclinic crystal structure with the space group is manifested [35].

Another common compound with great practical value and which is of great interest is xonotlite $Ca_6Si_6O_{17}(OH)_2$; the stoichiometric molar ratio of this mineral is CaO/SiO_2=1.0. This compound features a unique double-chain structure and is denoted by a number of beneficial properties for producing high temperature thermal insulation or other applications, such as: a catalyst [36], polymers [37], medical applications [38]. Other compounds of the wollastonite group are nekoite $Ca_3Si_6O_{15}\cdot 7H_2O$ and okenite $Ca_{10}Si_{18}O_{46}\cdot 18H_2O$ which are obtained in contact of metamorphosed limestone or in zeolites from the alteration of basalts.

The second group of calcium silicate hydrates is named *tobermorite* which is one of the main minerals in the class. The compounds in this group are characterized by variable basal spacing which is expressed in nanometres. There are three main polymorphs of tobermorite which are classified according to their hydration degree. 1.4 nm tobermorite ($Ca_5Si_6O_{16}(OH)_2\cdot 7H_2O$) is the most hydrated member of the group [39]. 1.13 nm tobermorite ($Ca_5Si_6O_{16}(OH)_2\cdot 4H_2O$) is one of the main phases found in the hydrated phase of concrete or during the autoclave treatment of silica products and 0.93 nm tobermorite ($Ca_5Si_6O_{16}(OH)_2$) [40]. The last one does not have any crystallographic water in its structure, which is a product of other polymorphs after heating in a certain thermal mode. Moreover, the tobermorite group also includes the semi-amorphous compound C-S-H(I) [41]. The structure of this compound is similar to the structure model of tobermorite, except that a part or the entirety of the bridging tetrahedral is missing. The C-S-H(I) phase occurs at the early stages of hydrothermal synthesis of calcium silicate hydrates which are thermodynamically unstable and are crystallized to tobermorite or another crystalline phase. The recrystallization of C-S-H(I) starts on the surface of the amorphous phase with the formation of crystal aggregates. The two thus formed occurring phases have irregular volume and surface structures. As a result, the molar ratio of C-S-H(I) varies and is generally expressed as CaO/SiO_2 <1.5 [42, 43].

Compounds within the jannite group include jannite, metajanite, and C-S-H(II). The group of these compounds is distinguished by the poorly crystallized structure, and C-S-H(II) is identified as semi-amorphous, or else C-S-H(II) gel is amorphous in the cement phase (44). The molar ratio (CaO/SiO_2) of this compound varies from 1.5 to 3.0 [45, 46]. The main compound of the group – jennite $Ca_9Si_6O_{18}(OH)_6\cdot 8H_2O$ – is another calcium silicate hydrate whose structure is crystalline; it features dreierkatte silicate chains similar to tobermorite. Yet, the stoichiometric molar ratio of CaO/SiO_2=1.5 is much higher than tobermorite [47]. Moreover, jennite is usually found in contact with 1.4 nm tobermorite in the nature or is synthesized from $Ca(OH)_2$ and hydrous silica under hydrothermal treatment [48]. Dehydration of jennite at 70–90 °C is distinguished by the loss of water molecules, which alters the structure of the interlayer thus resulting in the shrinkage in the *c* direction. In order to stabilize the structure of the compound, it recrystallizes into matajennite $Ca_9[Si_6O_{16}(OH)_2](OH)_8\cdot 2H_2O$ [49].

The following minerals are included in the gyrolite group: fedorite, K-phase, Z-phase, reyrite, truscottite and gyrolite. The main compound of the group, gyrolite, is similar to other calcium silicate hydrates such as: tobermorite, xonotlite or C-S-H(I) [50]. The chemical formula of gyrolite is $Ca_{16}Si_{24}O_{60}(OH)_8 \cdot 14H_2O$; thus its stoichiometric ratio is CaO/SiO_2=0.66. The latter mineral is the focus of interest of a number of scientists due to a greater absorption capacity in comparison with other calcium silicate hydrates [51]. Literature indicates that gyrolite substituted with aluminum ions has potential to be applied for waste disposal [52]. Moreover, gyrolite is suitable for sorption of heavy metal ions, for example, Cd^{2+}, Zn^{2+}, Cu^{2+}, and the cation exchange capacity of the material depends on the initial concentration of ions in the solution [53]. This compound is synthesized under hydrothermal conditions only at temperatures higher than 120 °C and remains stable up to 200 °C. Moreover, at 200 °C, this compound starts to recrystallize into truscottite $Ca_{14}Si_{24}O_{58}(OH)_8 \cdot 2H_2O$, but metastable gyrolite under certain conditions can be obtained at temperatures up to 270 °C. During the hydrothermal synthesis of gyrolite, the intermediate compound called Z-phase ($Ca_9Si_{16}O_{40}(OH)_2 \cdot (14+xH_2O)$ is obtained, especially in mixtures of lime and amorphous silica within the temperature range of 140–240 °C [54]. Moreover, K-phase $Ca_7Si_{16}O_{38}(OH)_2$ is easily obtained from Z-phase, which requires either higher temperatures of synthesis (350 °C), or dehydration of Z-phase at 450 °C [55].

The main compounds of the γ-C_2S group minerals are calcium chondrodite, kilhonite, γ-Ca_2SiO_4 [56].

Other calcium silicate hydrate compounds are: afwillite, α-C_2SH, cuspidine, dellaite, jaffaite, killalaite, poldervaartite, rosenhahnite, suolunite, tilleyite, Y-phase. Most of these compounds are more generic and are distinguished from other groups by their structure and origin. In addition, a largely common compound formed during hydrothermal synthesis is α-C_2SH ($2CaO \cdot SiO_2 \cdot nH_2O$) whose stoichiometric molar ratio is CaO/SiO_2=2 [57]. α-C_2SH is distinguished for its hydraulic cementitious properties and is the subject of many scientific researches [58].

1.3 Characterization of specific calcium silicate hydrates: 1.13 nm tobermorite and xonotlite

One of the major crystalline minerals of the calcium silicate hydrate group, which is called tobermorite, is the subject of research in many scientific fields. This mineral appears in binders of autoclaved concrete, sand-lime bricks, the hydration of cement (C_2S, C_3S), and in heat insulating materials. Other applications to be mentioned are sorption of heavy metals in the slurry, sorption of nuclear waste, semiconductors, and the field of medicine [59–61]. The extensive application of tobermorite is due to the differences in the physical behavior of the crystal, such as the solid state, the fiber and nanoparticles of this compound [62]. This compound occurs under a saturated steam or under hydrothermal conditions in the autoclave. Moreover, tobermorite remains stable in mixtures within the range of the molar ratio CaO/SiO_2 = 0.66–0.83 [63].

As described above, the structure of tobermorite is based on a layer-type structure where, between the silicate chains, there is an interlayer filled with calcium

ions. A simplified structure schematic of these tobermorite polytypes is presented in Figures 1.2 and 1.3. Although, unlike other calcium silicate hydrates, the structure of tobermorite has a variety of basal spacing which depends on their hydronation degree [64]. In addition, the names of these compounds are given by angstrom or nanometres which describe the gap among silicate chains [65].

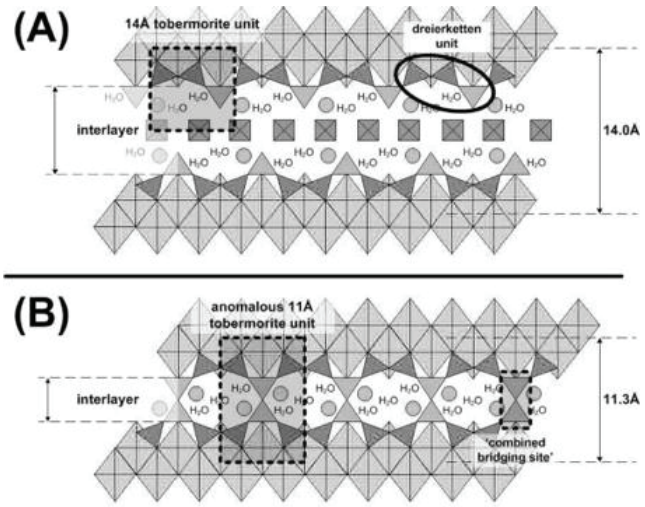

Fig. 1.2. Schematic sublattice representations of (A) 14 Å tobermorite, (B) anomalous 11 Å tobermorite [22]

It was determined that anomalous 1.13 nm tobermorite has a bound water to Si ratio H_2O/Si = 5/6 which corresponds to $[Ca_4Si_6O_{15}(OH)_2 \cdot 5H_2O]$ (Fig. 1.2, B). Moreover, normal 1.13 nm tobermorite has the same water to Si ratio H_2O/Si = 5/6; however, it contains 0.25 atoms of calcium per 'dreierketten' unit, which corresponds to $[Ca_{4.5}Si_6O_{16}(OH) \cdot 5H_2O]$. The formation of anomalous tobermorite is promoted by the following factors: a high molar ratio, CaO/SiO_2 = 1.0, short synthesis duration, a low temperature, stirring, the presence of Al, and the small size of a quartz particle [66].

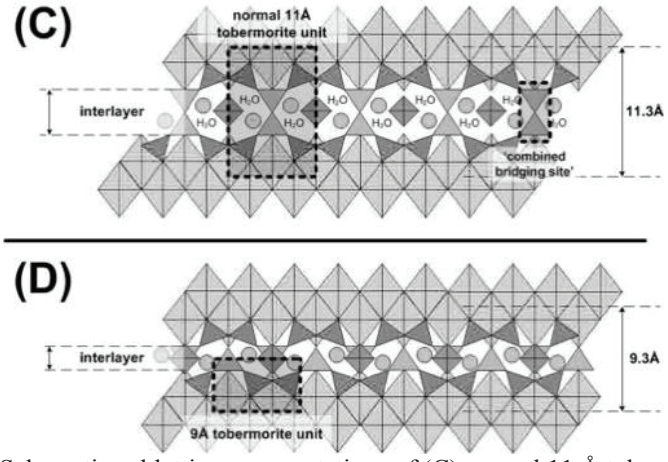

Fig. 1.3. Schematic sublattice representations of (C) normal 11 Å tobermorite, and (D) 9 Å tobermorite [22]

The gap between the layers varies from 1.4 to 0.93 nm, and only adjacent silicate chains of 1.13 nm tobermorite are directly joined with Si−O−Si cross-links. Literature indicates two types of 1.13 nm tobermorite: 'normal' 1.13 nm tobermorite in the interlayer structure contains calcium ions which shrink during dehydration (Fig. 1.3, C), while 'anomalous' 1.13 nm tobermorite without calcium ions in the dreierketten structure is protected from shrinkage (Fig. 1.2, B).

Xonotlite $Ca_6Si_6O_{17}(OH)_2$, due to its unique physical and chemical properties, is the field of work of a number of scientists [67]. This compound is obtained in the $CaO–SiO_2–H_2O$ system via the process of hydrothermal synthesis at 200–350 °C (68). The obtained xonotlite fibers form needle-shaped crystals [69]; they exhibit several excellent characteristics, such as a light weight, flame-retardancy and high compressive strength, which makes it very efficient for heat insulating and fire-resistant building materials [70]. Moreover, literature indicates that these xonotlite fibers due to their large specific surface area and the nano-scale effect could also be applied in catalysis of hydrogen generation [71].

Literature indicates that, when obtaining this calcium silicate hydrate, mixtures must contain a specific molar ratio which is characteristic of xonotlite. Moreover, researchers [72] suggested possibilities of using mixtures of various CaO/SiO_2 molar ratios: from 0.41 up to 1.66 for the synthesis of xonotlite [16]. However, according to the literature data, hydrothermal synthesis goes in the most favorable way when $CaO/SiO_2 = 1.0$ [73].

For the first time, Mamedov *et al*. proposed a structural model of xonotlite, which was later confirmed by Eberhard *et al*. The chemical formula $Ca_6Si_6O_{17}(OH)_2$ and the structure of xonotlite share some similarities with tobermorite and wollastonite [74]. The structure of this compound is based on layers consisting of Ca-polyhedra and Si-tetrahedra joined in a chain which is similar to two wollastonite chains joined in parallel. An ordinary unit of xonotlite is composed from a layer of Ca-polyhedra connected with three different elements: one of them is a distorted octahedron, and two of the elements have seven oxygen atoms. Meanwhile one of

the silicate tetrahedrals from the silicate chain through the -O-Si-O- bond is joined to the Ca layer. Therefore, two calcium oxide polyhedral chain layers separated by the $[SiO_4]^{4-}$ tetrahedra chain are merged into the repeating layer. This results in a large number of xonotlite polymorphs that differ in the arrangement of the silicate double chain in with other Ca layers [75]. Literature indicates six different polytypes: four ordered and two disordered [76].

1.4 Formation of tobermorite and xonotlite during hydrothermal synthesis

The formation of calcium silicate hydrates is complex, and compounds are closely related to each other in their chemical composition and structure. Moreover, studies on the formation of these compounds are further complicated by semi-amorphous compounds (C-S-H(I)), or metastable crystalline phases (Z-phase) can occur during hydrothermal synthesis. For this reason, it is hard to obtain single-phase, pure and high crystallinity degree materials [41].

The formation of xonotlite from mixtures of lime-silica when the molar ratio is CaO/SiO_2 = 1.0 proceeds through the following intermediates: C-S-H(I), α-C_2SH, and tobermorite [77, 78]. At the early stages of hydrothermal synthesis, after Ca-rich C-S-H gels have been formed while quartz has not completely reacted, then, tobermorite starts forming from C-S-H gels as an intermediate phase. The obtained tobermorite is not stable if there are free calcium ions in the reaction medium. The stoichiometric molar ratio is disturbed, and tobermorite starts recrystallizing into xonotlite [79]. Conversion from tobermorite to xonotlite is topotactic, which means that the compound occurs with no change in the particle morphology [80]. Due to this reason, synthetic xonotlite often slightly lacks calcium ions, and the stability of the compounds is achieved by Si–OH groups [81].

The mechanism of the phase transition from raw materials into the target compound is summarized in Fig. 1.4. The early synthesis stages start with calcium oxide which dissolves and goes around the particle of quartz due to the negative charge of SiO_3^{2-}. After a rapid reaction, amorphous C-S-H gel is generated, which leads to decreased fluidity. Thus, a large amount of Ca^{2+} ions is restricted in the C-S-H gel body, which leads to the shortage of free calcium ions in the system. With prolonging the duration of crystallization, many siliceous species participate in the reaction, and needles or laths (tobermorite) are formed on the surface of quartz grains which consist of calcium ions and silicates. After prolonging the duration of crystallization, more and more SiO_3^{2-} groups participate in the reaction. Due to the lack of free Ca^{2+} ions and the deficient fluidity, a large amount of Na^+ ions can easily form the structure of tobermorite at this reaction stage. Tobermorite absorbs water molecules and swells, which causes the temporary super saturation, and the needle works as the original crystal nucleus. With further prolonging of the crystallization duration, needles recrystallize into fibers, and more Ca^{2+} ions are released to participate in the crystalline structure [23].

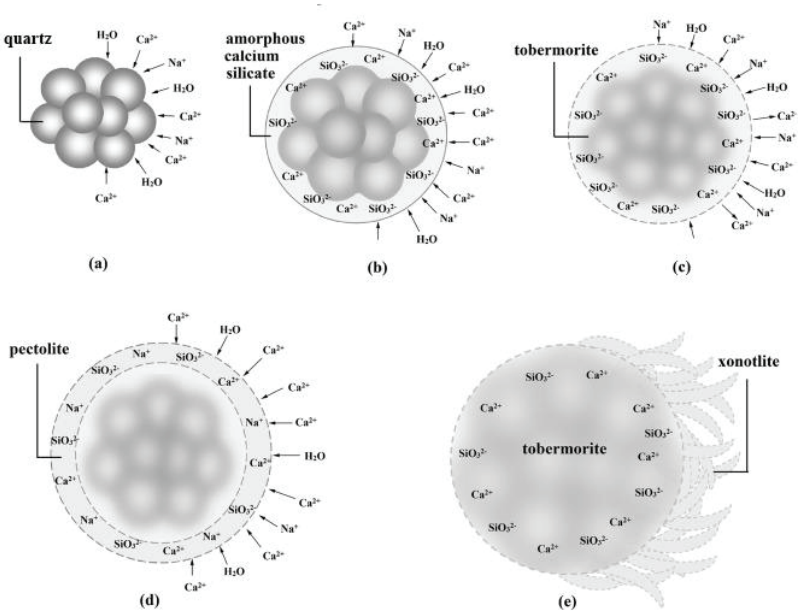

Fig. 1.4. Mechanism of tobermorite and xonotlite formation during hydrothermal synthesis [23]

1.5 Parameters of hydrothermal synthesis

The synthesis of 1.13 nm tobermorite as well as the formation of the intermediate compounds, their stability intervals, purity, crystallinity, and crystal lattice parameters significantly depend on the hydrothermal synthesis conditions (temperature, duration, stirring intensity, water to solid (W/S) ratio, etc.). Some authors attempted to synthesize 1.13 nm tobermorite at near-room temperature [82]. It was determined that this method of synthesis is only suitable for the scientific purpose, yet not for application in production. The temperature increase had a significant impact on the reaction kinetics; the synthesis duration decreased from a hundred days to mere hours. Many researchers started focusing on the temperatures between 90 and 210 °C [83]. Nevertheless, the synthesis of tobermorite is a complex process where the temperature affects the stability of the compound. Depending on the impurities in the used raw materials, 1.13 nm tobermorite may lose stability at 200 °C [23] and start recrystallizing to xonotlite [84]. However, the published data implies that, under certain conditions, tobermorite can be synthesized at 200 °C or even at a higher temperature [23]. The intensity of the characteristic to 1.13 nm tobermorite peaks in the X-ray diffraction patterns has a tendency to augment when the synthesis temperature is increased. A higher temperature leads to a better condition of the synthesis of this mineral, even though other calcium silicate hydrates are formed together. Moreover, the literature data indicates that hydrothermal synthesis is usually carried out at 180 °C [13, 85]. Under these conditions, 1.13 nm tobermorite crystals form at a competitive speed and reach a sufficient crystallinity degree.

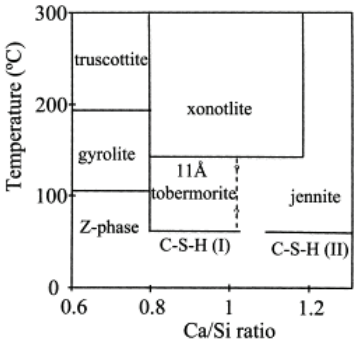

Fig. 1.5. Diagram of the dependence of the stability of calcium silicate hydrates on the parameters of hydrothermal synthesis [79]

From the literature data, it was determined that the parameter of hydrothermal synthesis, such as temperature, is more important in the synthesis of xonotlite than 1.13 nm tobermorite (Fig. 1.5). As mentioned above, 1.13 nm tobermorite can be obtained at room temperature, but xonotlite only begins to form at 180 °C [86, 87]. It was found experimentally that the optimal condition to obtain xonotlite during hydrothermal synthesis is in the temperature range between 200–300 °C [68, 72]. Moreover, xonotlite is obtained only after recrystallization from the intermediate phases, as shown in Figure 1.5. Nevertheless, Yanagisawa *et al*. presented a method of synthesis when a special thermal mode does not allow for forming C-S-H(I), C-S-H(II), tobermorite, and, after that, xonotlite occurs without the formation of any intermediate compounds [88]. The authors found that the ratio of raw materials CaO/SiO_2 and their additives does not affect the process of continuous xonotlite synthesis. Yet, the main product obtained by this method is xonotlite. In addition, this method of xonotlite synthesis is only suitable at a high ratio of W/S = 200–1000. Hartmann *et al*. studied xonotlite formation during hydrothermal synthesis by using a variety of mixtures with various CaO/SiO_2 molar ratios within a large range from 0.41 up to 1.66 [16]. During the first stage of the reaction, due to the low dissolution rate of quartz, calcium hydroxide dissolves rapidly thus forming calcium-containing zones [89]. Duo to this reason, xonotlite can be separated from the intermediate products during the hydrothermal synthesis by slightly increasing the molar ratio of CaO/SiO_2 from 1.0 to 1.24 while maintaining the temperature above 200 °C.

Literature data suggests that the duration of hydrothermal treatment and mixture dispersity has significant influence on xonotlite formation as well as on the degree of crystallinity. In case of a short synthesis duration from mixtures prepared from SiO_2 powder and lime, the products of interaction are tobermorite and xonotlite. Moreover, xonotlite starts recrystallizing from tobermorite only after a longer duration of hydrothermal synthesis. Literature sources indicate various durations of xonotlite conversion, but it generally varies from 6 to 8 hours. Literature indicates that, when the mixture molar ratio of CaO/SiO_2 varies from 0.8 to 1.0 while using ground quartz whose particle size is 10–20 μm, xonotlite can be obtained via hydrothermal synthesis only at 250 °C [90]. The temperature of hydrothermal synthesis of xonotlite can be reduced from 250 °C to 200 °C by using

mixtures when the particle size of quartz is 2–5 μm, and at W/S ratio of the suspension being 20–35. However, the higher temperature during hydrothermal synthesis leads to the formation of bigger xonotlite crystals, but the number of crystals with defects also increases. Moreover, crystal morphologies of the target compound crystal morphology increase by prolonging the duration of hydrothermal synthesis.

Maoqiang *et al*. investigated the dynamic hydrothermal synthesis of xonotlite by using continuous mixing of the suspension at a speed of up to 200 min^{-1} [91]. Competitive results were obtained in comparison to using water solids W/S = 20 when the temperature was set at 220 °C, when, after 8 hours of synthesis, crystallized xonotlite was identified. Stirring during hydrothermal synthesis is emphasized as a major factor in the formation of the target compound. From the analysis of the provided information, it is obvious that the synthesis of xonotlite takes place in the presence of a relatively higher water content than the synthesis of 1.13 nm tobermorite. Literature indicates that the formation of xonotlite is significantly accelerated by using a high W/S = 190 ratio and intensive mixing of the suspension at a speed of up to 300 min^{-1}, but this method is characterized by high energy consumption and a low efficiency of the hydrothermal treatment equipment [92].

1.6 Raw materials for tobermorite and xonotlite synthesis

The temperature, duration, stirring intensity and the water to solid (W/S) ratio have a significant impact on hydrothermal synthesis of calcium silicate hydrates. However, the chemical composition, purity and dispersion of the raw materials have no less impact on the rate of formation, the mineral composition and the crystallinity degree of the resulting products. The quality of the raw materials is particularly important when using natural rocks and industrial by-products as the external ions from impurities very often determine the kinetics of synthesis [93, 94]. Numerous studies of hydrothermal synthesis of 1.13 nm tobermorite have been carried out while using various sources of SiO_2 and CaO. Quartz, amorphous SiO_2, and limestone are the best examples of these materials thoroughly examined by Taylor, Mitsuda, McCoonnell and others [87, 95–97]. The above listed researchers formulated the key statements regarding the use of mixtures made from various raw materials in hydrothermal synthesis. The field of study was further developed, and additional data pertaining to the use of new silica sources was obtained: silica fume *Elkem*, silica fume *Grace Davison*, silica sand *Dorsilit* [98], and marble [98] were discussed. Therefore, researches started looking for raw materials containing the more reactive part of silica or containing additives which could accelerate the synthesis of 1.13 nm tobermorite. Some unconventional materials, such as: kaolinite and metakoaline (2), K-feldspar [99], igneous rocks trachyte [100], and fuka [101], sedimentary rock opoka [102] were used for these goals. The data provided in the literature supports the idea that tobermorite can be synthesized from industrial by-products and wastes: coal fly ash [103], biomass ash [104], high alumina fly ash

[83], blast furnace slag [105], steel slag [106], oil shale fly ash [107], newsprint recycling waste [108].

In general, xonotlite can be formed via a hydrothermal process by using various kinds of high purity siliceous materials and calcareous materials as well as raw materials, such as quartz, sodium silicate, or calcium oxide. However, former researches always focused on the temperature, time or additions to the synthesis process. Very little effort was directed towards the study on the fiber material involving issues such as the sources of the material, impurities, the crystalline degree of the fiber material, the crystal growth and its mechanisms, which is the essence of the process of synthesis. Literature indicates that the preparation method for the xonotlite fiber material when using acid residue and carbide slag was developed for the first time; it was aimed at finding an effective way to deal with millions of tons of residue and carbide slag, while synchronously seeking a cheap raw material to prepare xonotlite [109]. Furthermore, literature suggested possibilities to use various sources of silica for xonotlite synthesis. Wieslawa Nocuò-Wczelik [110] reports on the synthesis of xonotlite by using: amorphous ($SiO_2 \cdot nH_2O$), ground quartz, *Degussa* (20.000 $cm^2 \cdot g^{-1}$), *Aerosil*. Moreover, Pei *et al*. used pure nanoscale SiO_2 powders [111], whereas Zou, Jingjing *et al*. used acid residue (SiO_2 = 55.74%) from extracting alumina [23].

1.7 Influence of impurities on the synthesis of tobermorite and xonotlite

As mentioned above, calcium silicate hydrate occurs as the main hydration product in cement, or else it can be synthesized by using hydrothermal synthesis. The raw materials which are used in both cases to obtain these compounds of calcium silicate hydrates commonly contain impurities.

One of the most common compounds found in impurities is aluminum which can interfere into the tobermorite structure. The tobermorite model with interrupting aluminum has the same layer-based structure with the silicate chain and calcium (hydro)oxide layers organized in the dreierketten structure [112]. During the crystallization of calcium silicate hydrates, the guest ions from the interlayer layer, especially aluminum ions, can interfere into the silicate chains [113].

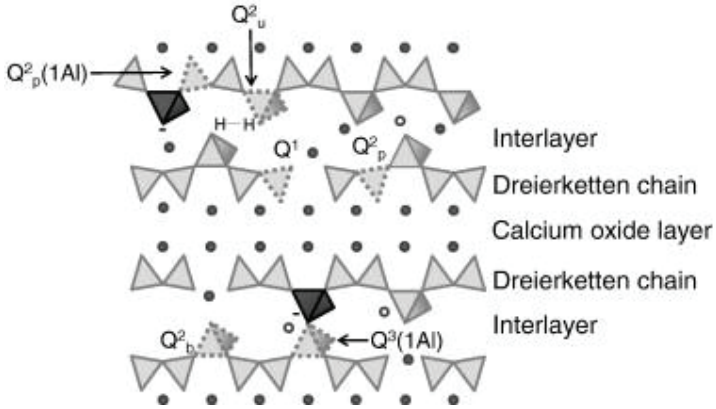

Fig. 1.6. Structure model of 1.13 nm tobermorite with aluminum interrupted into the crystal lattice [114]

Nuclear magnetic resonance (NMR) studies of ^{27}Al and ^{29}Si in the tobermorite structure showed that aluminum atoms can be: tetra-coordinated Al^{IV}, penta-coordinated Al^{V}, and hexa-coordinated Al^{VI}. In addition, aluminum atoms coordinated Al^{V} and Al^{VI} can replace calcium ions in the interlayer space [115, 116]. Moreover, about 10% of aluminum in the tobermorite structure is present as penta-coordinated Al^{V} regardless of the molar ratio of the compound [7, 117]. Literature data suggests that one of the silicate tetrahedra can be replaced with Al^{+3} in the silicate chain. Al^{V} and Al^{VI} compensate the negative charge in the silicate chain [118]. In this way, the structure of 1.13 nm tobermorite is stabilized and protected from crystallization to other compounds under hydrothermal treatment. Moreover, aluminum replaces the bridging tetrahedron rather than the adjacent pairs of the silicate tetrahedra in the silicate chain [116]. In addition, aluminum does not occupy the end of silicate chain. Richardson *et al*. suggested a mechanism of aluminum incorporation [119]. According to researchers, aluminum replaces the linker monomer in the bridge position of two dimeric silicate chains by formatting the pentameric chain.

Examination of the literature data shows that aluminum substituted tobermorite is mostly obtained from the reaction compositions falling into the following molar component ratios:

$$0.80 < CaO[SiO_2 + Al_2O_3] < 0.85$$
$$0.00 < Al_2O_3 l[Al_2O_3 + SiO_2] < 0.17$$

It was determined that the long duration of hydrothermal synthesis and the increased amount of aluminum over 15% of Si contained in tobermorite leads to the formation of hydrogarnets, such as katoite or others, as additional phases to Al-substituted tobermorite [120, 121]. However, Mostafa *et al*. reported that aluminum significantly influences the crystallization of tobermorite at the early stages of synthesis [121]. Subsequently, aluminum improves the conversion of semi-amorphous C-S-H into more structured and well-developed crystalline forms [110]. Moreover, stabilized tobermorite structure by aluminum additives prevents the recrystallization into xonotlite (79).

Alkaline additives significantly affect the formation and further transformation of crystalline forms of tobermorite. After examination of the Na_2O-CaO-SiO_2-H_2O system, researchers found that NaOH accelerates hydrothermal synthesis which occurs in the transition from C-S-H into tobermorite. Moreover, if the molar ratio C/S = 0.83 is constant and only the $NaOH/SiO_2$ ratio varies (from 0.05 to 0.63), after the synthesis, tobermorite is highly disordered [110, 122, 123]. In addition, if the prepared mixture contains impurities up to 10% by weight of Na_2O together with a content of silica of up to 55% by weight, no other phase occurs apart from C-S-H(I). At a higher SiO_2 content, pectolite can be detected as a result of autoclaving [110].

Literature data shows that the concentration of sodium ions has a significant effect on the phase composition and morphology formation of xonotlite during hydrothermal synthesis. Liu *et al*. in their study found that, when using mixtures containing less than 5wt% impurities of Na_2O, synthesis results in the formation of

xonotlite whose structure is similar to a fiber [124]. Moreover, as the amount of Na_2O increases, the obtained xonotlite recrystallizes into pectolite, and the morphology changes from a fibrous shape to a broom-like shape. When the amount of Na_2O is over 15 wt%, pectolite is identified as main crystalline compound in the products [125, 126]. In summary, the formation of xonotlite with the fiber structure in the $CaO\text{-}SiO_2\text{-}H_2O$ system when the molar ratio is CaO/SiO_2=1.0 requires careful monitoring of Na_2O content.

Literature indicates that sulphate additives found in raw materials affect the formation of calcium silicate hydrates. Copeland *et al*. stated that S^{6+} interrupts into the structure of calcium silicate hydrates and replaces the (Si^{4+} + $2H^{+}$) group [127]. Moreover, Mostofa *et al*. investigated the effect of SO_4^{2-} ions on the formation of 1.13 nm tobermorite and found that it speeds up compound formation during hydrothermal synthesis (127). The influence of this compound formation is greater with the addition of such sulphates as $Al_2(SO_4)_3$ and $CaSO_4$. Literature data shows that sulfate ions may intervene in the 1.13 nm tobermorite lattice; it was shown by scientific studies that tobermorite can accept up to 4% of SO_4^{2-} ions. In general, both aluminum and sulphate ions intervene into the tobermorite crystalline lattice, which has a significant impact on the transition from a low crystallinity degree to high-crystallinity levels. However, a certain amount of sulphate ions in moistened mixtures inhibits the conversion of C-S-H gel into compounds of a high crystallinity degree.

1.8 Thermal insulating materials from calcium silicate hydrates

Environmental issues and energy shortages are the two main challenges for a sustainable society. The energy consumption of buildings accounts for more than 10% of the total energy consumption in the world [128]. The use of high-performance thermal insulation materials is an effective way to significantly reduce energy consumption. The decrease of the level of energy consumption not only protects the environment, but also reduces the maintenance costs. Moreover, common organic polymer boards, such as polystyrene boards and polyurethane boards, are widely used as thermal insulation materials for buildings. However, organic polymer boards with a low utilization temperature are flammable; thus they easily lead to a fire in the building. Inorganic thermal insulation materials, such as foamed concrete, porous calcium silicate, mineral wool, expanded perlite, etc., which are incombustible and are denoted by a high utilization temperature, are alternatives to polymer boards [129, 130]. However, they usually have higher thermal conductivity and a larger apparent density [131]. By designing nano-porous inorganic thermal insulation materials, their thermal conductivity could be considerably reduced [132–134]. A typical example is silica aerogel with a thermal conductivity of 0.017−0.041 W K^{-1} m^{-1} which is regarded as the best insulation material [135–138]. Yet, silica aerogel is brittle and very expensive, therefore, it cannot be used in large scale building insulation. For building insulation, the challenge is to develop high performance inorganic thermal insulation materials sporting a low cost. For this purpose, the prerequisite is to find inexpensive and abundant raw materials to prepare thermal insulation materials [139].

High temperature thermal insulating materials obtained from calcium silicate hydrates are a subject of many fields of scientific research [140–143]. These compounds exhibit several excellent characteristics, such as being lightweight, fireproof and eco-friendly, which makes them very efficient for heat insulating and fire-resistant building materials. Literature indicates that insulating materials from C-S-H can be divided into two groups: low-density and high-density [144]. Insulating products are considered lightweight (i.e., low density) when their density is less than 300 kg/m^3. These products are usually suitable for coating of short pipes or blocks for industrial ovens. Low density impacts the final insulating product strength or resistance against damage and should be used where these effects are minimal.

High level thermal insulation products from calcium silicate hydrates are defined as having a density of more than 300 kg/m^3, and, commonly, the density varies from 560 to 1000 kg/m^3. These high-density materials are distinguished for good thermal insulating properties with sufficient strength and durability. Moreover, large sheets of this type of an insulating product can be used for self-supporting walls as building materials or refractory materials in metallurgical and glass-melting furnaces. Unlike low-density materials, the insulation of high-density calcium silicate hydrates goes along with good nailing, cutting and bolting retention properties and can be treated in the same way as many other building materials.

The classification of calcium silicate insulations is based on the compounds which form an insulation matrix. Each calcium silicate hydrate is denoted by different properties and conditions of synthesis, but, most importantly, different thermal stability and heat resistance [145, 146]. Moreover, the crystalline compounds of the insulating matrix can vary among tobermorite, xonotlite and others, depending on the reaction conditions involved. The low resistance against temperature compared to other materials characterizes the heat-insulating products based on tobermorite. Compared with fire-retardant fibers, xonotlite has excellent insulating performance, such as low thermal conductivity, environmental friendliness, high strength, and wide temperature ranges, all of which have been recognized in recent years by researchers and are of substantial interest to the industry [143].

The apparent density of the final product was largely controlled in the past by regulating the proportion of water in the suspension and the residual water is removed from the product after it has hardened to its final shape and size. In some processes (the so-called filter press processes), a portion of the suspension medium is expressed from the reactive mixture at an intermediate stage where sufficient reaction has taken place to produce a self-supporting but compressible gel. In such processes, the density of the final product is determined by the amount of water which was pressed out from this intermediate gel [144]. According to another class of processes (the so-called baking or casting processes), the suspension is simply poured into baking molds of the desired shape and induced under appropriate conditions, and the final apparent density is largely determined by the proportion of water in the stock solution [147].

2. Materials and Methods

In this work the materials used as the source of silica are: silica-calcite sedimentary rock opoka from Stoniskiai-Zemaitkiemis quarry, granite sawing powder waste from *JSC Granitas* (both from Lithuania), and amorphous $SiO_2 \cdot nH_2O$ (*Reachim*, Russia, analytical grade); as well as limestone from Karpenai quarry (Lithuania). The elemental composition of rocks was determined by employing the XRF method and recalculated to oxides (Table 2.1).

Table 2.1. Chemical composition of natural raw materials

Material	Oxides, wt%								Other	Ignition losses, wt%
	SiO_2	**CaO**	**Al_2O_3**	**K_2O**	**Na_2O**	**MgO**	**Fe_2O_3**	**SO_3**		
Opoka	54.60	22.10	2.53	0.83	0,09	0.55	1.66	0.58	0.74	16.41
Granite	58.41	3.95	15.41	3.86	3.45	2.87	7.17	0.19	0.48	4.31
Limestone	4.38	50.88	0.22	0.23	–	1.67	0.70	0.53	–	41.39

X-ray powder diffraction analysis of opoka (Fig. 2.1, curve 1) showed three different crystal modifications of SiO_2: quartz (d = 0.426; 0.335; 0.228; 0.182 nm), tridymite (d = 0.431; 0.410; 0.381 nm) and cristobalite (d = 0.408; 0.249 nm). Other identified minerals are: calcite $CaCO_3$ (d = 0.303; 0.228; 0.192 nm), dolomite $CaMg(CO_3)_2$ (d = 0.286; 0.218; 0.177 nm) and muscovite $KAl_2(AlSi_3O_{10})(F,OH)_2$ (d = 0.319; 0.257 nm).

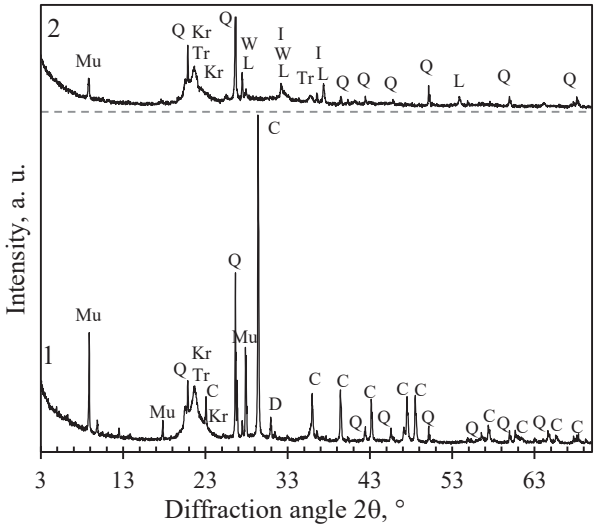

Fig. 2.1. XRD patterns of raw (*1*) and calcined opoka (*2*). Indexes: Q – quartz, Kr – cristobalite, Tr – tridymite, D – dolomite, C – calcite, Mu – muscovite, W – wollastonite, L – lanite, I – calcium oxide

The data received from Rietveld analysis showed that opoka contains ~2.5 times more cristobalite (one of SiO_2 modifications) than quartz (which is a much

more common material). Moreover, after summing up all three different crystal modifications of SiO_2 (35 %), it was found that opoka contains 19.6% of amorphous components which can be attributed to amorphous SiO_2. These assumptions were made because, after having examined the elemental composition of opoka, it was found that this material contains 54.6% of Si.

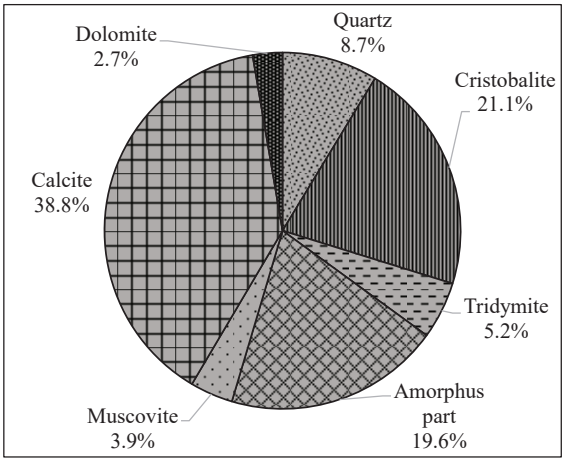

Fig. 2.2. Rietveld refinement results (wt%) of raw opoka

Under hydrothermal conditions, calcite and dolomite react with SiO_2 very slowly. In order to increase their reactivity, it is necessary to decompose these carbonates by thermal treatment. The curve of simultaneous thermal analysis shows that decarbonization of opoka starts at a temperature of 657 °C and ends at 791 °C. The mass loss was 16.41%, which equals to 37.32% of $CaCO_3$ available in the material. An exothermal peak at 887 °C shows the reaction between CaO and SiO_2 in which wollastonite ($CaO{\cdot}SiO_2$) was formed (Fig. 2.2).

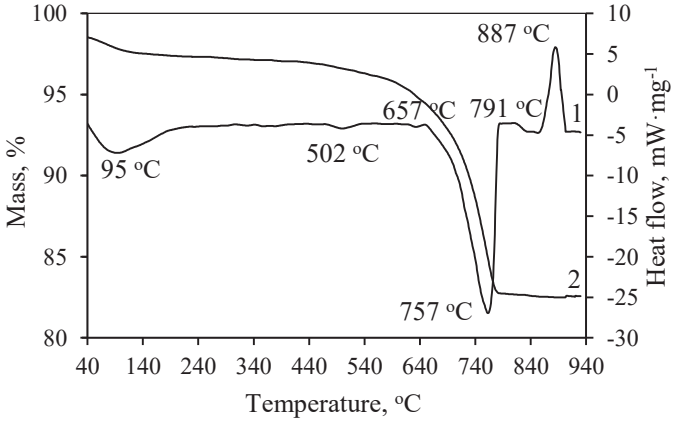

Fig. 2.3. DSC (1) and TG (2) curves of raw opoka

With reference to the previously published data, opoka was calcined at 775 °C for 1 h (148). After the calcination of raw material (Fig. 2.1, curve 2) the maximum

amount of CaO_{free} was obtained (50.67% of total CaO) under these conditions. In addition, crystalline modifications of SiO_2 remained after calcination (Fig. 2.1, curve 2). It should be underlined that, in the XRD curve, the amorphous part of SiO_2 was not detected, although, in previous researches it had been identified. It can be assumed that the amorphous part was consumed to obtain wollastonite because this compound is obtained during heat treatment. After calcination, pellets were milled in a ball mill until $S_a \approx 970\ m^2 \cdot kg^{-1}$ and used to obtain the mixtures.

The particle size distribution of opoka (Fig. 2.4) was determined to be as follows: 90% particles of a diameter less than 53.17 μm, 50% of a diameter of less than 6.08 μm, and 10% of a diameter less than 0.81 μm. The main particle diameter was determined to be 17.74 μm.

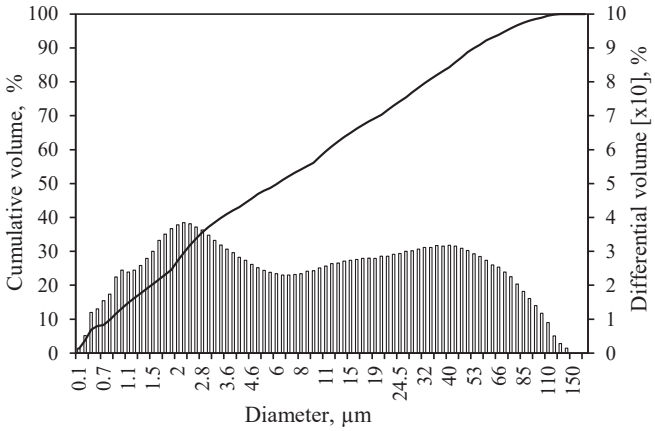

Fig. 2.4. Particle size distribution of opoka calcined at 775 °C

Granite sawing powder waste was milled in ball mill until $S_a \approx 905\ m_2 \cdot kg^{-1}$. XRD analysis (Fig. 2.5) shows one crystal modification of silica: quartz. Other identified minerals are listed in the random order. Annite $KFe_3AlSi_3O_{10}(OH)_2$ (PDF No. 00-002-0045; *d* = 1.01; 0.337; 0.266; 0.218; 0.118 nm) – a phyllosilicate mineral from the mica family. Albite $NaAlSi_3O_8$ (PDF No. 00-009-0466; d = 0.639; 0.403; 0.378; 0.368; 0.351; 0.319 nm) and anorthite $CaAl_2Si_2O_8$ (PDF No. 04-015-4238; *d* = 0.643; 0.404; 0.388; 0.376; 0.364; 0.347; 0.321; nm) – a plagioclase feldspar mineral. Actinolite $K_{0.01}Na_{0.05}Ca_{1.9}Mg_{3.4}Mn_{0.1}Fe_{1.5}Al_{0.2}Si_{7.9}O_{22.1}(OH)_{1.9}$ (PDF No. 04-013-2277; *d* = 0.906; 0.845; 0.489; 0.313; 0.244 nm) – an amphibole class mineral. Labradorite $Ca_{0.52}Na_{0.48}(Si,Al)_4O_8$ (PDF No. 05-001-0013; *d* = 0.644; 0.404; 0.374; 0.363; 0.336; 0.322; 0.318; 0.242 nm) – a feldspar mineral. Microcline $(K_{0.95}Na_{0.05})AlSi_3O_8$ (PDF No. 01-084-1455; *d* = 0.422; 0.383; 0.336; 0.329 nm) – is one of the family of igneous rocks. It should be noted that calcite was not identified in the XRD curve, but the chemical composition showed 3.95% of CaO. This can be explained by the fact that the amount of Ca^{+2} ions in granite is small, and it is present in other compounds, such as actinolite, anorthite, labradorite.

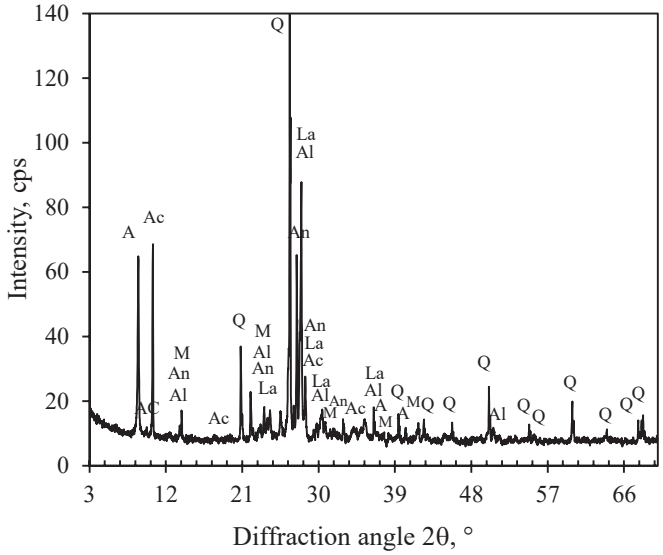

Fig. 2.5. XRD pattern of raw granite sawing waste. Indexes: A – annite, Ac – actinolite, An – anorthite, Al – albite, La – labradorite, M – microcline, Q – quartz

Rietveld analysis data showed that the largest part of granite sawing powder waste consists of quartz which constitutes 23.4% (Fig. 2.6). However, a moderate amount of other compounds was also found in granite sawing powder which is presented in Figure 2.6. Unfortunately, it should be noted that the accuracy of the identification is only average. The value of R_{np} (a statistical descriptive factor of the resulting profile) is 7.74, and R_{exp} (the value of the statistical reliability factor which is sought) is 1.34.

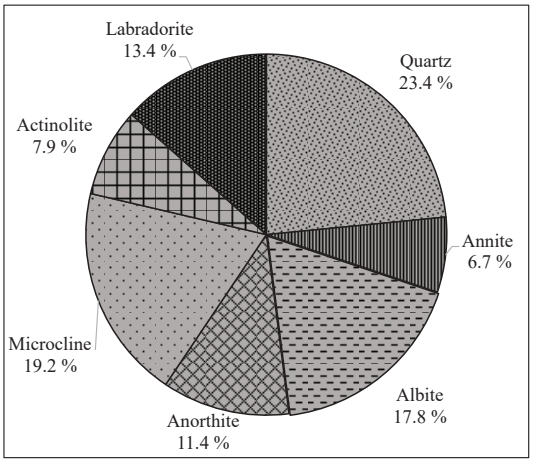

Fig. 2.6. Rietveld refinement results (wt%) of raw granite

The particle size distribution of the granite sawing waste is presented in Figure 2.7. It was determined to be as follows: 90% of the particles with a diameter of less

than 17.41 μm, 50% with a diameter of less than 3.99 μm, and 10% with a diameter of less than 0.85 μm. The main particle diameter was determined to be 10.33 μm.

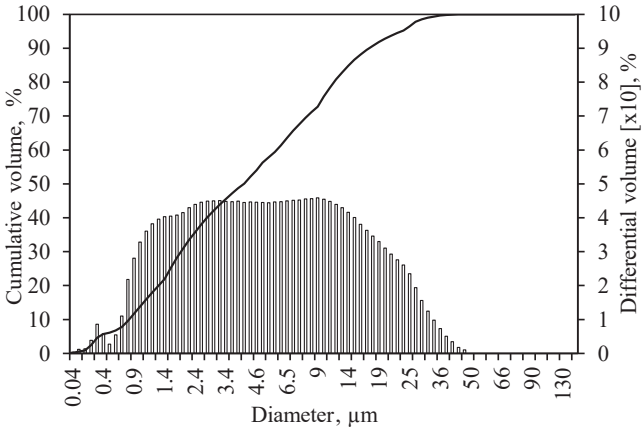

Fig. 2.7. Particle size distribution of granite sawing powders

Amorphous $SiO_2 \cdot nH_2O$ (reagent, 99.8%) was milled by using a ball mill where $S_a \approx 1000\ m^2 \cdot kg^{-1}$ was obtained; the loss on ignition is 18.32%.

Lime was obtained by burning limestone of *AB Naujasis kalcitas* (Akmenė District Municipality, Lithuania) at 900 °C for 1 h in a laboratory kiln *Nabertherm* LV 15/11/P330, and, after calcination, milled to $S_a \approx 650\ m^2 \cdot kg^{-1}$. The activity of the product (the amount of free CaO) was equal to 85.2%.

Lime (EN 459-1:2010; CaO_{free} = 92%) was sourced from *Lhoist Bukowa Sp.* (Poland) and milled in a ball mill until reaching S_a= 650 $m_2 \cdot kg^{-1}$.

$Ca(OH)_2$ (*Stanchem*, Poland, analytical grade) was calcined at 950 °C for 1 h and milled in a ball mill until reaching Sa = 616 $m^2 \cdot kg^{-1}$. The amount of free CaO was equal to 98%.

Aluminum hydroxide was purchased from *Sigma-Aldrich*, Germany, analytical grade. Al_2O_3 was obtained by burning aluminum hydroxide at a temperature of 475 °C for 5 h.

The mixtures of the granite sawing waste and lime were prepared with a molar ratio of CaO/SiO_2 = 0.83; 1.0. A molar ratio of the primary mixture from calcinated opoka and calcinated limestone was CaO/SiO_2 = 0.83; 1.0; 1.2. The mixtures were prepared in order to compare the sequence of reactions during the synthesis of calcium silicate hydrates in a pure (model) system from the following reagents: CaO, $SiO_2 \cdot nH_2O$, Al_2O_3. The mixtures whose composition corresponds to the molar rations $CaO/(SiO_2 + Al_2O_3)$ = 0.83; 1.0 and $Al_2O_3/(SiO_2 + Al_2O_3)$ = 0 or 0.025 were prepared.

Hydrothermal synthesis was carried out in unstirred suspensions (the water/solid ratio was equal to 10.0) in 25 ml volume PTFE cells which were placed in an autoclave (*Parr Instruments*, Germany) under saturated steam pressure at temperatures between 180–220 °C; the duration of isothermal curing was 4–72 h. The products of the synthesis were filtered, rinsed with acetone to prevent

carbonization, dried at a temperature of 100±1 ºC, and thrust through a sieve with an 80-μm mesh. In addition, hydrothermal synthesis was carried out in a stirred suspension in a (*Parr Instruments*, Germany) 600 ml autoclave at 180; 200 and 220 °C, for 4–72 h (the water/solid ratio was equal to 20.0).

X-ray diffraction analysis (XRD) was performed on a *D8 Advance* diffractometer (*Bruker AXS*, Germany) operating at the tube voltage of 40 kV and the tube current of 40 mA. The X-ray beam was filtered with a Ni 0.02 mm filter to select the CuKα wavelength. The diffraction patterns were recorded in a Bragg-Brentano geometry by using a fast counting detector *Bruker Lynx Eye* based on the silicon strip technology. The samples were scanned over the range of 2θ = 3–70° at a scanning speed of 6°/min by using the coupled two theta/theta scan type. The program used for compound identification was *Diffrac.eva v3.0*.

Quantitative phase (Rietveld) analysis, i.e., the determination of the quantity of phases in a multicomponent system, is based on the fact that the area of the phase diffraction peak is proportional to the amount of a given compound in the mixture and is performed by comparing with each other the diffraction peak profiles of the test phase and the standard. XRD analysis was complemented by Rietveld refinement. For this, 10% of ZnO was added to the sample as an internal standard for the quantitative determination of the amorphous phase. The samples for the QXRD analysis were dried at 40 °C for 48 h and ground to pass a 32 μm sieve. Quantitative analysis was performed by using *Topas* software which calculated the theoretical diffraction profile (by the least squares approximation), and we compared the results with the profile of the recorded diffraction curve.

XRD software *Diffrac.Eva* was used for the calculation of the crystallite size. The crystallite size of 1.13 nm tobermorite from the crystalline plane *h k l* (*d*–spacing 1.133 nm) and xonotlite (*h k l*; *d*–spacing 0.702 nm) was determined by following the Scherrer equation:

$$D_{hkl} = \frac{k_{hkl} \cdot \lambda}{\beta_{hkl} \cdot \cos\theta} \tag{1}$$

where λ is the wavelength of the CuKα radiation, θ is the Bragg's diffraction angle, β_{hkl} is the full width at half maximum intensity, and k is a shape factor (the value used in this study was 0.94).

The area computations were performed on an interval between two points called the 'entry points' or the Left Angle and the Right Angle. These are the angles (in degrees) of the scan point that are the closest from the entry points. These are statistical computations assuming that there is a unique peak in the interval. It supplies information about the position of the peak maximum and the net area of the peak. Dedicated software *Diffrac.Eva* was used for this purpose.

The highest value in the interval may not be pertinent information due to noise fluctuations. The position of the peak maximum was located by fitting a parabola through the points around the highest value and is given in a scan unit (plus *d* in Å, because the scan was 2θ). The output Gross height is the intensity of the fitting parabola, in cps. We calculated the Net height which is obtained from the Gross height minus the background intensity which is determined by the linear background

between the left and the right extremities. Software *Diffrac.Eva* was used for this purpose.

The chemical composition analysis of the samples was performed by X-ray fluorescence spectroscopy (XRF) on a *Bruker X-ray S8 Tiger WD* spectrometer equipped with a Rh tube with the energy of up to 60 keV. Powder samples were measured in Helium atmosphere, and the data was analyzed with *SPECTRA Plus QUANT EXPRESS* standardless software.

Thermal analyzer *Linses* (Germany) was applied to simultaneous thermal analysis (STA; differential scanning calorimetry (DSC), and thermogravimetric (TG)) studies. Heating was carried out under air atmosphere at a heating rate of 10 °C·min^{-1}; the temperature ranged from 40 up to 1000 °C. Ceramic sample handlers and crucibles of Pt were used. Differential scanning calorimetry (DSC) was performed by using *Netzsch DSC 214 Polyma*. The heating rate was 10 °C·min^{-1}, the temperature ranged from 15 °C up to 600 °C under N_2 atmosphere. Linear thermal expansion analysis of the samples was performed with a *Linseis 75PT 1600* dilatometer (Germany) by using a corundum Al_2O_3 support tube (the temperature interval was 30–1100 °C, the heating rate was 10 °C·min^{-1}, N_2 flux equaled to 20 cm^3·min^{-1}). Samples of 5 mm in diameter and ~30 mm in length were formed from the plastic mass and dried to a constant weight at 100 °C. The ends of the specimens were polished to be perpendicular to the axis.

Scanning electron microscopy (SEM) was performed by using *CARL ZEISS NTS EVO MA-15* and *JEOL-JSM-6301F*. Powder was mounted on the top of the carbon tape and coated with an Au-Pd layer.

FT-IR spectra were carried out with the help of a spectrometer *Perkin Elmer* FT–IR system *Spectrum X*. Specimens were prepared by mixing 1 mg of the sample in 200 mg of KBr. The spectral analysis was performed in the range of 4000–400 cm^{-1} with a spectral resolution of 1 cm^{-1}.

The specific surface area of the raw materials was determined by using CILAS LD 1090 or by the Blaine method with an air permeability apparatus (model *7201*, *Toni Technik Baustoff GmbH*). The mixing of raw materials was performed in a homogenizer *Turbula Type T2F* for 1 h at 49 rpm. The amount of free CaO was determined by following the standard *ASTM C114–11b*.

The compressive strength was determined right after the curing by using an *ELE International* 250 kN *Automatic Cement Compression Machine*, *EL39-1501/01* at a loading rate of 1.5 kN·s^{-1}. For statistical accuracy, at least three samples of each batch were tested, and the average value of the compressive strength was used.

The amount of free CaO was determined by following the standard *ASTM C114–11b*.

Surface area and particle size distribution

1) The particle size distribution of the materials was measured by using a laser particle size analyzer *CILAS 1090 LD* with a sensitivity range from 0.04 μm to 500 μm. The dispersion phase was compressed air (2.5 bar), the distribution of solid

particles in the air flow was 12–15%, the measurement time was 15 s. The specific surface area was calculated from the obtained measurement data.

2) The specific surface area of the synthesis products was determined by employing the Brunauer, Emmet and Taller (BET) method. Measurements were performed on a *KELVIN 1042 Sorptometer* (*Costech Instruments*, USA) by using a nitrogen adsorption isotherm at 77 K. The specific surface area was calculated according to the BET equation by using N_2 adsorption isotherm data in the range of ($0.05 < p/p_0 < 0.35$):

$$\frac{1}{X\left(\frac{p_0}{p}-1\right)} = \frac{C-1}{X_m \cdot C} \cdot \frac{p}{p_0} + \frac{1}{X_m \cdot C}, \tag{2.1}$$

where X is the mass adsorbed on the sample at relative pressure p/p_0 (p is the partial pressure of adsorbate, and p_0 is the saturated vapor pressure of adsorbate), X_m is the mass of N_2 adsorbed on the surface when a monolayer is formed, C is a constant which is a function of the heat of the adsorbate condensation and the heat of adsorption (C_{BET}).

The values of the BET equation are correct if it yields a straight line when $\frac{1}{X\left(\frac{P_0}{p}-1\right)}$ is plotted $\frac{p}{p_0}$. The angle of the slope $S = tg\alpha = \frac{C-1}{X_m \cdot C}$ and the length of the segment intersecting in the ordinate axis $I = \frac{1}{X_m \cdot C}$ were used to determine X_m and C. In order to calculate these parameters, the equations were rewritten as follows: $X_m = \frac{1}{S+I}$ and $C = \frac{1}{I \cdot X_m}$. The BET equation plot provides linear change in the range of p/p_0 = 0.05–0.35. The total surface area S_t of the sample is calculated from the following equation:

$$S_t = \frac{X_m \cdot N \cdot A_{cs}}{M}, \tag{2.2}$$

where A_{cs} is the cross-sectional area of the adsorbate molecule ($A_{ad} = 16.2 \cdot 10^{-20}$ m^2), M is the molecular weight of the adsorbate, N is Avogadro constant ($6.023 \cdot 10^{23}$).The specific surface area is calculated from the following equation:

$$S_{BET} = \frac{S_t}{m}, \tag{2.3}$$

where m is the mass of the sample of the product obtained after hydrothermal synthesis.

The total pore volume and the radial distribution of the pores were calculated according to the correlated Kelvin equation and a scheme developed by Orr *et al.* when using the N_2 desorption isotherm at 77 K. The Kelvin equation describes the vapor pressure depression of an adsorbate in a capillary of a given radius:

$$ln\frac{p}{p_0} = -2\frac{\gamma \cdot V_m \cdot cos\theta}{R \cdot T \cdot r_K}, \tag{2.4}$$

where p is the saturated vapor pressure in equilibrium with the adsorbate condensed in a capillary or a pore, p_0 is the normal adsorbate saturated vapor pressure, γ is the surface tension of nitrogen at its boiling point (γ=8.85 erg·$(cm^2)^{-1}$), V_m is the molar volume of liquid adsorbent N_2 (V_m=34.7 $cm^3 \cdot mol^{-1}$), θ is the surface adsorption angle (usually taken as 0° and thus cosθ=1), R is the universal gas constant (R=8.134·10^7 ergs· $deg^{-1} \cdot mol^{-1}$), T is the boiling point of liquid nitrogen (T=77 K), and r_K is the Kelvin radius of a pore.

The thickness t of the adsorbed layer is calculated according to the following equation:

$$t = \frac{V_a}{V_m} \cdot \tau; \tag{2.5}$$

where V_m is the volume of the absorbed gas, mm^3/g, and τ is the thickness of the monomolecular adsorbent, mm.

Since we use a cylindrical pore model $r_p = r_k + t$ then we get the following equation:

$$V_p = \left(\frac{\bar{r}_p}{\bar{r}_k}\right)^2 \cdot (V_L - \Delta t \cdot \sum A); \tag{2.6}$$

where $\bar{r}_p$ is the actual average of the pore radius in the range of r_2–r_1, Å;

The volume of desorbed liquid in any desorption isotherm range is related to the volume of gas evolved $\Delta V_p = \Delta V_d$ (1.54·10^{-3}). Cylindrical pores are calculated by using the following equation:

$$A = \frac{2 \cdot \Delta V_p}{\bar{r}_p} \cdot 10^4; \tag{2.7}$$

where ΔV_p is the volume of the emitted gas, cm^3.

Parallel plate type pore are calculated by using the following equation:

$$\overline{d_p} = r_k + 2t; \tag{2.8}$$

where r_k is the measured distance between two plates, Å; $\overline{d_p}$ is the actual distance between two plates, Å.

The volume of pores between two parallel plates is calculated by using the equation :

$$V_p = \frac{\overline{d_p}}{\bar{r}_k} (\Delta V_L - 2\Delta t \sum A); \tag{2.9}$$

The theoretical surface area A of the pore walls is calculated by the following equation:

$$A = \frac{2V_p}{d_p}; \tag{2.10}$$

The calculations are completed by using any model wherever $\Delta t \cdot \Sigma A$ exceeds ΔV_L value.

3. Results and discussion

3.1. Hydrothermal synthesis of 1.13 nm tobermorite from granite sawing powder waste

Calcium oxide ($Ca(OH)_2$; calcined at 950 °C for 1 h) was added into granite sawing powders in order to obtain mixtures with a molar ratio $CaO/SiO_2 = 0.83$, and hydrothermal synthesis was carried out in unstirred suspensions. X-ray diffraction analysis data of the obtained synthesis products is shown in Figure 3.1. It was determined that 1.13 nm tobermorite (d = 1.133; 0.548; 0.308; 0.298; 0.282; 0.184 nm), was identified in the synthesis products during all the examined durations. However, after 4 h of isothermal curing, only traces of 1.13 nm tobermorite were identified in the product (Fig. 3.1, curve 1). Together with it, we identified other compounds, such as: annite, actinolite, anorthite, albite. These minerals were identified in the raw granite sawing powder waste; thus, after 4 h of synthesis, they do not participate in the formation of calcium silicate hydrates. This can be explained by the fact that the solubility of these minerals is very low. Due to this reason, Ca^{2+} could not react with annite, actinolite, anorthite, or albite. Unexpectedly, the intensity of the peaks of these minerals in the XRD curves increases slightly with the increasing duration of synthesis. We assume that the semi-amorphous C-S-H type calcium silicate hydrates formed at the beginning of the synthesis may cover the surface of unreacted granite sawing waste minerals, which results in a lower intensity of their peaks in the RSDA curves. Later, with the formation of crystalline compounds, this shielding effect is attenuated, and higher peaks are obtained

However, the XRD results indicate that labradorite reacted as early as after 4 h of hydrothermal treatment; meanwhile, albite reacted only after 72 h (Fig. 3.1, curves 1 and 5).

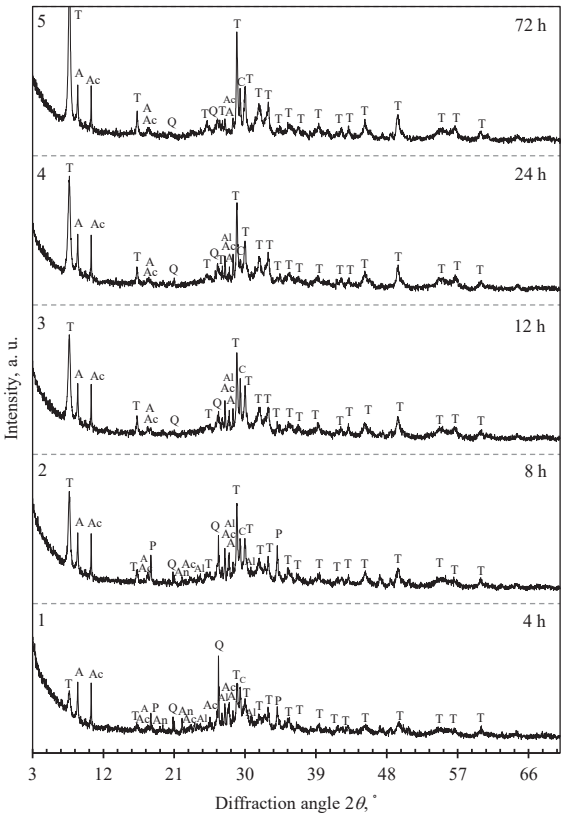

Fig. 3.1. XRD patterns of the synthesis products from CaO-granite mixture with CaO/SiO_2 = 0.83 at 180 °C. Indexes: A – annite, Ac – actinolite, An – anorthite, Al – albite, C – calcite, T – 1.13 nm tobermorite, P – portlandite, Q – quartz

In addition, calcite (PDF No. 00-002-0623) was identified by XRD analysis, and its existence was confirmed by simultaneous thermal analysis where the thermal effect of decarbonization at 747 °C is observed (Fig. 3.4, curve 3). Part of carbonates was brought along with the raw materials, whereas, the other part of carbonates was formed during the drying of the synthesis products. It is in good agreement with the literature data which indicates that some quantity of synthesis products could be carbonated when the samples are prepared for instrumental analysis (149–151).

It was determined that the intensity of the peaks and the size of 1.13 nm tobermorite crystallite increases significantly after 8 h of synthesis (Figs. 3.2 and 3.3). The obtained results indirectly indicate that the formation of 1.13 nm tobermorite was accelerated significantly thus changing only the duration of the synthesis. By extending the synthesis duration to 12 h, the crystallite size of tobermorite increases slightly, and this change is not as large as that observed in the 4–8 h interval. Moreover, the size of 1.13 nm tobermorite crystallites constantly increases with prolonged hydrothermal synthesis, meanwhile, the intensity remains unchanged. After this period, the formation of 1.13 nm tobermorite accelerates again, because, after 72 h of isothermal curing, the intensity increases even more. It

can be assumed that the formation of 1.13 nm tobermorite is slow at 4 h of synthesis; hence, it is necessary to prolong the duration of the synthesis.

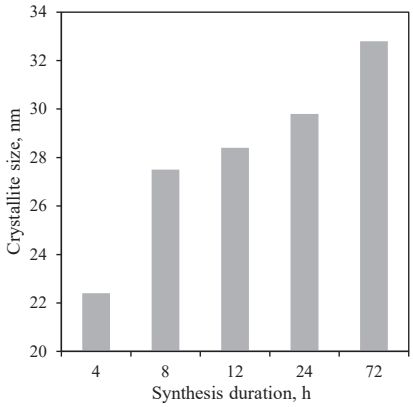

Fig. 3.2. Dependence of the size of 1.13 nm tobermorite crystallites on the duration of synthesis

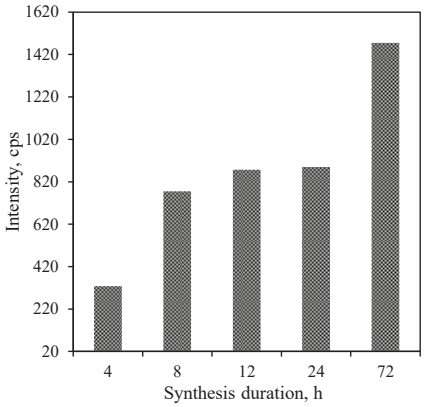

Fig. 3.3. Intensity of the main peak (d = 1.13 nm) of tobermorite from CaO-granite mixture

The results of simultaneous thermal analysis confirmed the above made assumptions, and, after 4 h hydrothermal synthesis, an endothermal effect at temperatures of 40–240 °C shows the dehydration of 1.13 nm tobermorite together with semi-amorphous C-S-H(I). However, the endothermal effect is very broad and vaguely expressed; due to this reason, it is impossible to distinguish between C-S-H(I) dehydration from 1.13 nm tobermorite (Fig. 3.4, curve 3). Other authors obtained similar results during the synthesis of 1.13 nm tobermorite from natural rocks and industrial waste materials with Al-containing impurities [152, 153]. According to TG analysis data, the mass loss between 40 °C and 190 °C is 4.28%, and it may be associated with the removal of adsorbed water and partial dehydration of 1.13 nm tobermorite and C-S-H(I) (Fig. 3.4, curve 1). The second endothermal effect at 456 °C is in good agreement with the XRD results where portlandite is identified. The TG analysis data also indicates that the mass loss during decarbonization is 3.65% (Fig. 3.4, curve 1), and the calculated quantity of $CaCO_3$ is 8.29%. The exothermic effect of recrystallization of C-S-H(I) into wollastonite is double and consists of two peaks, with the maximum at 872 °C and 902 °C. This means that the synthesized semi-amorphous calcium silicate hydrates without a clear crystal structure consist of two phases: C-S-H(I) and C-S-H(II). The latter compound (C-S-H(II) is likely to be formed at the beginning of the synthesis due to the low solubility of quartz and the higher molar ratio in the reacting region than it should be due to the stoichiometry of the initial mixture. The obtained results are well in line with the literature data [28, 45, 154].

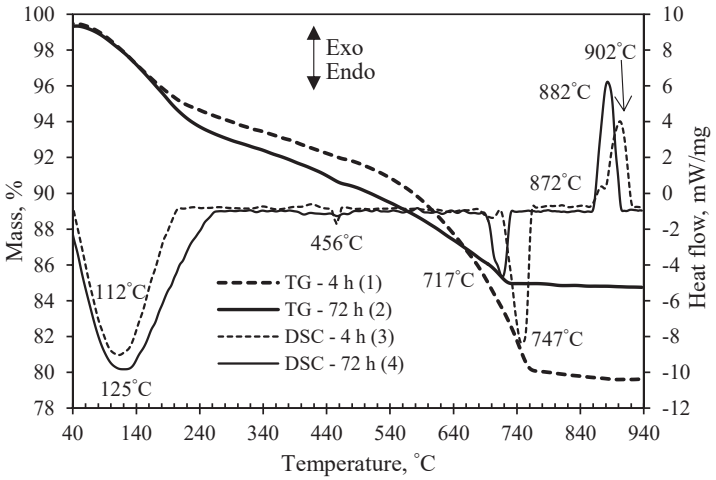

Fig. 3.4. TG (*1*, *2*) and DSC (*3*, *4*) curves of the synthesis products from CaO-granite mixture with CaO/SiO_2 = 0.83 at 180 °C after 4 h (*1*, *3*) and 72 h (*2*, *4*)

Samples obtained after 4 and 72 h of hydrothermal synthesis were examined by simultaneous thermal analysis (Fig. 3.4). The main dehydration effect of 1.13 nm tobermorite and C-S-H(I) at temperatures ranging between 40–240 °C is broader, and the mass loss is greater (6.0%) in the case of 72 h synthesis duration (Fig. 3.4, curve 2), which was observed by other scientists as well [155]. We can only assume, but not reliably state, that this is due to the higher amount of formed 1.13 nm tobermorite (this is evidenced by the XRD curves, see Fig. 3.1) because part of the adsorbed and crystalline water is removed from these calcium silicate hydrates almost simultaneously, and the endothermic effects overlap. The endothermic effect at 456 °C (Fig. 3.4, curve 3) indicates that, after synthesis of a short duration, the product still contains unreacted portlandite.

We also want to draw attention to the TG curves. In a 4-h synthesis product, the mass loss in the 180–640 °C range is ~8.5%, and in the 72-h synthesis product it is ~6.5% (Fig. 3.4, curves 1 and 2). 1.13 nm tobermorite loses most of its crystalline water (4.5 molecules) before reaching 240 °C, and the remaining 0.5 molecules show this effect only at ~700 °C. Meanwhile, C-S-H(I) loses water slowly but consistently over the entire mentioned temperature range. Thus, the TG results show that the products synthesized from CaO–granite sawing waste mixture at 180 °C contain a sufficient amount of semi-amorphous C-S-H type calcium silicate hydrates.

The tight thermal effect in the DSC curve at 717 °C indicates the existence of some amount of carbonates in the product (Fig. 3.4, curve 4). The mass loss at this temperature is about 1.25% (Fig. 3.4, curve 2), and the calculated quantity of $CaCO_3$ is 2.84%, e.g., which is much lower than in the case of synthesis of 4 h duration. Moreover, the heat flow of the exothermic effect at a temperature of 882 °C is increased by 37.74% (Fig. 3.4, curve 4). In addition, the identified peak at 902 °C disappears, which means that C-S-H(II) recrystallized into wollastonite and larnite.

It is known that the higher is the basicity of semi-amorphous C-S-H, the higher is its recrystallization temperature to wollastonite [155]. Thus, it can be stated that the 4-h synthesis product contains C-S-H(I) and C-S-H(II) (with exothermic effects at 872 and 902 °C), and the 72-h synthesis product is only C-S-H (I) (at 882 °C) type calcium silicate hydrates. Although the heat flow of the exothermic effect at 882 °C is 37.74% higher (Fig. 3.4, curves 1 and 2), this does not directly mean that more C-S-H(I) is formed – the amount of heat released from the recrystallization of these compounds to wollastonite differs.

Scanning electron microscopy (SEM) data of a 4-h synthesis sample (Fig. 3.5) shows that most of the new compounds are obtained as large agglomerates which are likely to be composed of semi-amorphous C-S-H(I). Unreacted starting materials such as quartz from the granite sawing waste (a 6-sided prism) and portlandite (hexagonal plates which look fibrous), are also visible in this image. Summarizing the results from the data of SEM, XRD, and DSC analyses after 4 h of isothermal curing at 180 °C, it can be stated that, after 4 h hydrothermal synthesis, 1.13 nm tobermorite crystallization processes are at the initial stage (Fig. 3.5, A).

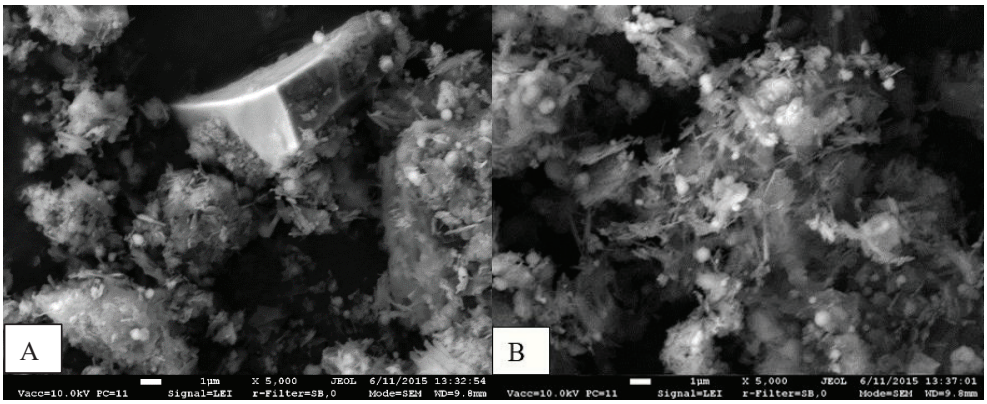

Fig. 3.5. SEM micrographs of synthesis products from CaO-granite mixture with $CaO/SiO_2 = 0.83$ after 4 h (A) and 72 h (B) at 180 °C

After prolonging the synthesis duration up to 72 hours, particles of unreacted quartz due to their low quantity are not visible in the products, and amorphous agglomerates are significantly smaller (Fig. 3.5, B). The accumulation of two morphologies of 1.13 nm tobermorite crystals can be noticed in the SEM image: 1–2 μm length needle-shaped crystals and 2–4 μm size plates or sheets are visible. This data is very similar to the results presented by other authors (98, 100) who noted that 1.13 nm tobermorite crystals can be of two types shaped either as needles or plates. It can be concluded that, after 72 h of hydrothermal synthesis at 180 °C, much more of 1.13 nm tobermorite is formed, and its crystals are distributed over the entire volume of the product.

It was determined that semi-amorphous C-S-H(II) was found in the case of short synthesis duration. This compound consumes most of the Ca^{2+} ions in the reaction medium, and the required mixture stoichiometry for the synthesis of 1.13

nm tobermorite may decrease. For this reason, a new mixture with a raised molar ratio of up to CaO/SiO_2 = 1.0 was prepared in order to increase the formation of the tobermorite rate at 180 °C.

The X-ray diffraction analysis data shows that, when the molar ratio of the mixture was increased up to 1.0, the intensity of 1.13 nm tobermorite peaks after 4 h of synthesis is low (Fig. 3.6, curve 1). Moreover, in the synthesis products, intense peaks of unreacted minerals, such as portlandite and quartz, were identified. Furthermore, the formation of tobermorite was not accelerated when the CaO content of the mixture was increased. Therefore, in the products, portlandite can be identified even after 24 h of hydrothermal synthesis. Due to slower hydrothermal reactions, in the products, 1.13 nm tobermorite as the main compound was identified only after 72 h (Fig. 3.6, curve 5). It can be assumed that tobermorite was obtained together along with semi-amorphous C-S-H(I) where a broad peak was identified in the angle of diffraction that varies from 27 ° to 31° (d=0.304; 0.278; 0.183 nm). It should be noted that 1.13 nm tobermorite remained stable and did not transform to a compound of the stoichiometric composition, i.e., xonotlite.

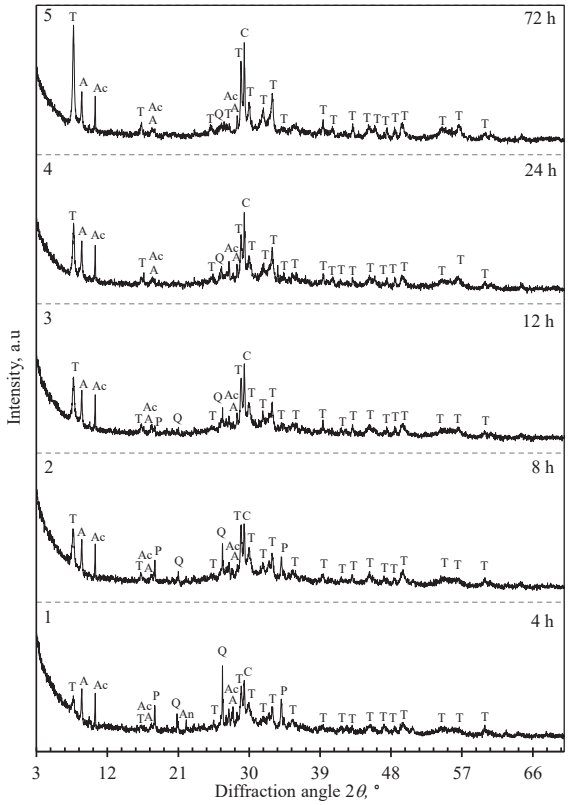

Fig. 3.6. XRD patterns of the synthesis products from CaO-granite mixture with CaO/SiO_2 = 1.0 at 180 °C. Indexes: A – annite, Ac – actinolite, An – anorthite, Al – albite, C – calcite, T – 1.13 nm tobermorite, P – portlandite, Q – quartz

The crystallite size of 1.13 nm tobermorite increased with the increasing duration of hydrothermal synthesis, especially when hydrothermal synthesis was performed at 8 h and 72 h (Figure 3.7). However, the intensity of the 1.13 nm tobermorite peaks increases as well (Figure 3.8). Furthermore, the results showed that, at a molar ratio of 1.0, after 4 h of isothermal curing, the crystallite size decreased by ~37%, and, after 72 h of synthesis, it went down by ~23% compared to mixtures with CaO/SiO_2 = 0.83. Hence, the increased amount of calcium oxide accelerates the formation of C-S-H(I) and C-S-H(II). Due to this reason, the size of tobermorite crystallite is significantly smaller compared to mixtures with the molar ratio CaO/SiO_2 = 0.83. Moreover, the intensity of 1.13 nm tobermorite peaks after 72 h of synthesis is lover by ~31% than for the cases when the molar ratio was CaO/SiO_2 = 0.83. This data indirectly shows that a lower amount of 1.13 nm tobermorite was formed.

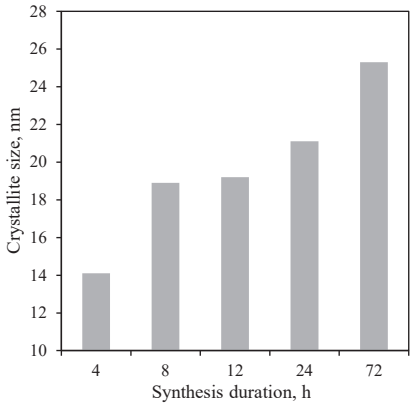

Fig. 3.7. Dependence of the size of 1.13 nm tobermorite crystallites on the duration of synthesis

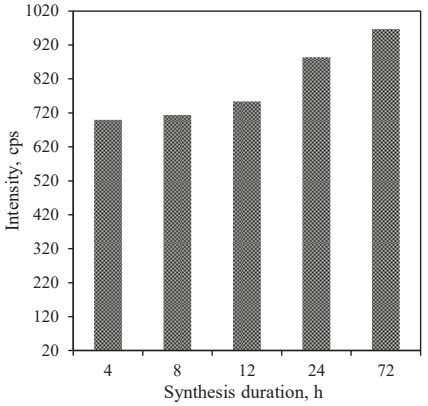

Fig. 3.8. Intensity of the main peak (d = 1.13 nm) of tobermorite from CaO-granite mixture

The results of simultaneous thermal analysis of the synthesis products obtained from mixtures with CaO/SiO_2 = 1.0 at 180 °C temperature are presented in Fig. 3.9. As in the case of mixture with CaO/SiO_2 = 0.83, after 4 h of hydrothermal synthesis, the endothermal effect at temperatures between 40–240 °C shows the dehydration of 1.13 nm tobermorite together with semi-amorphous C-S-H (I). TG analysis showed that the mass loss during this process is 6.32% (4 h, Fig. 3.9, curve 1) and 6.07% when hydrothermal synthesis was performed for 72 h (Fig. 3.9, curve 2). The second endothermal effect at 757 °C is associated with $CaCO_3$ decomposition of the 4-h synthesis product (Fig. 3.9, curve 3), whereas, at 730 °C, that of 72 h of the synthesis product is visible (Fig. 3.9, curve 4). The results of TG analysis showed that the mass loss is 5.11% (Fig. 3.4, curve A1) and 2.12% (72 h; Fig. 3.9, curve 2), accordingly. Thus, when increasing the molar ratio of the mixture from 0.83 to 1.0, the weight loss in the 72 h synthesis product almost doubles. This indirectly confirms our previous observations that as long as the CaO content of the mixture increases, more semi-amorphous calcium silicate hydrate is present in the synthesis

products (the latter carbonizes faster than 1.13 nm tobermorite). Furthermore, in the DSC curve, we identified only one exothermal effect which is related to calcium silicate hydrates recrystallizing into wollastonite. Literature indicates that the thermal effect of C-S-H(II) recrystallization occurs at a higher temperature than for C-S-H(I) [29]. On this basis, we can state that, after 4 h of hydrothermal synthesis, together with 1.13 nm tobermorite, C-S-H(II) forms as well (Fig. 3.9, curve 3), and, after 72 h of treatment, C-S-H(I) is formed (Fig. 3.9, curve 4).

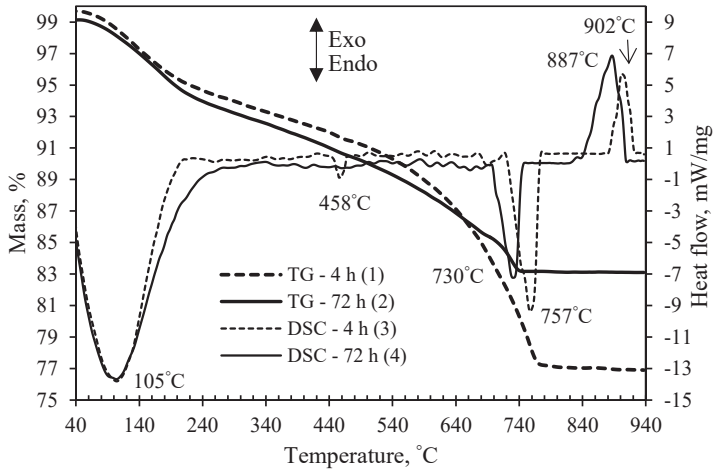

Fig. 3.9. TG (*1*, *2*) and DSC (*3*, *4*) curves of the synthesis products from CaO-granite mixture with CaO/SiO_2 = 1.0 at 180 °C after 4 h (*1*, *3*) and 72 h (*2*, *4*)

The obtained dilatometry analysis data from powders after 4–72 h of synthesis (Fig. 3.10) confirms and supplements the previously collected data from XRD and STA analysis. Literature indicates that semi-amorphous C-S-H type calcium silicate hydrates do not feature a clear crystalline structure and shrink when they recrystallize into wollastonite [156–158]. It can be assumed that the more crystalline structures (in this case, 1.13 nm tobermorite) are obtained in the synthesis products during hydrothermal synthesis, the smaller length changes will occur. It was determined that, when prolonging the synthesis duration from 4 h up to 72 h, the shrinkage of the sample decreases by nearly 7% (Fig. 3.10, curve A) when the molar ratio CaO/SiO_2 = 0.83 is used. However, the shrinkage in the samples obtained using the molar ratio CaO/SiO_2 = 1.0 regardless of the curing duration remained at 32%. This is also confirmed by the fact that a larger amount of 1.13 nm tobermorite was obtained after 72 h of hydrothermal synthesis when using mixtures with CaO/SiO_2 = 0.83.

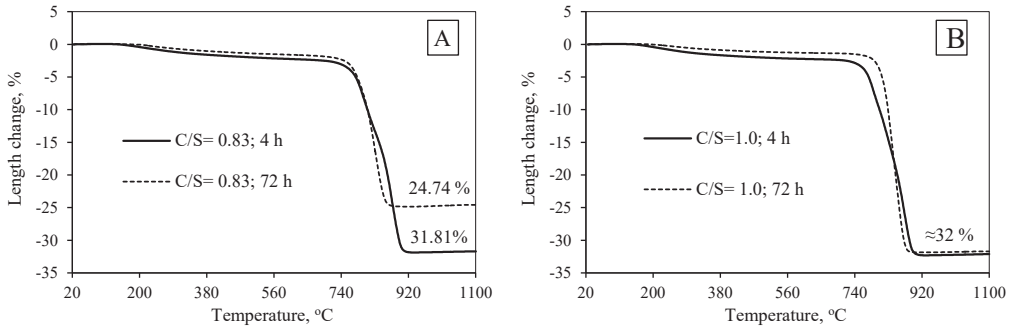

Fig. 3.10. Dilatometric curves of the synthesis products at 180 °C when CaO/SiO_2 = 0.83 (A) and 1.0 (B)

In order to establish the difference in the mineral composition of the synthesized products at different durations, the samples after combustion at 940 °C for 0.5 h were examined by XRD analysis (Fig. 3.11). It was determined that, regardless of their molar ratio (CaO/SiO_2 = 0.83 or 1.0) and the duration of isothermal curing (4 or 72 h), the qualitative composition of the products is the same: wollastonite (PDF No. 00-066-0271), gehlenite (PDF No. 04-014-4683), larnite (PDF No. 00-049-1673), annite and actinolite are formed. Nonetheless, the peak intensity of these compounds is highly dependent on the duration of hydrothermal synthesis. The peaks of wollastonite, after calcination of the synthesis product with CaO/SiO_2 = 0.83 for 72 h, are significantly intensive, meanwhile, the peaks of gehlenite are substantially lower (Fig. 3.11, curve 2) in comparison with the 4 h synthesis product (Fig. 3.11, curve 1). In our opinion, with the prolongation of the hydrothermal treatment, Al-bearing compounds (e.g., anorthite, albite, labrodorite) decompose, and Al^{3+} ions interrupt in the crystal lattice of calcium silicate hydrates. The more of these compounds are present in the synthesis product, the more wollastonite gets formed during combustion. A sample from a mixture CaO/SiO_2 = 1.0 in comparison with 0.83 after 72 h hydrothermal curing reveals a significantly lower intensity of wollastonite peaks (Fig. 3.11, curve 4). This is due to the lower amount of 1.13 nm tobermorite and because C-S-H(I) is formed (Figs. 3.1 and 3.6, curves 5). This is also confirmed by the curves of dilatometric analysis: the product with CaO/SiO_2 = 1.0 exhibits less shrinkage, which indicates that it contains less C-S-H (I) and C-S-H (II) (Fig. 3.10, B). By increasing the synthesis duration, the amount of gehlenite is virtually unchanged in mixtures with CaO/SiO_2 = 1.0. The highest intensity of larnite peaks was identified after the combustion of a sample obtained from a mixture with CaO/SiO_2 = 1.0 within 4 h. This is due to the higher molar ratio of the initial mixture and the higher amount of the formed C-S-H(II). Annite and actinolite from the granite sawing powder waste remained after calcination, but only traces of these minerals were identified.

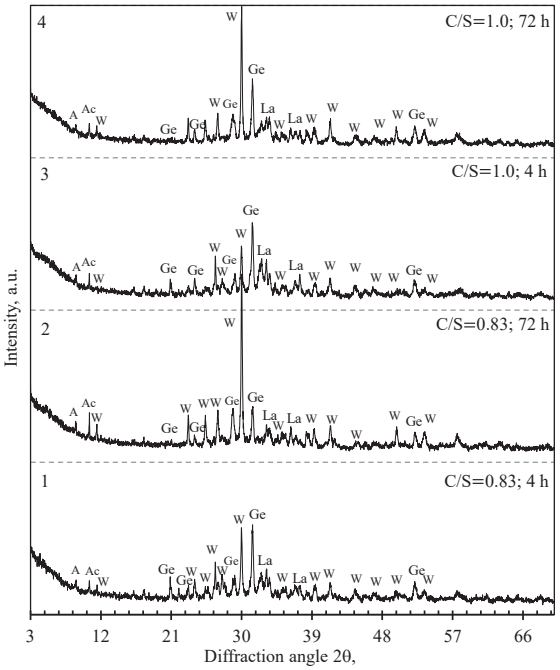

Fig. 3.11. XRD patterns of synthesis products from CaO-granite at 180 °C which were calcined at 940 °C. Indexes: A – annite, Ac – actinolite, An – anorthite, Ge – gehlenite, Lr – larnite, W – wollastonite

Summarizing the collected data, it can be stated that the composition of CaO and the granite sawing powder waste mixture for the production of 1.13 nm tobermorite should be $CaO/SiO_2 = 0.83$. In general, many hydrothermal reactions accelerate with increasing the temperature of saturated water vapor. Since the synthesis of 1.13 nm tobermorite at a temperature of 180 °C was slow enough, it was decided to investigate its synthesis at 200 °C.

It was determined that 1.13 nm tobermorite forms within the first 4 h of hydrothermal curing from a mixture with $CaO/SiO_2 = 0.83$ (Fig. 3.12, curve 1). However, the peaks of portlandite were identified as well; they remained in the synthesis products up to 8 h. Moreover, in the XRD curve, we identified peaks of quartz which decreased significantly when the duration of synthesis was prolonged, yet, after 12 h of hydrothermal synthesis, only its traces remain.

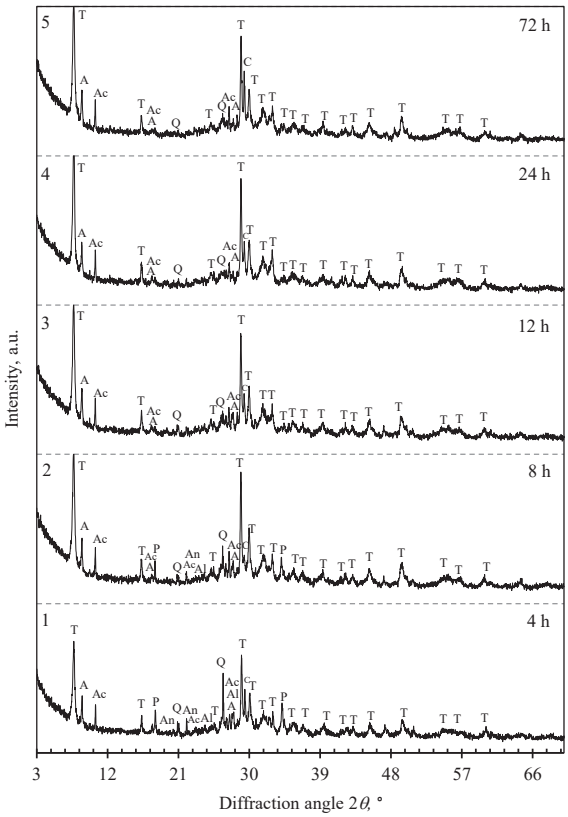

Fig. 3.12. XRD patterns of the synthesis products from CaO-granite mixture with CaO/SiO_2 = 0.83 at 200 °C. Indexes: A – annite, Ac – actinolite, An – anorthite, Al – albite, C – calcite, T – 1.13 tobermorite, P – portlandite, Q – quartz

The intensity of the main peak of 1.13 nm tobermorite increased by 4 times after 4 h of hydrothermal synthesis at 200 °C (Fig. 3.14) than for the case when synthesis was performed at 180 °C (Fig. 3.3). Therefore, the calculations of the crystallite size showed a 33.72% (Fig. 3.13) increase compared to the previous results (Fig. 3.2). Moreover, the intensity increased significantly after 8 h of isothermal curing. Hence, 1.13 nm tobermorite after 8 h of hydrothermal treatment becomes the dominant compound among the formed calcium silicate hydrates. Furthermore, the intensity of the main peak of 1.13 nm tobermorite gradually but constantly continues to increase with prolonging the duration of hydrothermal synthesis. Meanwhile, the size of crystallites increases slightly after extending the duration of the synthesis. It can be summarized that a large amount of tobermorite is formed within 8 h of synthesis, i.e., 9 times faster than when hydrothermal synthesis is carried out at 180 °C.

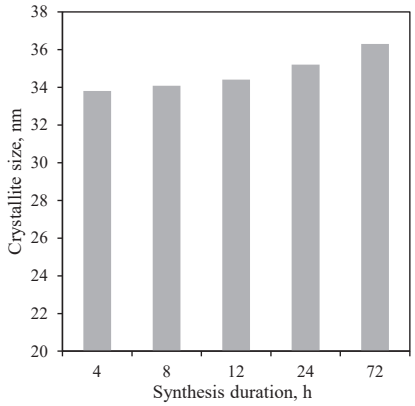

Fig. 3.13. Dependence of the size of tobermorite crystallites on the duration of synthesis

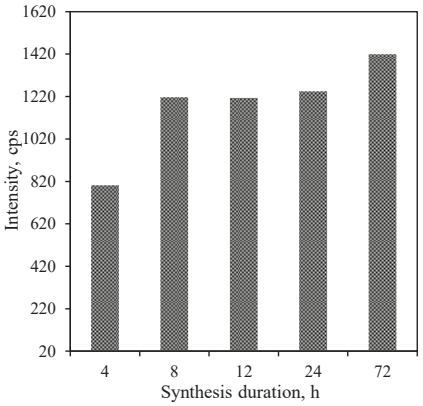

Fig. 3.14. Intensity of the main peak (d = 1.13 nm) of tobermorite from CaO-granite mixture

Other granite minerals are virtually not involved in the formation of new compounds: the area of the main peak of annite (d = 1.01 nm) and actinolite (d = 0.845 nm) remains similar when prolonging the duration of hydrothermal synthesis up to 72 h.

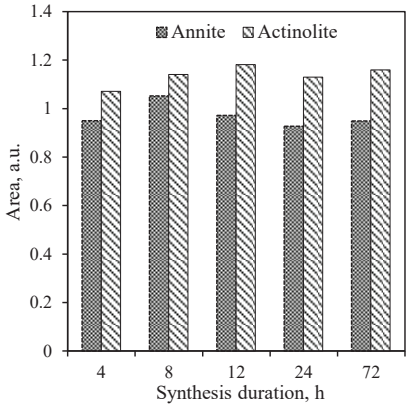

Fig. 3.15. Dependence of the main peak area of annite and actinolite on the duration of synthesis

The products were examined by simultaneous thermal synthesis as well (Fig. 3.16). Exothermic effects were identified at 869 °C (Fig. 3.9, curve 3) and 873 °C (Fig. 3.9, curve 4). When comparing the results after 4 h and 72 h of hydrothermal synthesis, we found that the duration does not have any impact on the heat flow – it is 5.89 mW/mg (4 h) and 5.82 mW/mg (72 h), respectively. In summary, the same amount of C-S-H (I) was formed regardless of the different durations of synthesis. Moreover, our results show that none of C-S-H(II) was obtained. It should be noted that tobermorite does not exhibit any exothermic effect at 800–900 °C. The mass loss during the decomposition of calcite in the 4 h synthesis product is 4.75% (Fig.

3.16, curve 1), yet it is much lower (2.02%) in the 72-h product (Fig. 3.16, curve 2). In addition, in the DSC curve, we identified an endothermal effect at 458 °C which is related to the decomposition of portlandite (Fig. 3.16, curve 3).

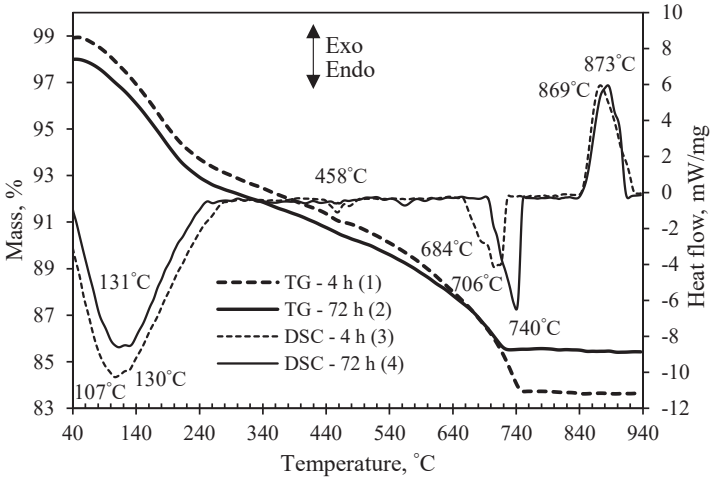

Fig. 3.16. TG (*1*, *2*) and DSC (*3*, *4*) curves of the synthesis products from CaO-granite mixture with CaO/SiO_2 = 0.83 at 200 °C after 4 h (*1*, *3*) and 72 h (*2*, *4*)

It was determined that 1.13 nm tobermorite, formed in a mixture with a molar ratio of CaO/SiO_2 = 0.83, is stable at 200 °C, and it does not recrystallize to other calcium silicate hydrates even after 72 h of synthesis. In order to determine the impact of the CaO content on the stability of this compound, the mixture with a molar ratio of CaO/SiO_2 = 1.0 was examined at 200 °C as well. As early as after 4 h of isothermal curing, 1.13 nm tobermorite becomes the dominant mineral among the newly formed compounds (Fig. 3.17, curve 1). Even after 72 h of hydrothermal curing, 1.13 nm tobermorite does not begin to recrystallize into thermodynamically stable xonotlite (Fig. 3.17, curve 2) whose composition corresponds to the molar ratio of the initial mixture.

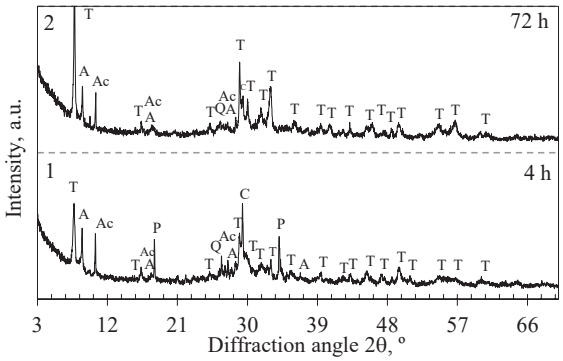

Fig. 3.17. XRD patterns of the synthesis products from CaO-granite mixture with CaO/SiO_2 = 1.0 at 200 °C. Indexes: A – annite, Ac – actinolite, C – calcite, T – 1.13 tobermorite, P – portlandite, Q – quartz

Summarizing the obtained results, it can be stated that the granite sawing waste is a suitable raw material for the synthesis of 1.13 nm tobermorite. However, from the mixture with the optimal molar ratio CaO/SiO_2 = 0.83 at 180 °C, after a short duration of the synthesis (from 4 h to 8 h), the intensity of 1.13 nm tobermorite is low. By increasing the synthesis temperature to 200 °C, the crystallization processes are significantly accelerated. This shows an increased intensity of the main peak of 1.13 nm tobermorite, and other peaks of this compound were most intense. It should also be noted that the size of 1.13 nm tobermorite crystallites as early as after 4 h of synthesis reaches 33.4 nm (at 180 °C – 224 nm), and the size of the crystallites of this compound is bigger than after 72 h of synthesis at 180 °C (32.8 nm). It should also be noted that the impurities in the granite sawing waste determine that 1.13 nm tobermorite does not recrystallize into xonotlite even in the mixtures with a molar ratio of CaO/SiO_2 = 1.0.

3.2. 1.13 nm tobermorite formation in lime–calcined opoka mixtures under hydrothermal conditions

As part of the granite sawing waste minerals do not react under hydrothermal conditions, it is not possible to obtain a product consisting of only 1.13 nm tobermorite. For this reason, it was decided to investigate the suitability of calcined opoka for obtaining tobermorite via hydrothermal synthesis. This raw material was used as a source of SiO_2. After adding the required amount of lime, a mixture with a molar ratio of Ca/SiO_2 = 0.83 was prepared. Hydrothermal synthesis was carried out in unstirred suspensions at 180 °C.

It was determined that, after 2 h of synthesis, only traces of 1.13 nm tobermorite were identified in the XRD curve (Fig. 3.18, curve 1). By prolonging the duration of hydrothermal treatment, the processes of formation of new compounds take place much more intensively, and 1.13 nm tobermorite is identified as the main mineral in the product as early as after 4 h of synthesis (Fig. 3.18, curve 2). However, together with this compound, we identified an intensive peak of quartz as well. All the other minerals which are present in calcined opoka, such as cristobalite, tridymite and muscovite, react under these conditions. By extending the synthesis duration to 8 h, no new compounds were formed, only the intensity of the 1.13 nm tobermorite peaks increased, whereas that of quartz decreased. Moreover, event after 72 h of isothermal curing, some quantity of quartz still remains. Literature indicates that if three main diffraction peaks of 1.13 nm tobermorite (*d*-spacing – 0.308; 2.975; 2.812 nm) are sharp and separated from other compounds, the crystallinity degree is high (159).

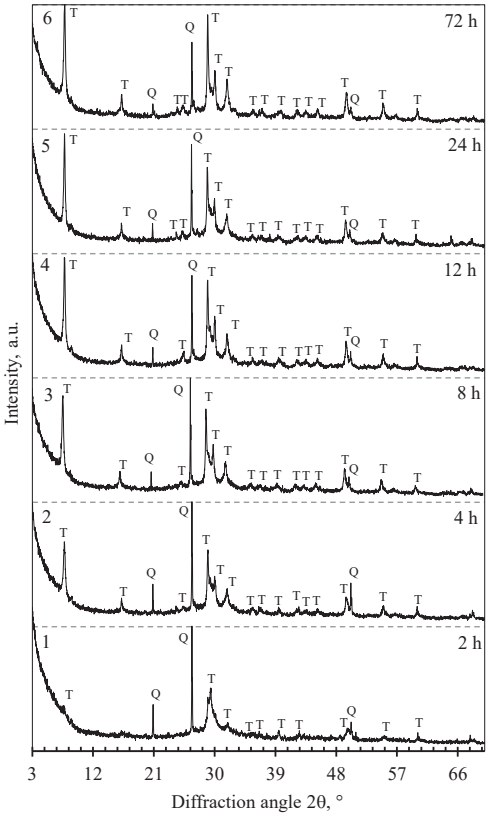

Fig. 3.18. XRD patterns of the synthesis products from lime-opoka mixture with CaO/SiO_2 = 0.83 at 180 °C after. Indexes: T – 1.13 nm tobermorite, Q – quartz

It should also be noted that the size of the formed 1.13 nm tobermorite crystallites also differs when using other raw materials. This is convincingly shown by the crystallite size calculations. This value after 4 h of synthesis increased by 24.32% (Fig. 3.19) compared to the analogous product from the granite sawing waste (Fig. 3.2). The biggest impact on the formation of 1.13 nm tobermorite was noticed when hydrothermal synthesis was prolonged from 8 h to 12 h – the peak intensity increased by 40.17%, and the size of the crystallite increased by 13.98%. Furthermore, the intensity of the 1.13 nm tobermorite peak gradually but constantly increased and reached 1099 cps (Fig. 3.20, curve 2) after 24 h of isothermal curing and increased slightly (1180 cps) after 72 h. When comparing these results with the synthesis products obtained when using the granite sawing waste (Fig. 3.8), it was found that the peak intensity of 1.13 nm tobermorite is 25.23% higher (Fig. 3.20, curve 2).

In summary, according to XRD data, 1.13 nm tobermorite begins to dominate in the synthesis products twice as fast with lime-calcined opoka mixture (4 h and 8 h), and, after 72 h of hydrothermal treatment, the intensity of its main peak is almost a quarter larger than in the case with the granite sawing waste.

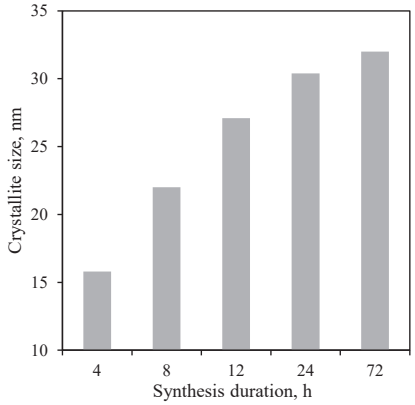

Fig. 3.19. Dependence of the crystallite size on the duration of synthesis from lime-opoka mixture

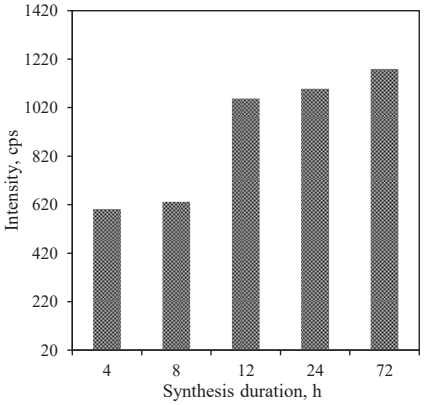

Fig. 3.20. Intensity of the main peak (d = 1.13 nm) of 1.13 nm tobermorite from lime-opoka mixture

Simultaneous thermal analysis shows that the dehydration effects of C-S-H(I) at 100–200 °C and 1.13 nm tobermorite at 200–240 °C temperature in the DSC curve is very broad and vaguely expressed (Fig. 3.21, curve 3). Literature data shows similar results obtained by other authors for the cases when the synthesis products contain aluminum (153). The results of TG analysis data show that the main mass loss occurs within the temperature range of 40–250 °C, and, regardless of the synthesis duration, the results are very close – 6.64% (4 h; Fig. 3.21, curve 1) and 6.83% (72 h; Fig. 3.21, curve 2). The values of the heat flow of exothermic effects at temperatures of 841 °C and 844 °C (recrystallization of C-S-H(I) to wollastonite) are similar – 13.48 mW/mg and 11.39 mW/mg. By summarizing these results and XRD data, we can state that C-S-H(I) formed at the beginning of the synthesis is sufficiently stable, and its amount does not change significantly throughout the studied period. The main changes that are taking place are the increase in the size of 1.13 nm tobermorite crystallites.

The narrow thermal effect in the DSC curve at a temperature of 389 °C (Fig. 3.21, curve 3) indicates the presence of a small amount of hydrogarnets in the product after 4 h of the synthesis. In addition, a negligible thermal effect at a temperature of 672 °C shows the decomposition of calcite (Fig. 3.21, curve 3). At this effect, the TG analysis curve is almost flat, which means that the mass loss is less than 0.5%. Furthermore, the total mass loss after 4 h of hydrothermal synthesis is 12.17%, whereas the mass loss after 72 h of synthesis is 10.67%.

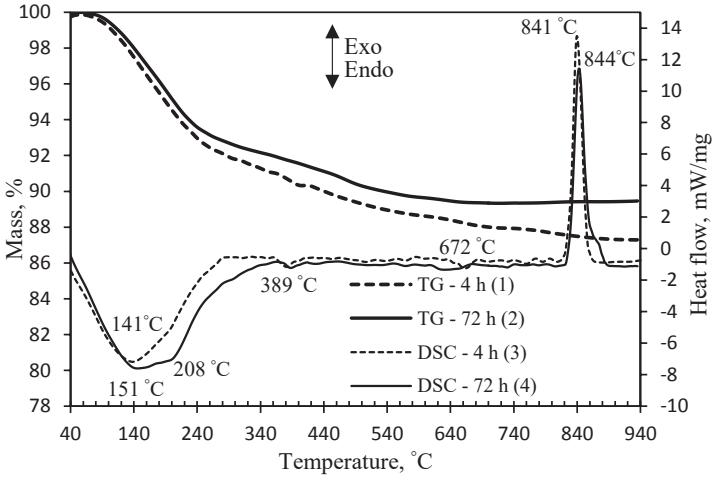

Fig. 3.21. TG (*1*, *2*) and DSC (*3*, *4*) curves of the synthesis products from lime-opoka mixture with CaO/SiO_2 = 0.83 at 180 °C after 4 h (*1*, *3*) and 72 h (*2*, *4*)

XRD and STA data was confirmed by SEM investigation as well. From the opoka-lime suspension during 4-h synthesis at a temperature of 180 °C, 1.13 nm tobermorite forms small plates or shavings (sheets) bound together into fine fibrous agglomerates by semi-amorphous C-S-H(I) (Fig. 3.22, A) that have not managed to recrystallize yet. By prolonging the isothermal treatment up to 72 h, significantly smaller accumulations of amorphous particles were detected. The morphology of 1.13 nm tobermorite also changes: needle-shaped crystals predominate in the length of 4–5 nm, although there is also a small number of slightly smaller plates (Fig. 3.22, B).

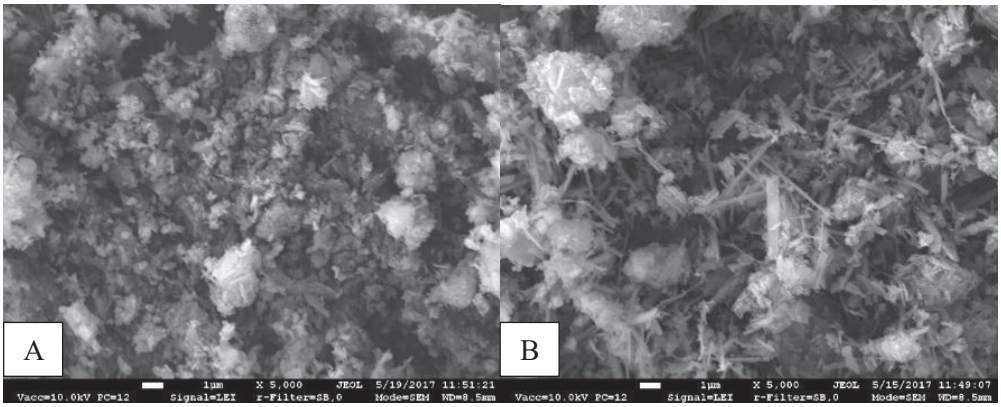

Fig 3.22. SEM micrographs of synthesis products from opoka-lime mixture with CaO/SiO_2 = 0.83; 4 h (A), 72 h (B)

A significant part of the energy consumption during the production of calcium silicate hydrates mainly occurs due to the temperature and duration of hydrothermal synthesis. The obtained results showed that calcined opoka is a promising raw

material for the synthesis of 1.13 nm tobermorite. When summarizing the data of the literature (see 160), we note that many authors draw attention to the formation of 1.13 nm tobermorite via hydrothermal synthesis from pure and industrial materials. However, our results cannot be directly compared with the literature data because opoka contains impurities containing Al^{3+}, K^{+}, Na^{+} ions, modifications of SiO_2 and their percentage also differ, etc. So, new results must be obtained under the same conditions and while using the same equipment. For this reason, the formation peculiarities of 1.13 nm tobermorite in opoka-lime and in model (reagents) CaO-$SiO_2 \cdot nH_2O$ mixtures (pure and with Al_2O_3 additive) were compared.

The synthesis products obtained during hydrothermal synthesis when using mixtures prepared from reagent CaO and amorphous $SiO_2 \cdot nH_2O$ when the molar ratio was $CaO/SiO_2 = 0.83$ were examined by X-ray diffraction analysis. It was determined that, after 4 h of isothermal curing, traces of 1.13 nm tobermorite were formed (Fig. 3.23, curve 1). However, the target compound co-exists with other calcium silicate hydrates. In the XRD analysis curve, we identified Z-phase (d = 1.152; 0.840; 0.417; 0.371 nm). This compound is not typical during hydrothermal synthesis when the molar ratio is bigger than $CaO/SiO_2 = 0.66$. Furthermore, for short duration times of the synthesis, we identified α–C_2SH (d-spacing 0.533 nm, 0.422 nm, 0.392 nm) which, as literature indicates, can be synthesized when the molar ratio is $CaO/SiO_2 = 2.0$ [58]. This sequence of the formation of new compounds leads to the assumption that in the reaction medium, at the beginning of the synthesis zones, different CaO/SiO_2 ratios are formed – around $Ca(OH)_2$ grains, mostly Ca^{2+} accumulate, whereas, around SiO_2 grains, we observe Si^{4+} ions. For this reason, non-stoichiometric compounds for the initial mixture – Z-phase (CaO/SiO_2 = 0.55) and α-C_2SH ($CaO/SiO_2 = 2.0$) – crystallize. It is in good agreement with the literature data as other researchers present similar results [110, 161]. It should also be noted that in the synthesis product we identified semi-amorphous C-S-H(I) type calcium silicate hydrate (d = 0.306; 0.281, 0.184 nm). The XRD curve of the synthesis product obtained after 8 h of synthesis showed minor changes, and, with the synthesis duration increased by two times, this did not manifest any effect on the formation of the target compounds (Fig. 3.23, curve 2). Furthermore, only after 24 h of isothermal curing, 1.13 nm tobermorite main peaks in the XRD pattern are seen in a well-expressed form (Fig. 3.23, curve 4).

Therefore, 1.13 nm tobermorite of a high crystallinity degree was obtained after 72 h of hydrothermal synthesis at 180 °C (Fig. 3.23, curve 5). Moreover, along with this, we identified another calcium silicate hydrate – gyrolite (d = 2.281; 1.126; 0.837 nm). Literature indicates that gyrolite can be obtained when hydrothermal synthesis is performed by using a mixture whose molar ratio is $CaO/SiO_2 = 0.66$ [161, 162]. It can be stated that the Z-phase formed in the initial stages of the synthesis becomes unstable and transfers to a compound of a lower basicity.

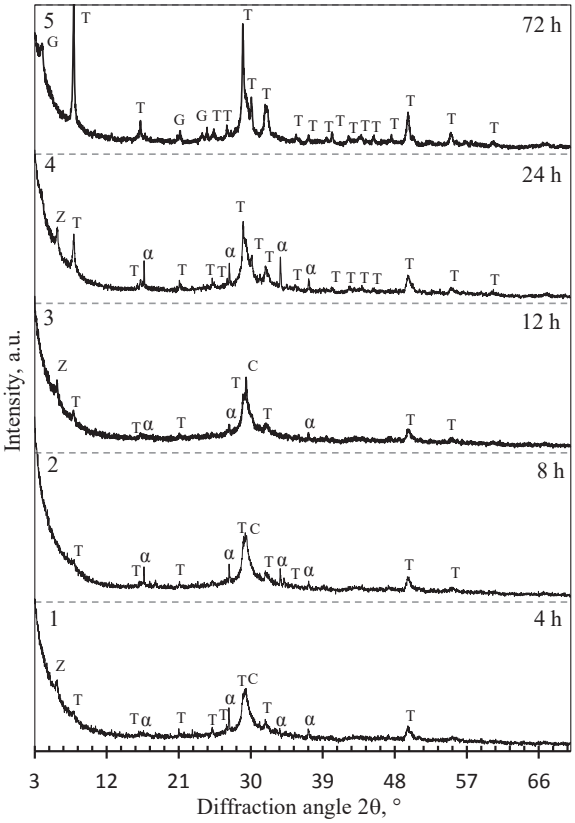

Fig. 3.23. XRD patterns of the synthesis products from CaO-SiO_2·nH_2O mixture with CaO/SiO_2 = 0.83 at 180 °C. Indexes: T – 1.13 nm tobermorite, Q – quartz, α – C_2SH, C – calcite, Z – Z-phase, G – gyrolite

The results of differential scanning calorimetry after 4 h and 72 h of hydrothermal synthesis are presented in Fig. 3.24. It was determined that, in the synthesis product obtained after 4 h of synthesis, we identified three endothermic effects (Fig. 3.24, curve 1). The first effect at 77 °C occurs due to the removal of the absorbed moisture from the sample. The second endothermal effect at 137 °C is related to Z-phase and C-S-H(I) dehydration. This result complements the assumptions made above that, after 4 h of hydrothermal synthesis, we mainly obtained semi-amorphous calcium silicate hydrates with some quantity of α-C_2SH and Z-phase (Fig 3.23, curve 1). The final endothermic effect at 446–462 °C is associated with the decomposition of α–C_2SH. Furthermore, in the DSC curve of 72 h synthesis, two endothermic effects are present (Fig. 3.24, curve 2). The first effect is related to the dehydration of C-S-H(I), however, the intensity of this effect is negligible. That shows the small quantity of this compound. It should be underlined that the endothermal effect at 191 °C shows dehydration of 1.13 nm tobermorite (Fig. 3.24, curve 2). It is in good agreement with the XRD results where 1.13 nm tobermorite of a high degree of crystallinity was identified (Fig 3.23, curve 5).

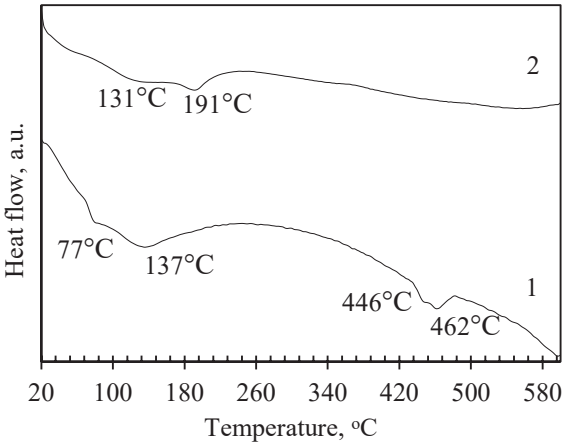

Fig. 3.24. DSC curves of the synthesis products from CaO-$SiO_2 \cdot nH_2O$ mixtures after 4 h (1) and 72 h (2) at 180 °C

The previous results obtained when using CaO-$SiO_2 \cdot nH_2O$ mixtures corresponded to the data of SEM analysis. It was determined that the irregularly shaped crystals of globules are attributed to semi-amorphous C-S-H(I) and Z-phase. Only a few separate rectangular plate-shaped crystals of formed α-C_2SH were observed in the SEM image of the product after 4-h synthesis (Fig. 3.25, A). The accumulation of crystals of two morphologies can be noticed in the SEM micrographs of the product after 72 h of synthesis (Fig. 3.25, B): plate-shaped crystals characteristic of 1.13 nm tobermorite, and gyrolite particles which consist of very small plate crystallites.

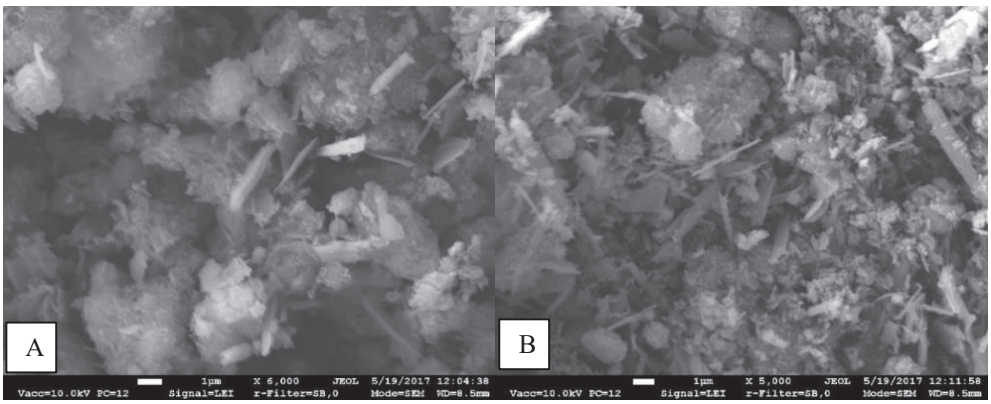

Fig. 3.25. SEM micrographs of synthesis products from CaO-$SiO_2 \cdot nH_2O$ mixtures with $CaO/SiO_2 = 0.83$ after 4 h (A) and 72 h (B) at 180 °C

The obtained results showed that the formation of 1.13 nm tobermorite via the hydrothermal synthesis from CaO and amorphous $SiO_2 \cdot nH_2O$ mixture is a very slow and long-lasting process. It is in good agreement with the literature data where researchers indicate that adding aluminum into the reagent system accelerates the

formation of tobermorite significantly [110]. Furthermore, obtaining pure 1.13 nm tobermorite is very difficult because it co-exists with other calcium silicate hydrates. Comparing these results with hydrothermal synthesis when using mixtures produced from opoka, the latter raw material is far more suitable for the synthesis of 1.13 nm tobermorite.

Chemical composition analysis showed that opoka contains 2.53% of aluminum. As literature indicates [110], Al^{3+} ions lead to significant acceleration of the reactions between CaO and amorphous SiO_2. Due to this reason, a mixture with the molar ratio of $CaO/(SiO_2 + Al_2O_3) = 0.83$ and $Al_2O_3/(SiO_2 + Al_2O_3) = 0.025$ was produced. The obtained new mixture is very close to the composition of the opoka-lime mixture, and it was examined under the same conditions. It was determined that aluminum significantly accelerates hydrothermal reactions, and 1.13 nm tobermorite was identified as the main compound in the XRD curve of the 4-h synthesis product (Fig. 3.26, curve 1). When comparing these results with the data obtained when using mixtures without Al^{3+} ions, it was found that neither α-C_2SH nor Z-phase was formed. Furthermore, prolonging hydrothermal synthesis up to 8 h leads to the significant increment in the intensity of 1.13 nm tobermorite peaks (Fig. 3.26, curve 2). Further investigation showed that the main peaks of the target compound constantly increased with prolonging the duration of isothermal curing. It should be noted that 1.13 nm tobermorite was not stable, and, after 72 h of hydrothermal synthesis, it started to recrystallize to xonotlite and gyrolite (Fig. 3.26, curve 5). As a result, the intensity of 1.13 nm tobermorite peaks decreased. Therefore, there is no favorable molar ratio for the formation of these compounds during hydrothermal synthesis. Due to the low rate of the formation of tobermorite, semi-amorphous C-S-H (with a variable molar ratio) formed instead. In this case, Al^{3+} ions accelerated the synthesis of calcium silicate hydrates, and a high degree of crystallinity of 1.13 nm tobermorite was reached. However, the amount of Al^{3+} ions in opoka did not stop the recrystallization of 1.13 nm tobermorite to xonotlite after 72 h of hydrothermal synthesis.

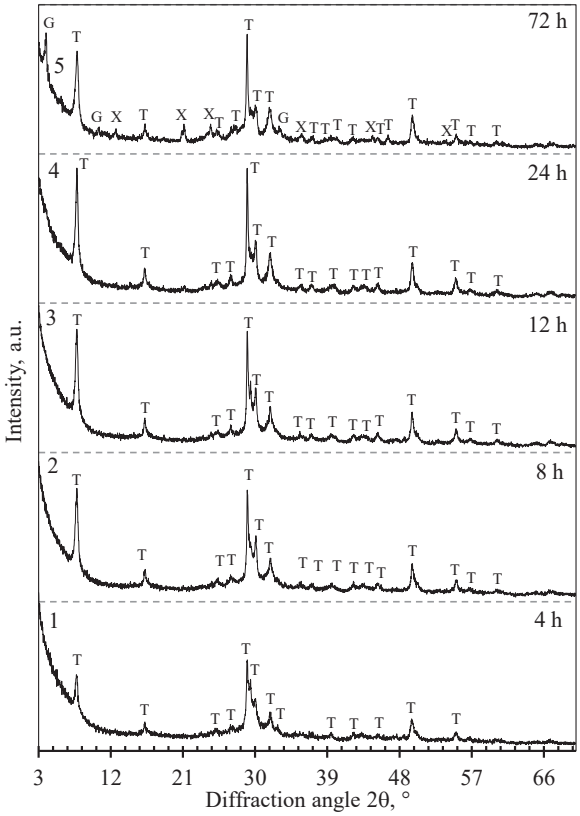

Fig. 3.26. XRD patterns of the synthesis products from $CaO\text{-}SiO_2\cdot nH_2O\text{-}Al_2O_3$ mixture with $CaO/(SiO_2+Al_2O_3) = 0.83$ and $Al_2O_3/(SiO_2+Al_2O_3) = 0.025$. Indexes: T – 1.13 nm tobermorite, G – gyrolite, X – xonotlite

In the XRD curve, the identified 1.13 nm tobermorite was additionally confirmed by differential scanning calorimetry where an endothermic effect was identified at 172 °C which is related to the dehydration of this compound (Fig. 3.27, curve 1). Moreover, the results of DSC show that 1.13 nm tobermorite obtained via 4 h hydrothermal synthesis co-exists with semi-amorphous C-S-H(I) (the endothermal effect at 112 °C). Furthermore, the examined products of synthesis obtained after 72 h of synthesis by DSC showed an endothermal effect at 133 °C and at 178 °C (Fig. 3.27, curve 1). This result is in good agreement with the XRD data, where 1.13 nm tobermorite and gyrolite were identified. It should be noted that endothermic effects of tobermorite become wide and blank when aluminum ions are present in the system. Moreover, there is data in the literature which suggests that, in the DSC curve, the endothermic effect related to the dehydration of 1.13 nm tobermorite is shifted to a lower temperature by 20–30 °C.

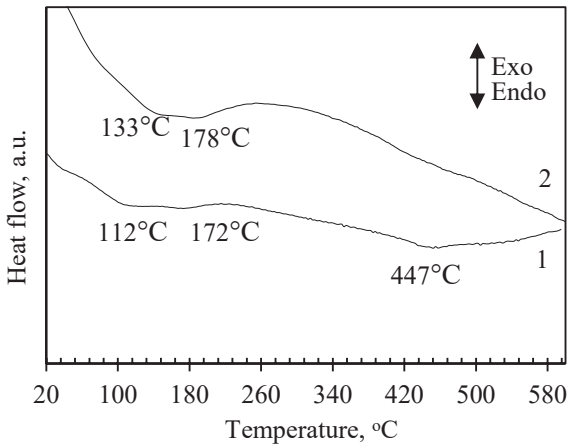

Fig. 3.27. DSC curves of the synthesis products from $CaO\text{-}SiO_2\text{-}Al_2O_3$ mixtures after 4 h (*1*) and 72 h (*2*) at 180 °C

SEM analysis indicates that Al_2O_3 additive in the $CaO\text{-}SiO_2 \cdot nH_2O$ mixture stimulates the formation of calcium silicate hydrates with a higher crystallinity. It was determined that only a few aggregates characteristic to semi-amorphous C-S-H(I) were observed in the SEM image of the product after 4 h of synthesis (Fig. 3.28, A). Plate-shaped crystals of 1.13 nm tobermorite are dominant in the product after 72 h of synthesis (Fig. 3.28, B).

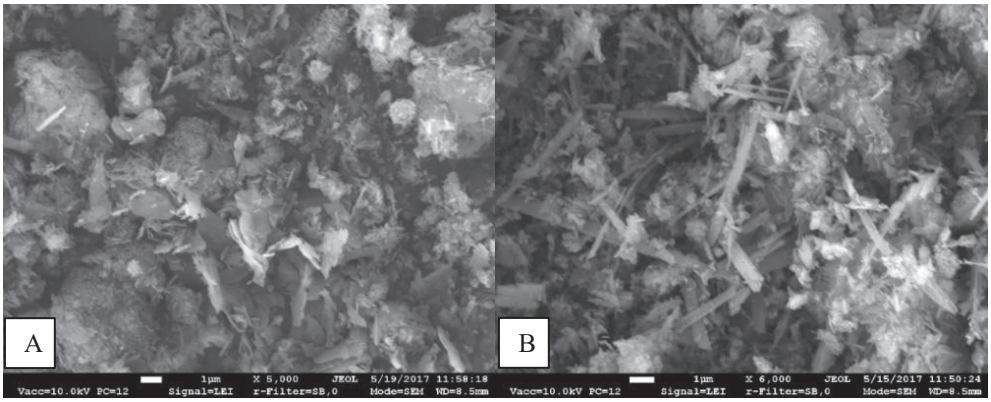

Fig. 3.28. SEM micrographs of the synthesis products from $CaO\text{-}SiO_2\text{-}Al_2O_3$ mixtures with $CaO/SiO_2 = 0.83$ after 4 h (A) and 72 h (B) at 180 °C

This data was confirmed by the method of FT-IR spectroscopy (Fig. 3.29). The most intense spectral vibration peak, the band at ~980 and ~972 cm^{-1}, is assigned to the Si–O–Si stretching vibration peak. The second most intense band at ~460 cm^{-1} is due to SiO_4 deformation, and the band at ~670 cm^{-1} is assigned to the O–Si–O bending vibration peak. A wide band near 3457 cm^{-1} means that molecular water forms hydrogen bridge links in the interlayers. The bands in the range of 1636 cm^{-1} frequency are assigned to $\delta(H_2O)$ vibrations and thus confirm this presumption.

According to literature data [127, 164], the above mentioned absorption bands are inherent for tobermorites. This data corresponds to XRD results. In addition, carbonation occurred when the products were dried in the air-conditioned chamber because the diffraction peaks characteristic to calcite (d-spacing = 0.304; 0.191 nm) were detected in the XRD patterns, and doublet bands of CO_3^{2-} at 1510–1470 cm^{-1} are seen in all the FT-IR curves as well.

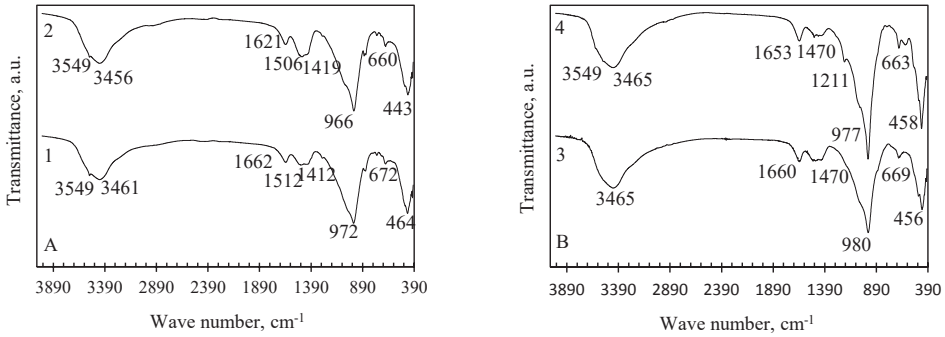

Fig. 3.29. FT-IR spectrum of synthesis products from CaO-SiO_2·nH_2O (A) and CaO-SiO_2-Al_2O_3 (A) mixtures after 4 h (*1, 3*) and 72 h (*2, 4*) at 180 °C

The usual X-ray diffraction analysis is not suitable for the quantitative determination of compounds, but the change in the peak intensity indicates the tendency for the amount and crystallinity of the test minerals to increase or decrease. In order to demonstrate the kinetics of the formation of tobermorite in various mixtures, Table 3.1 presents data on the intensity of the main 1.13 nm tobermorite diffraction peak (*d*-spacing – 1.133 nm) dependence on the hydrothermal synthesis duration at 180 °C.

It was determined that, after 4 h of hydrothermal treatment, only traces of 1.13nm tobermorite were formed in CaO-SiO_2·nH_2O mixtures where no additional aluminum was added. Therefore, only after 24 h of hydrothermal treatment, the intensity of the 1.13 nm tobermorite peak increased up to 334 cps. However, Al_2O_3 added into the CaO-SiO_2·nH_2O mixture accelerated the formation of the target compound, and, after 4 h of hydrothermal treatment, the intensity of the tobermorite peak surpasses the intensity of the peak obtained after 24 hours in CaO-SiO_2·nH_2O mixtures. These results are in good agreement with the literature data where the formation of the target compound was significantly accelerated by additives. In addition, other calcium silicate hydrates, such as gyrolite and xonotlite, start forming in the CaO-SiO_2·nH_2O-Al_2O_3 mixture after 72 hours of isothermal curing. Due to this reason, the peak intensity of 1.13 nm tobermorite decreased significantly. Comparing the results, the most intensive peak of the target compound was obtained as early as after 4 h when using lime-opoka mixtures. By prolonging the duration of hydrothermal synthesis, the intensity of the 1.13 nm tobermorite peak constantly increases, and it is higher by 12.29% after 72 h of synthesis. Summarizing this data, it can be stated that tobermorite is formed much faster in the lime-calcined opoka mixture, and its main peak intensity is higher than in the other mixtures.

Table 3.1. Intensity of the 1.13 nm peak (cps) in the hydrothermal synthesis products obtained at 180 °C, from various mixtures

Duration of hydrothermal synthesis, h	**4**	**8**	**12**	**24**	**72**
Lime-calcined opoka	604	633	1058	1099	1180
$CaO\text{-}SiO_2 \cdot nH_2O$	51	55	63	331	1035
$CaO\text{-}SiO_2 \cdot nH_2O\text{-}Al_2O_3$	344	619	803	1008	391

The crystallite size of 1.13 nm tobermorite when using various mixtures after hydrothermal treatment was calculated and presented in Table 3.2. It was determined that, after 4 h of isothermal curing, the biggest crystallites were obtained from the lime-opoka mixture. With further prolonging of the duration of hydrothermal synthesis, the size of the crystallites steadily increases. The obtained results showed that the size of the target compound crystallites formed in the $CaO\text{-}SiO_2 \cdot nH_2O\text{-}Al_2O_3$ mixture is slightly smaller compared to lime-opoka. Moreover, due to the formation of other compounds after 72 h of synthesis, the size of tobermorite crystallites decreased.

Table 3.2. Dependence of the crystallite size (nm) of tobermorite on the duration of hydrothermal synthesis at 180 °C, from various mixtures

Duration of hydrothermal synthesis/h	**4**	**8**	**12**	**24**	**72**
Lime-calcined opoka	296	320	375	422	428
$CaO\text{-}SiO_2 \cdot nH_2O$	-	-	-	304	372
$CaO\text{-}SiO_2 \cdot nH_2O\text{-}Al_2O_3$	258	288	292	306	224

As the previously obtained results show, when using the granite sawing waste as a raw material, the formation of 1.13 nm tobermorite, especially in the case of a short duration of the synthesis, was accelerated after raising the temperature of hydrothermal synthesis up to 200 °C. Calcined opoka is denoted by a higher amount of active SiO_2 modifications, and 1.13 nm tobermorite formation processes proceed rapidly enough as early as at 180 °C. However, literature suggests that elevated temperature also improves the formation of other calcium silicate hydrates, especially when mixtures contain amorphous $SiO_2 \cdot nH_2O$ [1].

The impact of temperature on the formation of calcium silicate hydrates via hydrothermal synthesis at 200 °C in unstirred suspensions when the molar ratio $CaO/SiO_2 = 0.83$ was investigated. It was determined that strong peaks of 1.13 nm tobermorite were identified as early as after 4 h of hydrothermal synthesis (Fig. 3.30, curve 1). Prolonging hydrothermal treatment up to 8 h does not have a huge impact on the formation of tobermorite or other compounds (Fig. 3.30, curve 2). Moreover, as in the previous cases, quartz is identified in these products. However, other modifications of SiO_2, such as cristobalite and tridymite, react under these conditions. Further, the intensity of the tobermorite peak gradually continues to increase with prolonging the duration of hydrothermal synthesis. Nevertheless, in all the cases, even despite the longest isothermal curing, strong peaks of quartz still remained in the synthesis products.

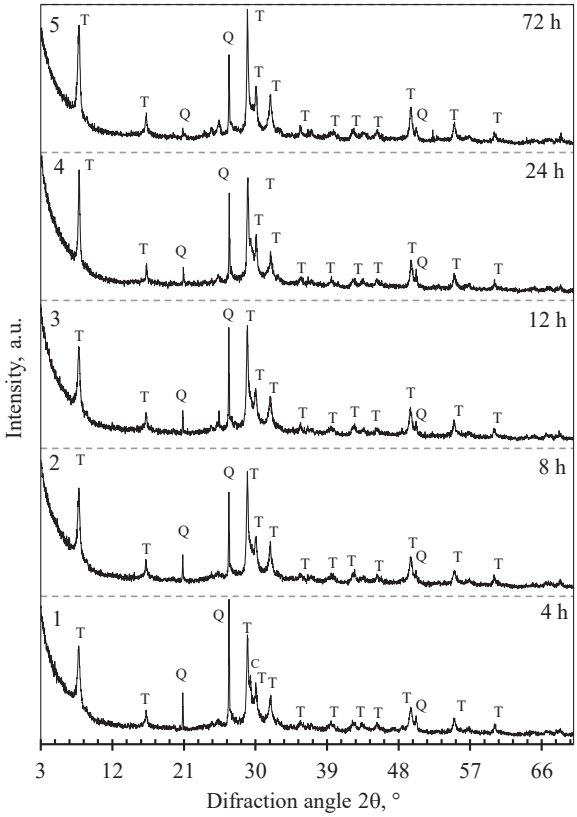

Fig. 3.30. XRD patterns of the synthesis products from lime-opoka at 200 °C when $CaO/SiO_2 = 0.83$. Indexes: T – 1.13 nm tobermorite, C – calcite, Q – quartz

The size of 1.13 nm tobermorite crystallites after 4 h of hydrothermal treatment at 200 °C increased only by 1.33% (Fig. 3.31) in comparison to the value of 180 °C (Fig. 3.19). This is one of the statements highlighting that the increased temperature, at least in the case of synthesis of a short duration, has no significant effect. Moreover, further crystallization of 1.13 nm tobermorite is accelerated, and the speed continues to grow until 24 h duration of hydrothermal synthesis. After prolonging the duration of the synthesis up to 72 h, the size of the crystallites of the compounds increased only slightly (Fig. 3.31). Moreover, the final size of a crystallite (after 72 h) increased by 4.28% comparing to the previously obtained results (Fig. 3.19). In addition, an increase in the intensity of the 1.13 nm tobermorite peak was not affected by the synthesis duration, and it increased significantly only after 24 h of hydrothermal synthesis. It can be assumed that the elevated temperature does not accelerate the formation of 1.13 nm tobermorite when using a mixture made from calcined opoka when the molar ratio is $CaO/SiO_2 = 0.83$.

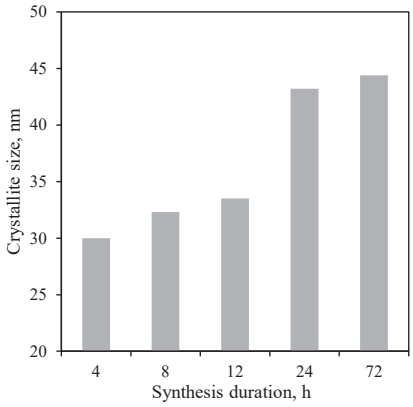

Fig. 3.31. Dependence of the crystallite size on the duration of synthesis from lime-opoka mixture

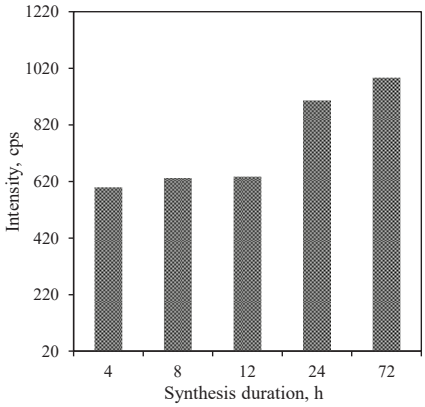

Fig. 3.32. Intensity of the main peak (d = 1.13 nm) of tobermorite from lime-opoka mixture

Simultaneous thermal analysis was performed for the synthesis products obtained via hydrothermal synthesis at 200 °C when the molar ratio equals CaO/SiO_2 = 0.83 (Fig. 3.33). It was determined that, in the DSC curve, we can identify three endothermic effects and one exothermic effect in both synthesis products obtained after 4 h and 72 h. The exothermic effect at 844 °C is related to C-S-H(I) recrystallization into wollastonite (Fig. 3.33, curve 3). Furthermore, the observed exothermic effect after 72 h of synthesis in the product is observed at the same temperature as for the product of synthesis after 4 h (Fig. 3.33, curve 4). When comparing these thermal effects, it was found that the heat flow from 12.05 mW (4 h) decreased to 11.61 mW (72 h). The small endothermic effect at 688 °C is related to the decomposition of calcite. Furthermore, in the synthesis product obtained after 72 h, the same thermal effect was shifted to a slightly lower temperature and identified at 655 °C. The TG analysis curve is almost flat, and it shows an insignificant amount of calcite (Fig. 3.33, curve 2). Due to this reason, the endothermic effect was shifted to a lower temperature. In addition, at 379–385 °C, we identified an endothermic effect which is related to the decomposition of hydrogarnets. It should be noted that this effect is insignificant, and the expected amount of this compound is small. Due to this reason, hydrogarnets were not identified in the XRD curve, and the peaks of this compound were obstructed by more intense peaks. TG analysis showed that the total mass loss is 12.05% (4 h) and 10.49% (72 h), respectively.

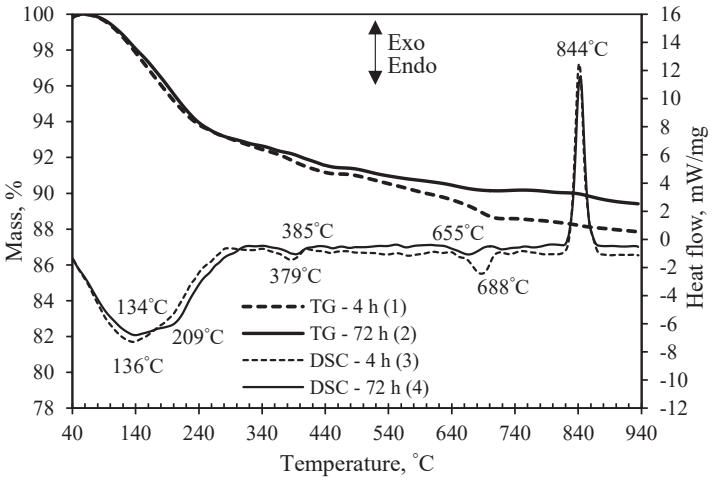

Fig. 3.33. TG (*1*, *2*) and DSC (*3*, *4*) curves of the synthesis products from lime-opoka mixture with CaO/SiO_2 = 0.83 at 200 °C after 4 h (*1*, *3*) and 72 h (*2*, *4*)

When summarizing the results, we determine that opoka calcinated at 775 °C is an excellent raw material for the synthesis of 1.13 nm tobermorite. This compound starts dominating in the product as early as after 4 h of hydrothermal synthesis at 180 °C. As the duration of isothermal treatment is prolonged, the size of crystallites of this calcium silicate hydrate increases and surpasses other competitors. In the lime-opoka mixture, 1.13 nm tobermorite is formed much faster than in the reagent $CaO\text{-}SiO_2\cdot nH_2O$ system. In addition, there is sufficient data in literature to suggest that the addition of Al compounds in a mixture of raw materials is a major way to promote the formation of 1.13 nm tobermorite. The obtained data shows that, in such a system, this compound is formed more slowly, and it exists for a shorter time than in the lime-opoka mixture. In our opinion, the high reactivity of opoka under hydrothermal conditions is due to its chemical composition, especially the presence of 2.53% Al_2O_3 and 0.83% K_2O. Compounds containing aluminum and potassium ions are evenly distributed throughout the raw material. Al^{3+} ions stimulate the reactions of amorphous SiO_2 and CaO, which results in faster formation of 1.13 nm tobermorite in the early stages of hydrothermal synthesis. K^+ ions accelerate the dissolution of SiO_2 crystalline modifications (quartz, tridymite and cristobalite) by destroying the surface of particles and thus increasing the concentration of SiO_4^{4-} ions.

It should also be noted that, in lime-opoka mixtures, the obtained 1.13 nm tobermorite in the all cases was stable, and it does not start to recrystallize into other calcium silicate hydrates thus prolonging the duration of synthesis. In fact, this stability is determined by the small amount of aluminum-containing compounds present in opoka.

3.3. Peculiarities of xonotlite synthesis from raw materials with various SiO_2 activity

The investigation of hydrothermal synthesis products from lime and natural raw materials (calcined opoka and granite sawing powder waste) and reagent $SiO_2 \cdot nH_2O$ showed that xonotlite synthesis is a complex process which is strongly influenced by the pozzolanic activity of SiO_2 raw materials.

Table 3.3. Pozzolanic activity of raw materials

Material	Activity, mgCaO/g, after		
	3 days	7 days	Final
Opoka	117.9	144.6	170.1
Granite waste	14.3	39.9	52.2
$SiO_2 \cdot nH_2O$	332.1	335.9	336.8

For this reason, it is necessary to determine the suitability of SiO_2-bearing natural raw materials with various levels of pozzolanic activity for the rapid synthesis of xonotlite and to explain the formation and existence of the intermediate phases. According to the data of XRD analysis, in the reagent $CaO\text{-}SiO_2 \cdot nH_2O$ mixture, after 4 h of isothermal curing at 200 ºC when $CaO/SiO_2 = 1.0$ (unstirred suspensions), only traces of 1.13 nm tobermorite together with semi-amorphous C-S-H(I) (Fig. 3.34, curve 1) were identified. The latter compound cannot be determined by the XRD analysis method only [155], but results are in good agreement with the STA data, where, in the DSC curve, we detected an exothermal effect at 837 °C related with C-S-H(I) recrystallization into wollastonite (Fig. 3.37, curve A). Moreover, strong peaks of portlandite were identified in the synthesis products. Due to this reason, non-stoichiometric composition calcium silicate hydrates were identified: α-C_2SH ($CaO/SiO_2 = 2.0$) and Z-phase ($CaO/SiO_2 = 0.55$).

After 8 h of hydrothermal synthesis, the intensity of 1.13 nm tobermorite increased (Fig. 3.35, curve 1). Therefore, previously detected α-C_2SH still remained in the synthesis product together with Z-phase. It can be assumed that the formation of 1.13 nm tobermorite is slow because other calcium silicate hydrates have already formed. By prolonging the duration of isothermal curing to 12 h, the formation of xonotlite begins as traces of this compound were determined in the XRD curve (Fig. 3.34, curve 3). Moreover, the intensity of 1.13 nm tobermorite increased by 37.4% (Fig. 3.35, curve 1). However, Z-phase under these conditions becomes unstable and starts recrystallizing into gyrolite which was identified in the obtained product (Fig. 3.34, curve 3). It should be highlighted that α-C_2SH was not detected under these conditions of synthesis. It can be assumed that the stoichiometric molar ratio during hydrothermal synthesis is more permanent throughout the entire volume of the mixture. Furthermore, the intensity of the main peak of xonotlite and tobermorite in the XRD curve is significantly increased after 24 h of isothermal curing (Fig. 3.35, curves 2 and 3). In addition, after 72 h of isothermal curing, the highest intensity compound was 1.13 nm tobermorite (Fig. 3.34, curve 5).

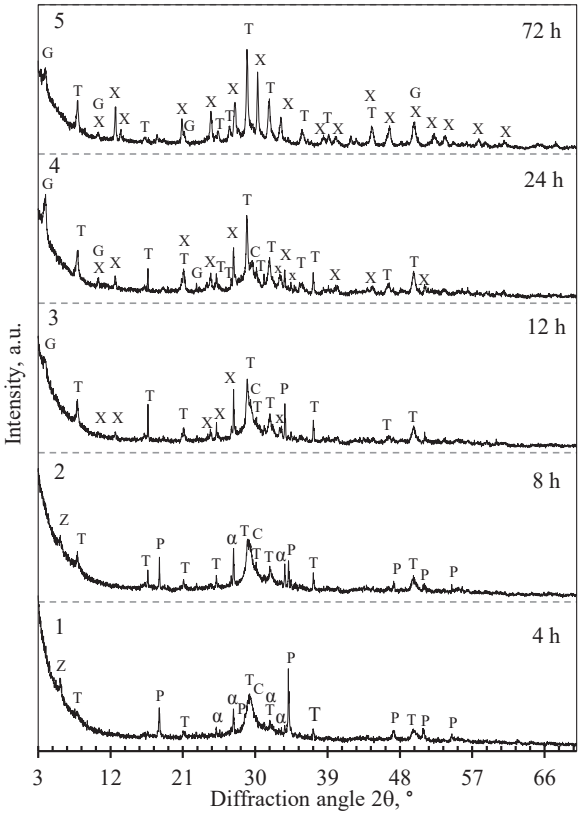

Fig. 3.34. XRD patterns of the synthesis products from CaO-SiO_2·nH_2O mixture with CaO/SiO_2 = 1.0 at 200 °C. Indexes: T – 1.13 nm tobermorite, X – xonotlite, P – portlandite, α – α-C_2SH, G – gyrolite, Z – Z-phase

It was determined that the size of tobermorite crystallites after 12 h of hydrothermal treatment is 371 nm, and it gradually increases with the increasing duration of synthesis (Fig. 3.35). In addition, the crystallites of xonotlite and gyrolite are larger than those of tobermorite. However, after prolonging the duration of synthesis from 12 h to 24 h, the size of gyrolite and xonotlite crystallites decreased. Meanwhile, the size of tobermorite crystallites continued to grow. Furthermore, with prolonging the duration of hydrothermal synthesis up to 72 h, the size of xonotlite crystallites slightly decreased. However, the size of gyrolite crystallites increased. The intensity of the tobermorite peak is constantly increasing with prolonging hydrothermal synthesis (Fig. 3.36). In addition, a different trend was observed in the formation of gyrolite in the synthesis products where the intensity of this compound decreased after 72 h of hydrothermal synthesis.

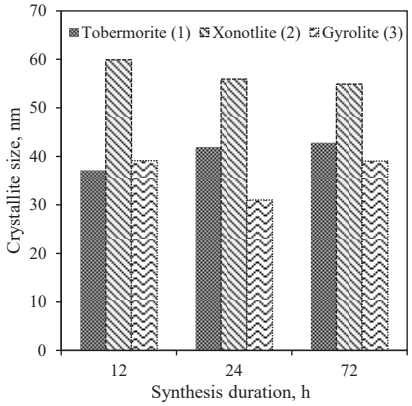

Fig. 3.35. Dependence of xonotlite (*1*), tobermorite (*2*) and gyrolite (*3*) crystallite size on the duration of synthesis from CaO-$SiO_2 \cdot nH_2O$ mixture

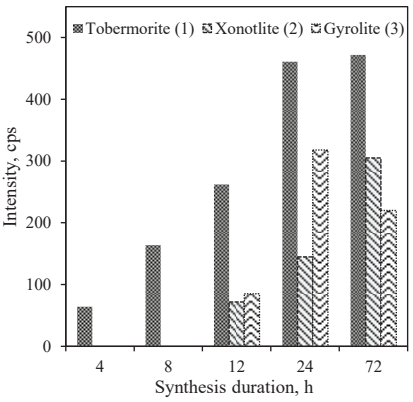

Fig. 3.36. Intensity of the tobermorite (*1*) (d = 1.13 nm), xonotlite (*2*) (d = 0.702 nm) and gyrolite (*3*) (d = 2.267 nm) peaks obtained from CaO-$SiO_2 \cdot nH_2O$ mixture

When examining the thermal analysis data, it was observed that the first endothermic effect at temperatures between 80–240 °C in the DSC curve is very broad and vaguely expressed. This thermal effect is related with the dehydration of the absorbed water from the atmosphere and the loss of bounded molecular water from the crystal structure of calcium silicate hydrates. With the formation of higher crystallinity compounds, these mass losses decrease: from 5.57% (4 h; Fig. 3.37, curve A1) to 2.19% (72 h; Fig. 3.37, curve B1). It should be noted that, in the DSC curve, before the decarbonation effect at 716 °C, we detected an effect at a temperature of 610 °C (Fig. 3.37, curve A). According to literature data, it is related with the decomposition of carbonated C-S-H gels which are easily carbonated during the preparation and storage due to their unstable state (165).

A considerable amount of portlandite was found in the samples after 4–8 h of the synthesis due to the presence of excess CaO in the stock solution: DSC analysis showed an endothermic peak at 461 °C related to the decomposition of portlandite (Fig. 3.37, curve 3). As a result, the molar ratio of CaO/SiO_2 of the mixture changed significantly, and calcium silicate hydrates which do not match the raw material molar ratio were formed – α-C_2SH (CaO/SiO_2 = 2.0) and Z-phase (CaO/SiO_2 = 0.55). Due to a significant amount of portlandite, the synthesis products easily absorb CO_2 from the atmosphere. This data is in good agreement with the STA data: an endothermic effect in the DSC curve at a temperature of 716 °C is related with the decomposition of calcite; TG analysis shows a mass loss of 4.13% (Fig. 3.37, curve 3), but the exothermic effect in the DSC curve at a temperature of 849 °C still remains (Fig. 3.37, curve 4). Literature data indicates that C-S-H(I) should no longer remain in these conditions, and that is proven by XRD analysis (d = 0.304 nm) [166]. The existence of an exothermic effect in the DSC curve may be explained by the recrystallization of gyrolite (Fig. 3.34, curve 5) into wollastonite.

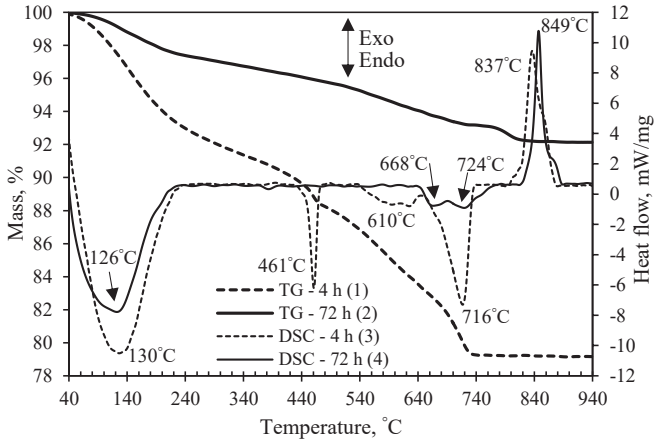

Fig. 3.37. TG (*1*, *2*) and DSC (*3*, *4*) curves of the synthesis products from CaO-$SiO_2 \cdot nH_2O$ mixture with CaO/SiO_2 = 1.0 at 200 °C after 4 h (*1*, *3*) and 72 h (*2*, *4*)

In summary, when using the SiO_2 component of a very high activity, intermediate phases are formed very rapidly which hardly recrystallize into thermodynamically stable minerals after prolonging the duration of hydrothermal treatment.

In the next stage of the work, xonotlite formation when using a CaO-granite mixture (where all SiO_2 is in the crystalline phase) was investigated, and the results are presented in Fig 3.38. The main peaks of 1.13 nm tobermorite after 4 h of hydrothermal synthesis were identified, but no peaks of xonotlite were detected (Fig. 3.38, curve 1). By prolonging the hydrothermal synthesis up to 8 h, the intensity of 1.13 nm tobermorite increased even more, almost by 3 times (Fig. 3.39, curve 1). Compared with $SiO_2 \cdot nH_2O$, the granite sawing waste reacts more actively, and the intensity of 1.13 nm tobermorite peaks is significantly higher. A possible reason is that in the composition of this raw material, there are minerals containing K^+ and Al^{3+} ions which promote the formation of 1.13 nm tobermorite. Therefore, the intensity of this peak is 4 times higher than when using $SiO_2 \cdot nH_2O$. Furthermore, when using mixtures prepared from the granite sawing waste, we obtained less C-S-H(I) in the synthesis products. This is indicated by thermal analysis where the peak in the DSC curve at 894 °C is 2 times less intensive (Fig. 3.41, curve 3). If we continue to prolong the duration of hydrothermal synthesis, the intensity of 1.13 nm tobermorite constantly increases (Fig. 3.39, curve 1). These results imply that tobermorite forms much faster when using the granite sawing waste rather than amorphous $SiO_2 \cdot nH_2O$ as the source of silica. However, a huge amount of Al^{3+} ions prevents the formation of xonotlite, yet, even then, the molar ratio is more favorable, and the synthesis temperature is balanced for the synthesis of this compound. In addition, the other identified minerals (annite and actinolite) in the granite sawing waste remain in the synthesis products even after 72 h of isothermal current.

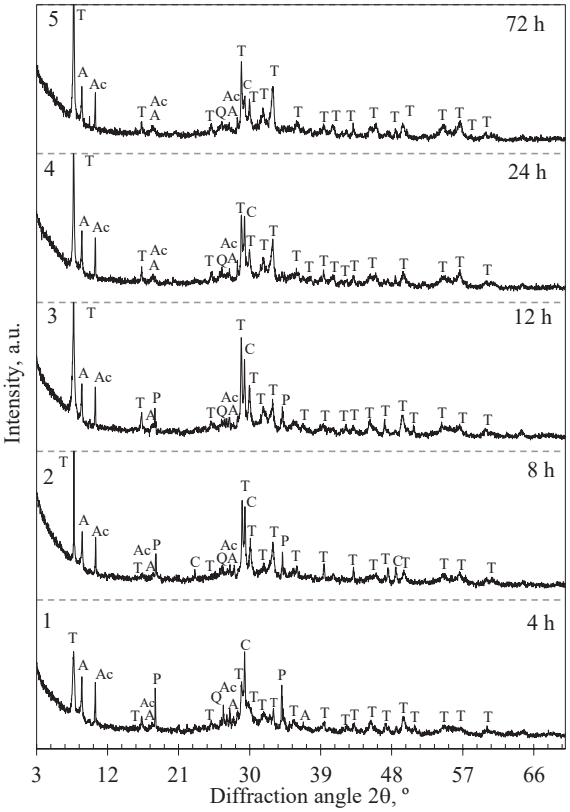

Fig. 3.38. XRD patterns of the synthesis products from CaO-granite mixture with CaO/SiO_2 = 1.0 at 200 °C. Indexes: A – annite, Ac – actinolite, C – calcite, P – portlandite, Q – quartz, T – 1.13 tobermorite

The size of tobermorte crystallites slowly increases when prolonging hydrothermal treatment from 4 h to 12 h (Fig. 3.39). Moreover, the size of the crystallites significantly increased when hydrothermal synthesis was performed for 24 hours and is bigger by 18% when obtained from amorphous $SiO_2 \cdot nH_2O$. However, crystallites no longer increase with the prolongation of isothermal curing. The intensity of 1.13 nm tobermorite after 4 h of hydrothermal synthesis is 3 times bigger than in the synthesis products obtained from a $SiO_2 \cdot nH_2O$ mixture. Furthermore, this trend persists even when the duration of synthesis is prolonged up to 72 h. These results indicate that, when using a mixture with granite, the amount of 1.13 nm tobermorite is higher than in the synthesis product obtained from amorphous $SiO_2 \cdot nH_2O$.

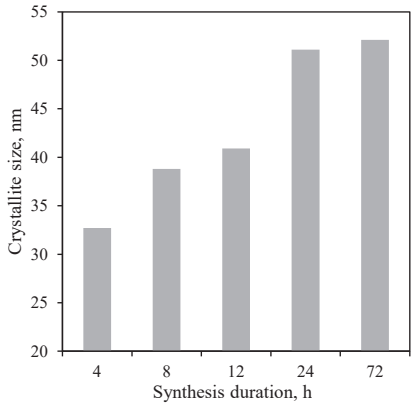

Fig. 3.39. Dependence of 1.13 nm tobermorite crystallite **s**ize on the duration of synthesis from CaO-granite mixture

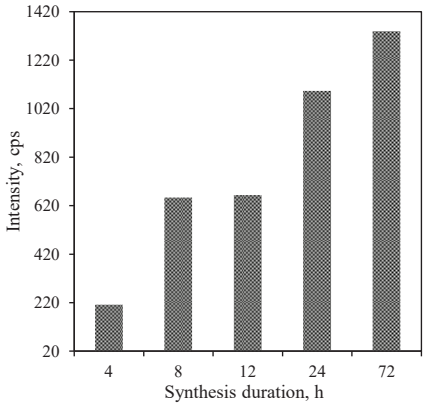

Fig. 3.40. Intensity of the main peak (d = 1.13 nm) of tobermorite from CaO-granite mixture

The obtained products of synthesis were examined by simultaneous thermal analysis whose data is presented in Figure 3.41. The first endothermal effect is broad, and, behind it, several effects underlie: at 40–100 °C, related to moisture removal, and, at 100–250 °C, related to C-S-H(I) and 1.13 nm tobermorite dehydration. Therefore, the mass losses at 100–250 °C during dehydration are 4.08% (4 h) and 5.41% (72 h). The second endothermal effect detected in the DSC curve at 462 °C is related to the decomposition of portlandite (Fig. 3.41, curve 3). It is in good agreement with the XRD results where this compound was identified (Fig. 3.38, curve 1). The endothermic effect at 749 °C shows the decomposition of carbonates, and the mass loss in the temperature range of 707–761 °C is fairly large – 5.07% (Fig. 3.41, curve 1). However, in the synthesis products obtained after 72 h, we observed a significant decrease of carbonates because the mass loss is 2.93 times smaller; it is equal to 1.73%. The exothermal effect at 894 °C was assigned to semi-amorphous C-S-H(I) recrystallization to wollastonite (Fig. 3.41, curve 3). Moreover, the exothermic effect at 879 °C in the synthesis products obtained after 72 h of hydrothermal treatment remains (Fig. 3.41, curve 4). This means that Al^{3+} ions incorporate not only in the 1.13 nm tobermorite crystal lattice but also in the C-S-H(I) structure. Do to this reason, the recrystallization temperature is shifted to the higher levels of temperature than usual.

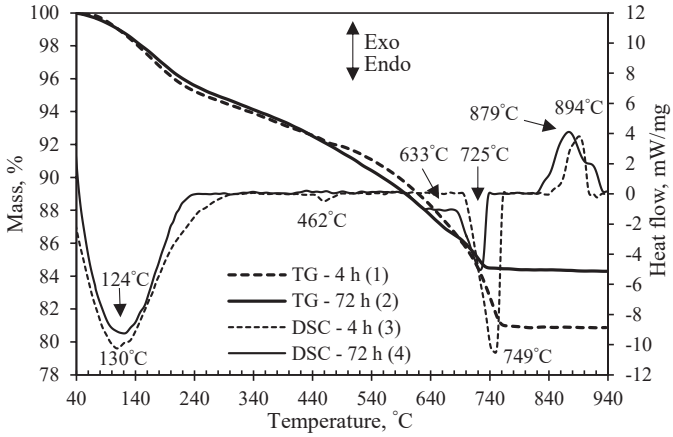

Fig. 3.41. TG (*1*, *2*) and DSC (*3*, *4*) curves of the synthesis products from CaO-granite mixture with CaO/SiO_2 = 1.0 at 200 °C after 4 h (*1*, *3*) and 72 h (*2*, *4*)

SEM data confirms that the specific crystal plates of 1.13 nm tobermorite after 4 h of hydrothermal synthesis are formed (Fig. 3.42, A). Also, visible large agglomerates composed of semi-amorphous C-S-H(I) were identified not only by XRD analysis, but also by STA. Furthermore, the SEM data showed clearly visible grains that, when evaluating the data obtained with other methods of instrumental analysis, are highly likely to be portlandite and calcite. After prolonging the synthesis duration up to 72 h, agglomerates of semi-amorphous compounds are still visible (Fig. 3.42, B). However, the SEM data indicates that crystals of 1.13 nm tobermorite are more widely distributed in the volume of the synthesis products than in the case of 4 h synthesis. These results are in good agreement with the previously obtained data and confirm the results of XRD analysis.

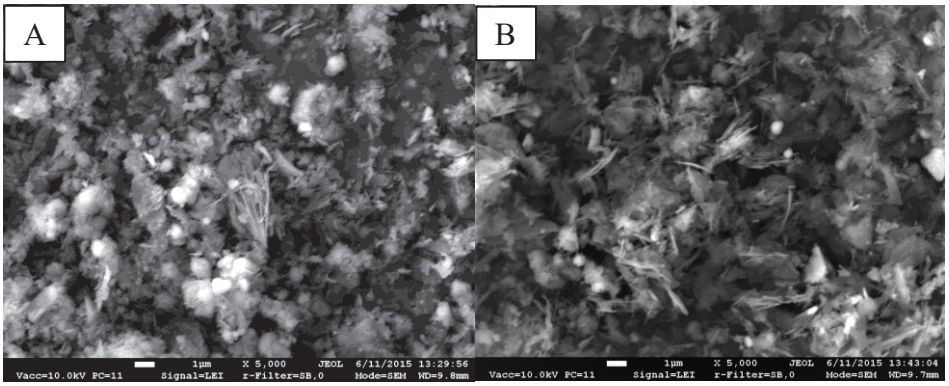

Fig. 3.42. SEM micrographs of synthesis products from CaO-granite mixture with CaO/SiO_2 = 0.83 after 4 h (*A*) and 72 h (*B*) at 200 °C

In order to compare materials of different pozzolanic activities, the hydrothermal synthesis at 200 °C from a lime-opoka mixture with a molar ratio of CaO/SiO_2 = 1.0 was performed as well. It was determined that, after 4 h of

isothermal curing, 1.13 nm tobermorite was identified as the main compound in the synthesis product (Fig. 3.43, curve 1). In addition, the peaks of quartz remained in the XRD curve, but neither tridymite nor cristobalite or portlandite were identified. It can be assumed that these minerals fully react during hydrothermal treatment within the shortest duration of synthesis. The formation of semi-amorphous calcium silicate hydrates compounds is low. Therefore, we indirectly confirmed it with the TG data – decarbonization results in a mass loss of only 1.91% (Fig. 3.46, curve A), and, when compared to previous results, a similar amount of carbonates was established only after 72 h of synthesis. It should be underlined that xonotlite was identified after prolonging the duration of synthesis up to 8 h (Fig. 3.43, curve 2). Furthermore, together with xonotlite, 1.13 nm tobermorite was identified. However, quartz remains in the synthesis products, but the intensity of its peaks decreases. After 12 h of isothermal curing, no new compounds were detected, and xonotlite, together with 1.13 nm tobermorite, dominate in the synthesis products (Fig. 3.43, curve 3). Furthermore, XRD analysis data shows that the profiles of the curves after hydrothermal treatment of 24 h and 72 h are very similar.

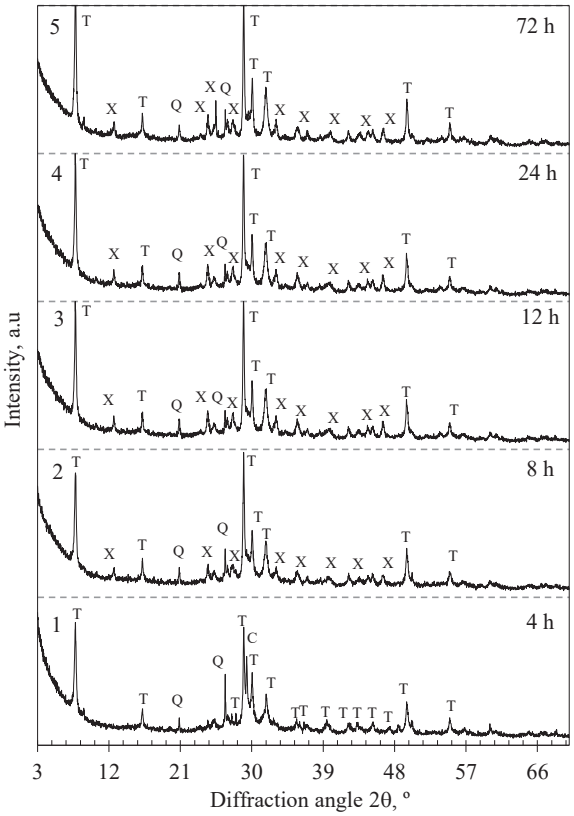

Fig. 3.43. XRD patterns of the synthesis products from lime-opoka mixture with CaO/SiO_2 = 1.0 at 200 °C. Indexes: T – 1.13 nm tobermorite, Q – quartz, X – xonotlite

It was determined that the crystallite size was found to be bigger (36.9 nm) as early as after 4 h of hydrothermal synthesis (Fig. 3.44) compared to the previously

obtained results (Fig. 3.39). By prolonging the duration of isothermal curing up to 8 h, the size of tobermorite crystallites increased only by 3.4% (Fig. 3.44). Furthermore, the intensity of the 1.13 nm tobermorite peak increases constantly by prolonging the synthesis duration up to 24 h (Fig. 3.45). However, intensity of the xonotlite peak increases slightly, whereas the 1.13 nm tobermorite peak increases significantly (Fig. 3.45). Moreover, when comparing with the previous results, it was determined that, after 72 h of isothermal curing, the highest intensity of 1.13 nm tobermorite was obtained when using lime-opoka mixtures. It can be assumed that synthesis goes in a more favorable way when in the mixtures there is some quantity of amorphous SiO_2 and impurities, which accelerates the formation of calcium silicate hydrates.

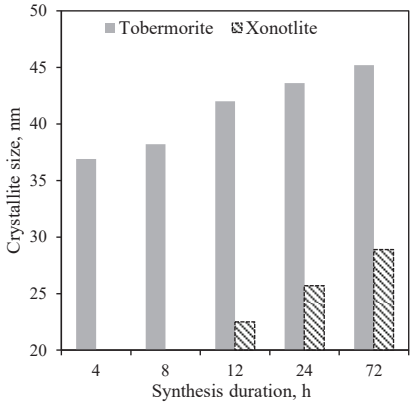

Fig. 3.44. Dependence of the 1.13 nm tobermorite (1) and xonotlite (2) crystallite size on the duration of synthesis from lime-opoka mixture

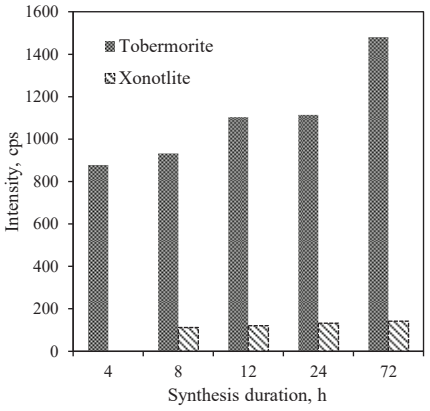

Fig. 3.45. Intensity of the tobermorite (d = 1.13 nm) and xonotlite (d = 0.702 nm) peak obtained from lime-opoka mixture

It was determined that, after 72 h of isothermal curing, the dehydration effect at 80–240 °C in the DSC curve was well expressed and shown in Fig. 3.28, curve B. This effect is divided into two stages, and dehydration of 1.13 nm tobermorite is clearly visible. The results of TG analysis showed that the mass loss at 40–100 °C is 0.65, whereas the mass loss at 100–240 °C is 6.08% (Fig. 3.46, curve 1). It was determined that, in DCS, the endothermal effect is observed at 337 °C, which is related to the decomposition of hydrogarnets which are formed at the beginning of hydrothermal synthesis (Fig. 3.46, curve 3). Due to this reason, as our chemical composition analysis showed, opoka contains some Al-containing compounds which were consumed and yielded hydrogarnets during hydrothermal treatment. It can be assumed that not all aluminum was interrupted into the tobermorite crystallite lattice. The endothermic effect of the decomposition of carbonates in the DSC curve is negligible, and the same results were obtained in the data of XRD analysis, where, the highest amount of xonotlite and 1.13 nm tobermorite after 72 h of isothermal curing was obtained. In addition, TG analysis showed that the total mass loss after 72 h is less than after 4 h of synthesis, and it reached 10.4% (Fig. 3.46, curve 2).

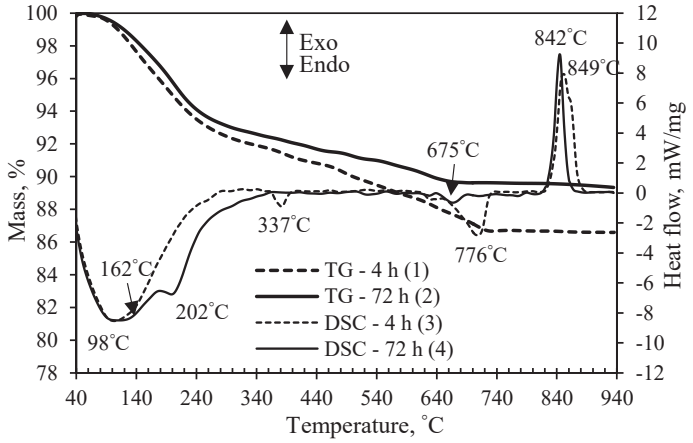

Fig. 3.46. TG (*1*, *2*) and DSC (*3*, *4*) curves of the synthesis products from lime-opoka mixture with CaO/SiO_2 = 1.0 at 200 °C after 4 h (*1*, *3*) and 72 h (*2*, *4*)

According to the SEM data, in the 72 h synthesis product, the needle-shaped crystals of xonotlite were well expressed, however, with 1.13 nm tobermorite crystals in the mix (Fig. 3.47). It is in good agreement with the XRD analysis data where, for xonotlite and 1.13 nm tobermorite, specific peaks were identified. Furthermore, the XRD data showed, and SEM analysis confirmed, that the highest crystallinity degree of xonotlite and tobermorite crystals was obtained after 72 h of isothermal curing.

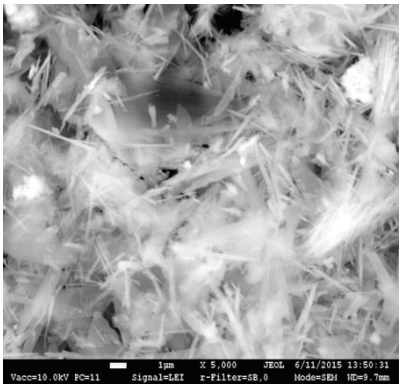

Fig. 3.47. SEM micrograph of synthesis products from lime-opoka mixture with CaO/SiO_2 = 1.0 after 72 h at 200 °C

The obtained samples from all the used mixtures after 4 h and 72 h of isothermal curing were investigated by the method of FT-IR spectroscopy (Fig. 3.48). CO_3^{2-} vibrations at 1442–1469 cm^{-1} and 878 cm^{-1} were determined in all the curves (Fig. 3.48). In all the spectra, we can distinguish a broad absorption band at 3520–3571 cm^{-1} which can be assigned to the hydroxyl group, and the second peak at 1630 cm^{-1} due to the bending vibration band of molecular H_2O. It was determined

that the band in the range of 1200–950 cm^{-1}, which is assigned to asymmetrical stretching vibrations of SiO_4 tetrahedra, was not identified. It is in good agreement with the results from XRD analysis where quartz reacted under the condition of hydrothermal synthesis. Moreover, the second important silicate band was characterized as the Si–O–Si bending vibration band which occurs at ~673 cm^{-1}, whereas the band at 480–533 cm^{-1} is assigned to the O–Si–O bending vibration. According to literature data, the above mentioned adsorption bands are inherent for tobermorite [167, 168]. Moreover, the obtained data from the mixtures with the granite sawing waste in the FT-IR spectroscopy curves showed the weakest peaks assigned to tobermorite. This data corresponds to our XRD results where poor crystallinity degree of 1.13 nm tobermorite was identified after hydrothermal synthesis.

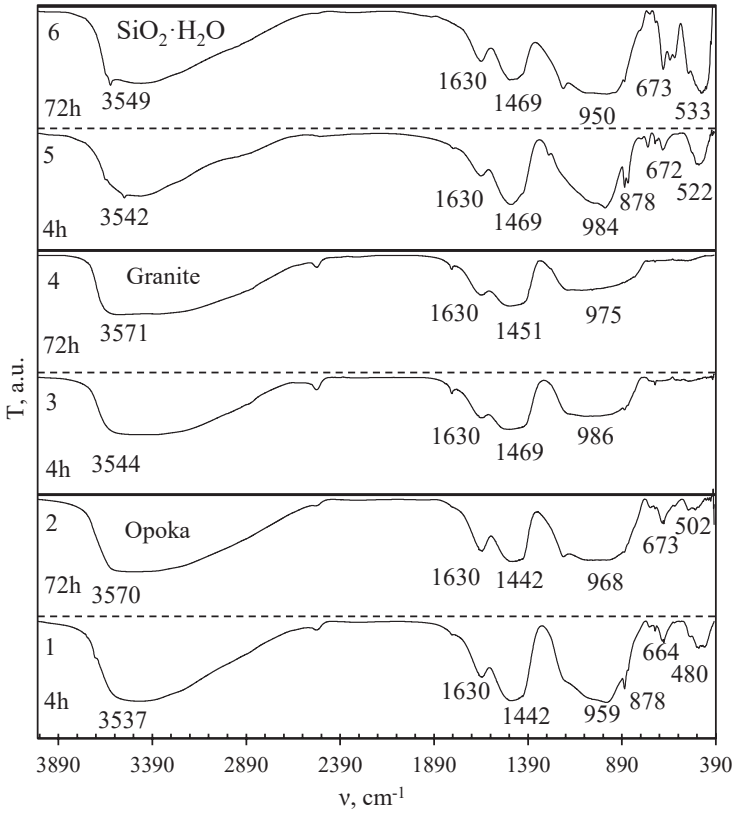

Fig. 3.48. FT-IR spectrum of products after 4 and 72 h synthesis from lime-calcined opoka (*1*, *2*)/granite sawing waste (*3*, *4*)/$SiO_2 \cdot nH_2O$ (*5*, *6*) mixtures with $CaO/SiO_2 = 1.0$ at 200 °C

To summarize, during hydrothermal synthesis, in CaO-granite mixtures, when the molar ratio is $CaO/SiO_2 = 1.0$, only 1.13 nm tobermorite was identified in the synthesis products, and, even after 72 h, xonotlite was not found. The granite sawing waste contains a significant amount of aluminum (15.41%) which completely prevents the formation of xonotlite. However, 1.13 nm tobermorite (calcium silicate

hydrate related to xonotlite) forms more rapidly and with a higher degree of crystallinity than in the cases of using mixtures with amorphous $SiO_2 \cdot nH_2O$.

Calcinated opoka is a suitable material for the synthesis of crystalline calcium silicate hydrates. Amorphous SiO_2 from opoka begins to react first, it is followed by tridymite and cristobalite. 1.13 nm tobermorite and xonotlite are formed at the beginning of the hydrothermal synthesis (4 h), and this greatly reduces the probability of the existence of semi-amorphous phases. The combination of various modifications of SiO_2 and a balanced amount of K^+ and Al^{3+} ions allows synthesizing xonotlite and 1.13 nm tobermorite of a high crystallinity degree. It can be assumed that the formation of crystalline calcium silicate hydrates is not solely dependent on the SiO_2 activity of the raw materials. The impurities contained therein may promote the formation of some other compounds (in this case, 1.13 nm tobermorite) and retard the synthesis of stoichiometric minerals (xonotlite).

3.4. Specific surface area and porosity of synthesis products obtained from raw materials with various SiO_2 activity

The important characteristics of the structure of materials with distinct open porosity are: the specific surface area, the pore diameter, and the pore volume. Nitrogen adsorption/desorption at 77 K is one of the main experimental methods to measure these parameters. The major adsorption equilibrium analysis and specific surface area calculations begin with the classification of the isotherms. The *Union of Pure and Applied Chemistry* (in the abbreviated form, *IUPAC*) provides empirical classification of six types of isotherms for gas-solid equilibria based on Langmuir [169] general equation grounded on kinetic calculation; Brunauer *et al*. [170], which introduced the Brunauer-Emmer-Teller (BET) equation for multimolecular adsorption [171].

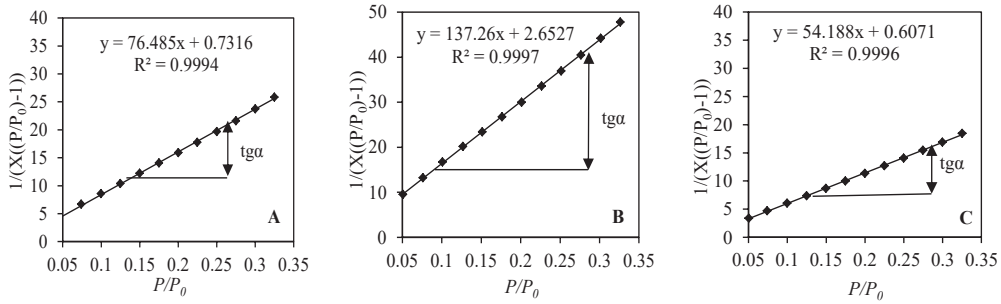

Fig. 3.49. Isotherm of N_2 adsorption at 77 K in BET plot of products after 12 h synthesis from mixtures: $SiO_2 \cdot nH_2O$–CaO (A), granite–CaO (B), opoka–CaO (C)

In order to calculate the characteristics of the microstructure of materials with distinct open porosity, the BET method was employed. When using the collected data of N_2 adsorption at the range of relative pressure $0.05 \leq P/P_0 \leq 0.35$ and applying the BET coordination $(1/(X[(P/P_0) - 1))$, we obtained values for further research. It was determined that, for all the samples, the BET equation yields a linear plot and a straight line of the correlation coefficient R^2 which is presented in Figures 3.49 and

3.50. The correlation coefficient R^2 remains very close to the unit, i.e., ~0.9999, and it could be assumed that the calculated parameters are correct.

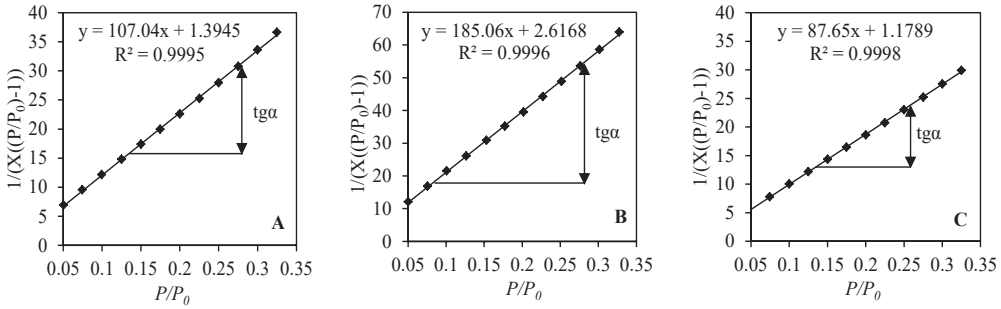

Fig. 3.50. Isotherm of N_2 adsorption at 77 K in the BET plot of products after 72 h synthesis from mixtures: $SiO_2 \cdot nH_2O$–CaO (A), granite–CaO (B), opoka–CaO (C)

The most reliable S_{BET} measurement data is obtained when the constant C_{BET} value is between 50–250 or equal to the extreme values. A lower value of the constant ($C_{BET} > 50$) indicates that N_2 condenses in the pores, and the calculated S_{BET} would be higher than the real one. The finding of condensates in the pores means that the multilayer of N_2 adsorbate was obtained, and, instead of a thin layer, the pore was fully filled. Conversely, $C_{BET} > 250$ shows that a chemical reaction takes place between the surface of the adsorbent and the adsorbate without the formation of a monolayer. It was determined that the calculated constant C_{BET} varies within the values of 52.74–87.38, which perfectly fits into the theoretical guidelines (Table 3.4). These results show that a stable monolayer was formed on the surface of hydrothermally synthesized samples from various raw materials, and, for this reason, S_{BET} was possible to be calculated accurately. It was determined that the measured surface area varies between 18.73–63.98 $m^2 \cdot g^{-1}$, and the highest value is obtained from the samples synthesized by using opoka. This is explained on the basis of the product mineral composition obtained by using opoka via hydrothermal synthesis. Moreover, another trend was observed that the surface area S_{BET} significantly depends on the duration of synthesis. In the samples obtained after 72 h of synthesis, the capacity of monolayer Xm decreases significantly. As a result, the calculated surface area S_{BET} is decreased by 27% in the sample obtained from $SiO_2 \cdot nH_2O$–CaO and by 25% from granite–CaO. Slightly different results were delivered in the sample obtained from opoka after 72 h of isothermal curing where the surface area decreased significantly – by 38 percent. Such a decrease in the surface area after a longer duration of hydrothermal synthesis is considered as the increased crystallinity degree of the material. It is in good agreement with the previous result where synthesis duration has a significant impact on 1.13 nm tobermorite and xonotlite crystallization.

Table 3.4. Calculated parameters of synthesis products obtained from various raw materials

Mixture	Duration	BET equation constants		C_{BET} Constant	Capacity of monolayer X_m, g	S_{BET}, $m^2 \cdot g^{-1}$
		Slope *S*	Intercept *I*			
$SiO_2 \cdot nH_2O$-CaO	12 h	74.52	$1.051 \cdot 10^{-1}$	71.88	0.0132	46.08
$SiO_2 \cdot nH_2O$-CaO	72 h	106.05	$1.466 \cdot 10^{-1}$	73.35	0.0093	32.39
Granite-CaO	12 h	137.26	$2.652 \cdot 10^{-1}$	52.74	0.0072	24.91
Granite-CaO	72 h	183.09	$2.816 \cdot 10^{-1}$	66.02	0.0054	18.73
Opoka-CaO	12 h	53.81	$6.230 \cdot 10^{-2}$	87.38	0.0182	63.98
Opoka-CaO	72 h	86.76	$1.303 \cdot 10^{-1}$	67.58	0.0114	39.55

N_2 adsorption-desorption isotherms of the sample obtained from various mixtures after 12 h and 72 h of hydrothermal synthesis are shown in Figure 3.51. It was determined that the adsorption curves are assigned to Type II isotherms and can be described with the BET equation. Moreover, this type of isotherm features the hysteresis loop associated with capillary condensation in mesopores and a limited uptake in the high p/p_0 range. The sharp increase of the synthesis product isotherms at P/P_0 ~0.05 shows micropores which are in the structure of the compounds.

It was determined that, in the synthesis products, N_2 adsorption/desorption isotherms show the formation of a monolayer in the range of P/P_0. These absorption-desorption isotherms do not coincide, and the desorption isotherm is shifted to the left of the adsorption isotherm. According to the IUPAC classification, four types of hysteresis loops are distinguished according to the different exhibited forms. The received data of the absorption-desorption isotherms of the products obtained after 12 h of synthesis when using amorphous $SiO_2 \cdot nH_2O$ showed that the occurrence hysteresis loop can be assigned to the type of H3 (Fig. 3.51, A). Currently, the above mentioned type of the hysteresis loop is associated with the parallel plate pore.

A different tendency was observed in the synthesis product obtained from granite (Fig. 3.51, B). It was determined that the desorption isotherm is narrow, and it ends at 0.45. Due to this reason, it is difficult to classify the hysteresis loop, and it may be between H1 and H3. The data does not precisely correspond to the classic shape of the hysteresis loop, and it will be clarified by using calculation.

The sample obtained from calcinated opoka features a desorption band that forms a hysteresis loop (Fig. 3.51, C). It can be classified as H1 hysteresis loop because it closes and merges with the absorption curve at a fairly high pressure (P/P_0 ~0.6). However, the desorption isotherm is narrow, and this shows that the obtained system is polydisperse, with some parallel plate pores formed with the cylindrical shape pores.

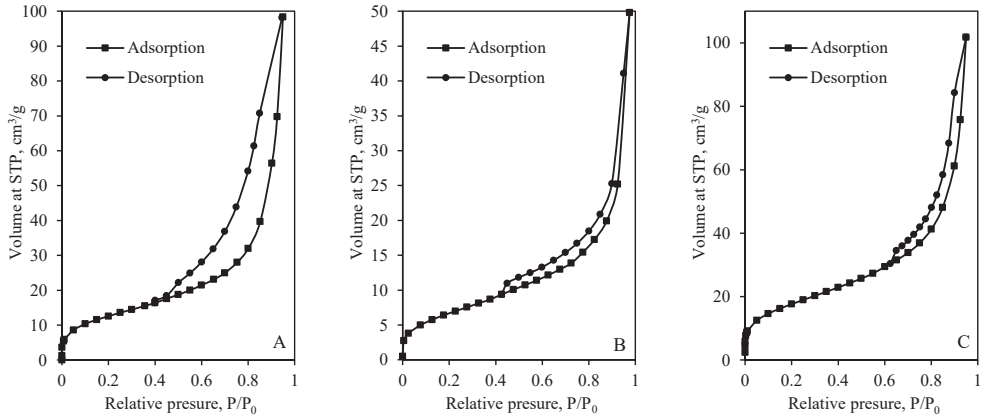

Fig. 3.51. N_2 adsorption-desorption isotherms of products (CaO/SiO_2 = 1.0 at 200 °C) after 12 h synthesis from mixtures: $SiO_2 \cdot nH_2O$-CaO (*A*), granite-CaO (*B*), opoka-CaO (*C*)

N_2 adsorption/desorption was examined in the samples obtained after 72 h of hydrothermal synthesis from various raw materials. It was determined that the duration synthesis prolonged by six times significantly impacted the sample obtained from the mixture with granite–CaO where the hysteresis loop was not identified (Fig. 3.52, B). To characterize this compound, it can be attributed to the second type of the isotherm which is assigned to a non-porous or macroporous material. In this case, the Kelvin equation cannot be used to calculate the pore parameters.

It was determined that the isotherms of the product obtained when using amorphous $SiO_2 \cdot nH_2O$ after prolonged synthesis duration showed that the desorption curve lies closer to the adsorption curve with a decreasing pressure of N_2, and this led to the narrowed hysteresis loops (Fig. 3.52, A). This effect is related to the volume of the pores being decreased due to the better reserialized sample grains after the prolonged duration of the synthesis. Despite the changes in the microstructure, the presently occurring hysteresis loop can be assigned to H3 type.

The microstructure of the synthesis sample obtained by using opoka–CaO changed significantly. It was determined that the pressure when the desorption curvemerges with the absorption curve decreases from P/P_0 ~0.6 to 0.45 and due to this reason, the type of hysteresis loop changes from H1 to H3. The prolonged synthesis duration leads to a change of the pore shape. It can be assumed that the pores change from cylindrical-shaped into plate-shaped.

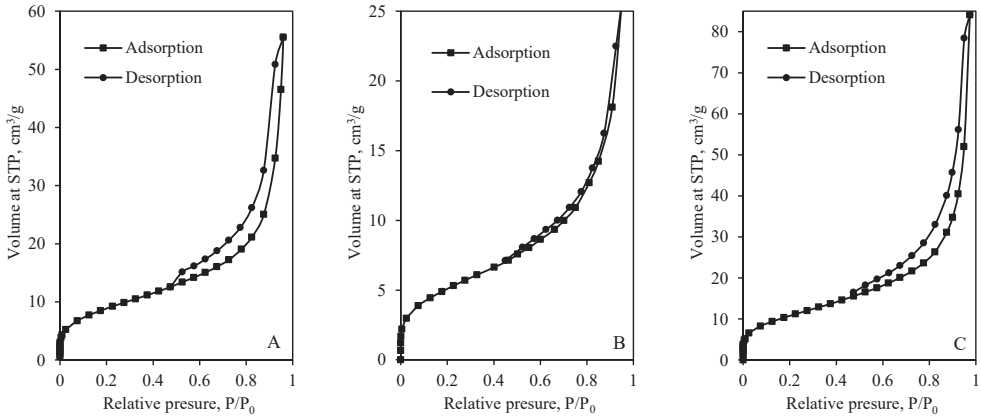

Fig. 3.52. N_2 adsorption/desorption isotherms of products (CaO/SiO_2 = 1.0 at 200 °C) after 72 h synthesis from mixtures: $SiO_2 \cdot nH_2O$–CaO (A), granite–CaO (B), opoka–CaO (C)

We determined only the shape of the dominant pores in the studied polydisperse system. The most suitable pore model is the one of the experimentally measured specific surface area whose S_{BET} value is the closest to the calculated ΣA value. In order to check which pore model better describes the texture of the fusion products, we performed calculations by using two models: the cylindrical pore, and the pore between parallel planes. The total pore volume and the radial distribution of the pore was calculated by using the following methodology: the correlated Kelvin equation, C. Orr methodology, and J.M. Dalla Valle methodology. The initial calculations are analogous and applicable to both models while using the measured amount of the adsorbed nitrogen volume at different relative pressures. The Kelvin radius of the pore and the thickness of the adsorbed N_2 layer are calculated from the Kelvin and Halsey equations. These values are used in further calculations when using various pore models; they are presented in Appendix 1. The total specific surface area ΣA is calculated by summing the theoretical surface area A of the pore walls as the relative pressure decreases. The calculations are completed when the difference between the total specific surface area and the nitrogen layer thickness ($\Delta t \cdot \Sigma A$) becomes greater than the value of the change in the volume (ΔV_L) of the evaporated liquid adsorbate. This indicates that the desorbed gas is not of the vapor origin of the liquid walls, but simply a desorbed gas.

By analyzing the obtained calculations, it was found that the pores of amorphous SiO2·nH2O formed in the synthesis product are best described by the parallel plate pore model (Table 3.5). However, the deviation remains large, and the possible system is polydisperse. It should be underlined that the calculation shows significant changes prolonging hydrothermal synthesis in the synthesis products after 72 h. Parallel plate shaped pores are replaced with cylindrical ones, and the deviations that describe this model are very small at only ~6%.

When we investigated a sample obtained from granite-CaO after 12 h of synthesis, the adsorption/desorption isotherm had a hysteresis loop which was classified as H3 type. However, the obtained calculations clarified that the system is

polydisperse, and none of the applied models fully describes the resulting system. Therefore, it can be stated that the system is polydisperse and dominated by poresof different shapes. Moreover, by prolonging the duration of the synthesis, the material becomes non-porous or macro-porous. Due to this reason, the hysteresis loop was not identified. In addition, these results are confirmed by the small surface area obtained in the sample after 72 h.

It was determined that, in the synthesis product obtained from the opoka–CaO mixture, the hysteresis loop is assigned to H1 type, and the predominant pore is of the cylindrical shape. Moreover, it is possible to observe that the shape of the hysteresis loop changed when the synthesis time was prolonged, and, in this case, the hysteresis loop can be classified as H3, which is characteristic of materials whose pores are formed between parallel plates, or else the pores are formed between disordered particles. The results of the calculations using the Kelvin equation coincide with the classification of the hysteresis loop because it is estimated that, after 12 h, cylindrical porespredominate, and the difference between the measurements and the calculations is insignificant (7%). Meanwhile, our calculations showed a much larger difference (40%) when using the parallel plate pore model. The calculations showed that, with the increase of the synthesis duration, the difference between the plate and the cylindrical pore model is similar. This indicates that the number of cylindrical pores is decreasing more, and more pores develop between the plates. Therefore, the cylindrical pore-shaped model is no longer suitable; there are not enough plates to fit this model. This is an intermediate state, and it is likely that, by prolonging the fusion time, the plate pores would begin to predominate in the sample. The values of the specific surface area measured and calculated by using different models describing the pore are given in Table 3.5.

Table 3.5. Values of the measured and calculated specific surface area of the synthesis samples obtained at 200 °C in unstirred suspensions with $CaO/SiO_2 = 1.0$

Mixture	Duration	Calculation results using the cylindrical pore model		Calculation results using the parallel plate pore model	
		ΣA, $m^2 \cdot g^{-1}$	$\lvert S_{BET} - \Sigma A \rvert$, %	ΣA, $m^2 \cdot g^{-1}$	$\lvert S_{BET} - \Sigma A \rvert$, %
$SiO_2 \cdot nH_2O$-CaO	12 h	84.39	83.13	56.38	22.35
$SiO_2 \cdot nH_2O$-CaO	72 h	38.45	6.06	19.00	13.39
Granite-CaO	12 h	31.07	24.72	16.73	32.83
Granite-CaO	72 h	-	-	-	-
Opoka-CaO	12 h	68.93	7.73	37.82	40.89
Opoka-CaO	72 h	50.63	28.01	27.18	31.22

It was determined that the biggest total pore volume (340 mm^3/g) formed in the product was determined in the mixture with amorphous $SiO_2 \cdot nH_2O$ after 12 h of isothermal curing at 200 °C (Fig. 3.53, A). Meanwhile, the smallest pore volume (80 mm^3/g) occurred in the sample obtained from the granite–CaO mixture. However, the total pore volume decreased significantly when the synthesis duration was prolonged up to 72 h – from 340 mm^3/g to 109 mm^3/g (in the case of $SiO_2 \cdot nH_2O$) and from 245 mm^3/g to 137 mm^3/g (in the case of opoka) (Fig. 3.53, B). This is in good agreement with the data presented in Fig. 3.35 and Fig. 3.44 – with prolonging

the duration of hydrothermal curing, the crystallite size increases, and the total pore volume decreases.

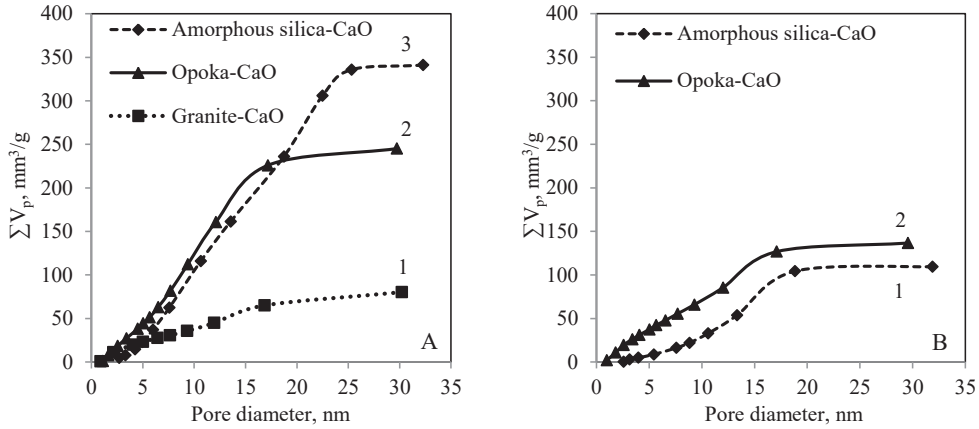

Fig. 3.53. Total pore volume of products (CaO/SiO_2 = 1.0 at 200 °C) after 12 h (*A*) and 72 h (*B*) of synthesis.

It was determined that the pores with 2 different diameter ranges are predominant: 1–2.5 nm and 5–20 nm (Fig. 3.54). The porosity of the obtained calcium silicate hydrates should provide good thermal insulation properties for the products made from them as no air convection occurs in the fine pores.

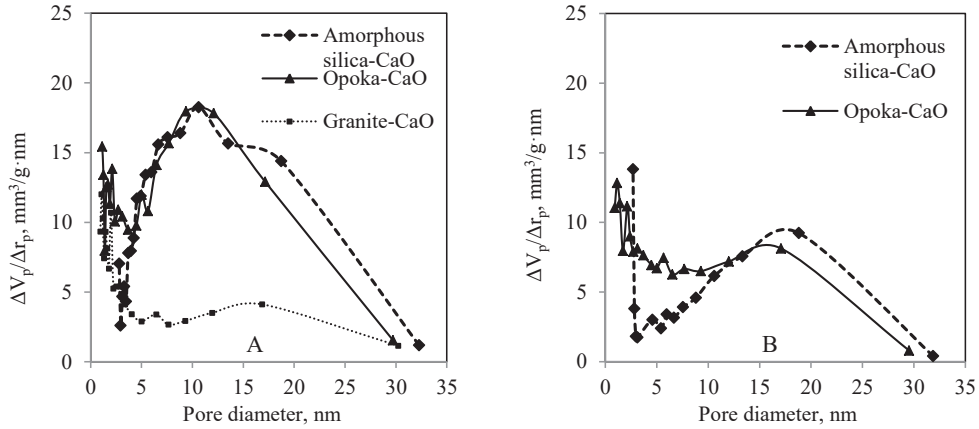

Fig. 3.54. Differential distributions of the pore sizes in the products (CaO/SiO_2 = 1.0 at 200 °C) after 12 h (*A*) and 72 h (*B*) of synthesis

3.5. Hydrothermal curing of opoka at 220 °C in non-stirred suspensions

The results of hydrothermal synthesis in unstirred suspensions using mixtures prepared from calcined opoka when the molar ratio is CaO/SiO_2 = 0.83 were discussed in the previous section. However, the formations of calcium silicate hydrates can be significantly affected by the temperature rise.

It was determined that, after 4 h of isothermal curing, traces of 1.13 nm tobermorite were identified (Fig. 3.55, curve 1). Therefore, the intensity of this compound is only 136 cps (Fig. 3.56). When comparing these results with the data obtained at 200 °C (Fig. 3.30, curve 1), the intensity decreases 4.4 times. Moreover, traces of gyrolite were identified in the synthesis product. Moreover, this compound has a lower molar ratio (CaO/SiO_2 = 0.66) than tobermorite (CaO/SiO_2 = 0.83) [172]. Meanwhile, in the temperature range between 180–200°C (Figs. 3.18 and 3.30), only 1.13 nm tobermorite was formed. With the prolonged synthesis duration up to 8 h, the intensity of the 1.13 nm tobermorite peak increased only slightly (Fig. 3.54).

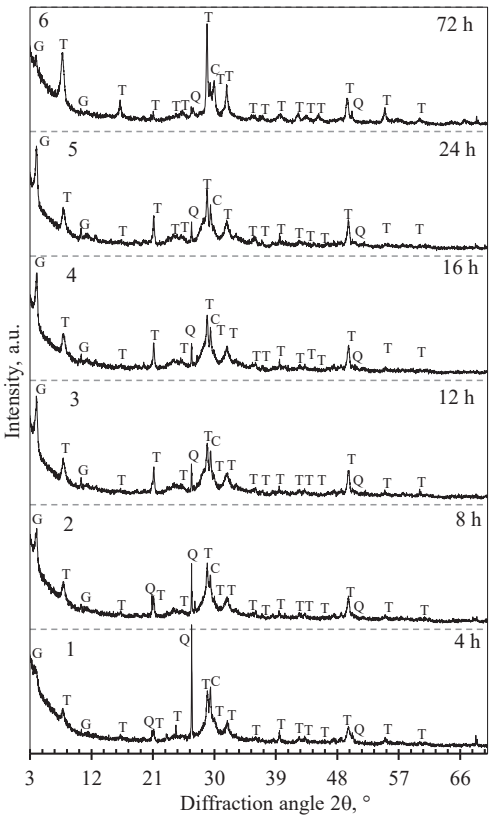

Fig. 3.55. XRD patterns of the synthesis products from lime-opoka mixture with CaO/SiO_2 = 0.83 at 220 °C. Indexes: C – calcite, T – 1.13 nm tobermorite, G – gyrolite, Q – quartz

This trend continues further – by extending the duration of the synthesis up to 24 h, the intensity of the peaks of calcium silicate hydrates increases; meanwhile, the intensity of quartz decreases (Fig. 3.55, curves 3–5). In addition, the intensity of gyrolite decreases until only traces are left after prolonging the hydrothermal treatment up to 72 h (Fig. 3.56). Instead of the formation of gyrolite from part of C-S-H(I), therefore, all of this compound can be used to form tobermorite. Due to this reason, the main peak of 1.13 nm tobermorite increases significantly (Fig. 3.56).

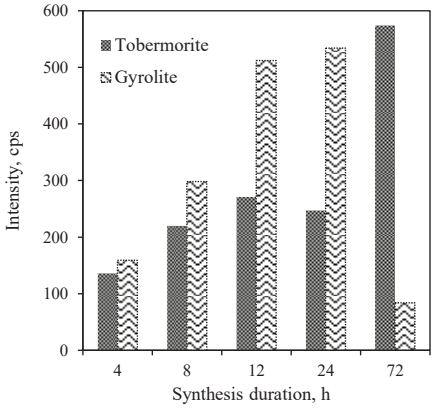

Fig. 3.56. Intensity of tobermorite (d = 1.13 nm) and gyrolite (d = 2.267 nm) peaks obtained from lime-opoka mixture

Simultaneous thermal analysis showed that, in the synthesis products obtained after 4 h, we could identify an exothermic effect at 844 °C (Fig. 3.57, curve 3) which is associated with C-S-H(I), and it is in good agreement with XRD data where only traces of 1.13 nm tobermorite and gyrolite were found (Fig. 3.57, curve 1). The same endothermic effect in the synthesis product obtained after 72 h is observed at a slightly higher temperature, specifically, at 855 °C (Fig. 3.57, curve 4). The results of TG analysis showed that, in the case of decomposition of calcite, the mass loss is 5.2% (4 h; Fig. 3.57, curve 1), and the mass loss in the products obtained after 72 h is 1.11% (4 h; Fig. 3.57, curve 2).

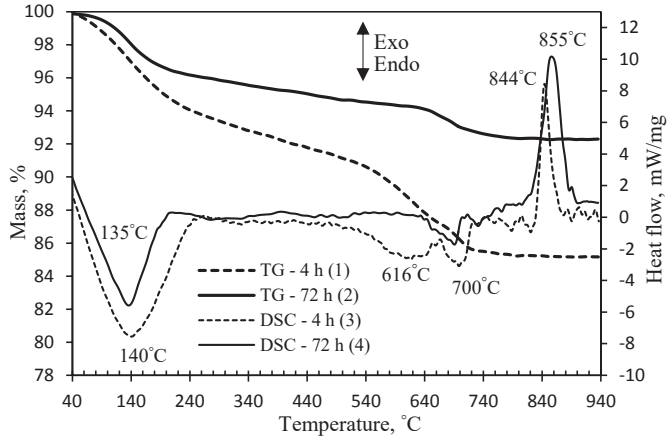

Fig. 3.57. TG (*1*, *2*) and DSC (*3*, *4*) curves of the synthesis products from lime-opoka mixture with CaO/SiO_2 = 0.83 at 220 °C after 4 h (*1*, *3*) and 72 h (*2*, *4*)

These results suggest that much less calcite can be found in the synthesis products obtained after 72 h because a higher amount of stable crystalline compounds is formed. The endothermic effect at 616 °C may be related to two processes – to the dehydration of C-S-H residues and to the decomposition of semi-amorphous calcium carbonates which form during atmospheric carbonization.

The results showed that there was no positive impact on the formation of 1.13 nm tobermorite after increasing the temperature up of hydrothermal synthesis to 220 °C when the molar ratio is $CaO/SiO_2 = 0.83$. For this reason, the CaO content in the initial mixture was increased to improve the formation of tobermorite. It was determined that, after 4 h of isothermal curing at 220 °C ($CaO/SiO_2 = 1.0$), we identified two main compounds: 1.13 nm tobermorite and xonotlite (Fig. 3.58). In the previous results, we determined that xonotlite was identified only after 8 h of synthesis at 200 °C (Fig. 3.43, curve 2). It can be assumed that the formation of xonotlite was accelerated, and a small amount of this compound can be obtained two times faster. Moreover, the intensity of the 1.13 nm tobermorite peak (Fig. 3.59) is three times smaller comparing to the previously obtained results (Fig. 3.45). It can be assumed that the formation of xonotlite goes faster than that of 1.13 nm tobermorite when hydrothermal treatment is carried out at 220 °C.

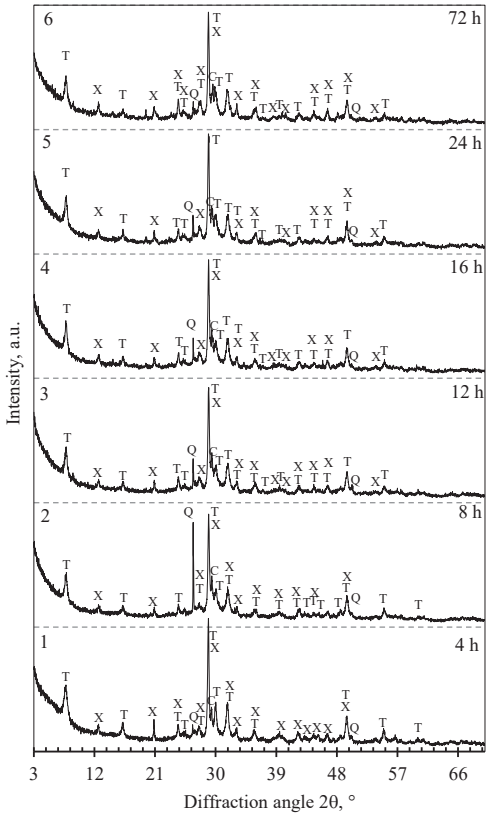

Fig. 3.58. XRD patterns of the synthesis products from lime-opoka mixture with $CaO/SiO_2 = 1.0$ at 220 °C. Indexes: C – calcite, T – 1.13 nm tobermorite, Q – quartz, X – xonotlite

Literature indicates that semi-amorphous C-S-H(I) is formed first, from which, recrystallization into 1.13 nm tobermorite takes place, and then, eventually, the formation of xonotlite begins [173]. It can be summarized that the intensity of the 1.13 nm tobermorite peaks must remain constant, but the intensity of the xonotlite

peaks must increase (Fig. 3.59). In our case, by prolonging the synthesis duration up to 72 h of isothermal curing, the intensity of the 1.13 nm tobermorite peaks remained very similar, but the peaks of xonotlite constantly increased.

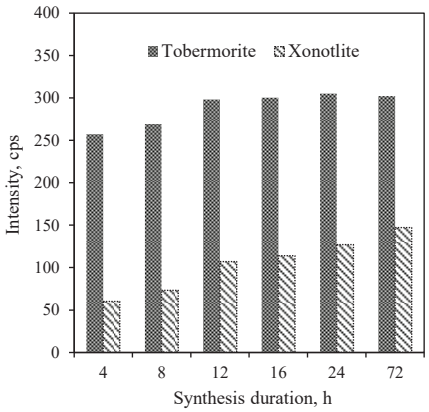

Fig. 3.59. Intensity of tobermorite (d = 1.13 nm) and xonotlite (d = 0.702 nm) peaks obtained from lime-opoka mixture

The results of simultaneous thermal analysis showed that the exothermic effect at 845 °C is related to semi-amorphous C-S-H(I) type of calcium silicate hydrate recrystallization into wollastonite (Fig. 3.60, curves A and B). When comparing the shape of this effect with the exothermic effect occurring in the synthesis product when the molar ratio is CaO/SiO_2 = 0.83, we can show that less C-S-H(I) is obtained. It is in good agreement with the XRD data where xonotlite and 1.3 nm tobermorite are identified. In addition, the thermal effect at a temperature of 700 °C shows the decomposition of calcite (Fig. 3.60, curves 3 and 4). It should be noted that the endothermic effect at 625 °C is related to the decomposition of semi-amorphous calcium carbonates which formed during atmospheric carbonization. The results of TG analysis show that the mass loss is 3.12% (Fig. 3.60, curve 1) and 1.03% (Fig. 3.60, curve 2). The three times lower mass loss indicates that more crystalline compounds are formed after 72 h of hydrothermal synthesis because C-S-H(I) gels can be easily carbonized. These results support the previously made assumption that the formation of the target compound goes much faster when using mixtures with an increased molar ratio when the synthesis temperature is 220 °C. Furthermore, the total mass loss after 4 h of hydrothermal synthesis is 11.53%, whereas the mass loss after 72 h of synthesis is 5.94% (Fig. 3.60, curves 1 and 2).

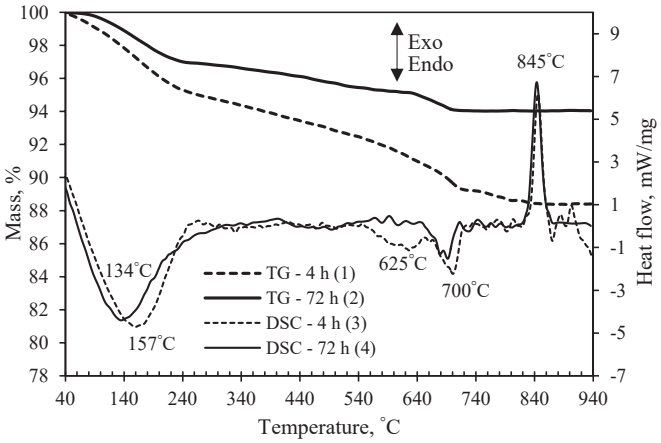

Fig. 3.58. TG (*1*, *2*) and DSC (*3*, *4*) curves of the synthesis products from lime-opoka mixture with CaO/SiO_2 = 1.0 at 220 °C after 4 h (*1*, *3*) and 72 h (*2*, *4*)

In summary, comparing to the previously obtained data at 180 °C and 200 °C (Figs. 3.20 and 3.32), the intensity of the 1.13 nm tobermorite peak is much less prominent. In addition, when comparing the intensity of the 1.13 nm tobermorite peak with the results obtained at 180 °C, the peak is ~2 times lower. Moreover, when the molar ratio is CaO/SiO_2 = 1.0, the intensity is lower by ~5 times than in the synthesis product obtained at 200 °C. It can be concluded that the formation of 1.13 nm tobermorite is slower at 200 °C than at 180 °C. However, the increased temperature impacted the formation of xonotlite as peaks of this compound were identified not after 8 h, but actually much earlier: after 4 h.

3.6. Formation of calcium silicate hydrates in stirred lime-opoka suspensions

During the study of the literature data, we observed that the formation of calcium silicate hydrates goes much faster when the mixture is stirred in an autoclave [96]. In order to verify these statements, hydrothermal synthesis with stirring the mixtures at 50 rpm was investigated. Calcined opoka was selected for further investigation because the best results were obtained when using this material. XRD analysis showed that, at 180 °C, only traces of 1.13 nm tobermorite were identified after 4 h of isothermal curing when the molar ratio was CaO/SiO_2 = 0.83 (Fig, 3.61, curve 1). Therefore, in this curve, we detected intensive peaks of quartz. Furthermore, probably, a large amount of semi-amorphous C-S-H(I) was formed in the synthesis products. It shows a broad peak in the interval from 27° to 31° (d=0.304; 0.278; 0.183 nm) which was identified and is related to the C-S-H(I) compound. The obtained results are supported by literature data [174–177]. The intensity of the tobermorite peak significantly increased after 8 h of hydrothermal synthesis. Moreover, it exceeded 600 cps (Fig. 3.61), and this value is similar to the product obtained under hydrothermal synthesis without stirring (Fig. 3.20). Further

extending of the duration of isothermal curing also showed similarities in the formation of 1.13 nm tobermorite under hydrothermal synthesis without stirring.

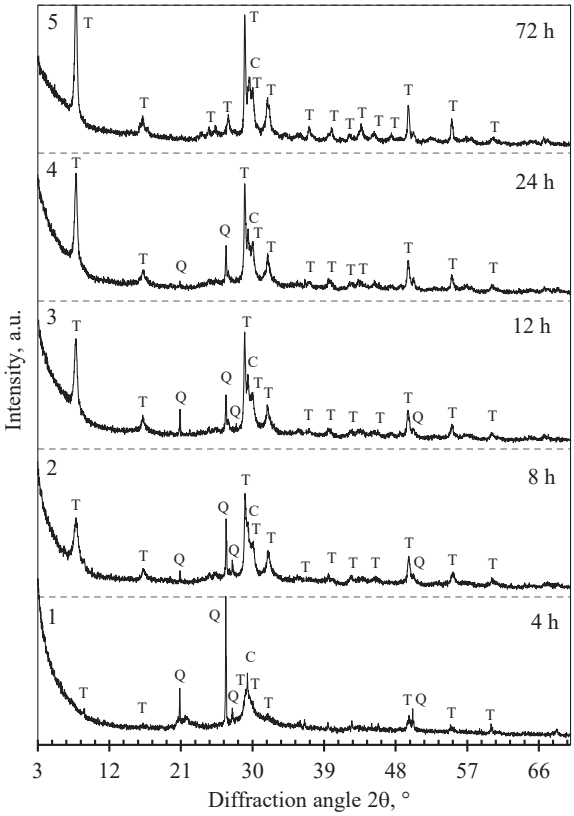

Fig. 3.61. XRD patterns of hydrothermal synthesis from opoka-lime mixture with CaO/SiO_2 = 0.83 at 180 °C under 50 rpm stirring. Indexes: C – calcite, T – 1.13 nm tobermorite, Q – quartz

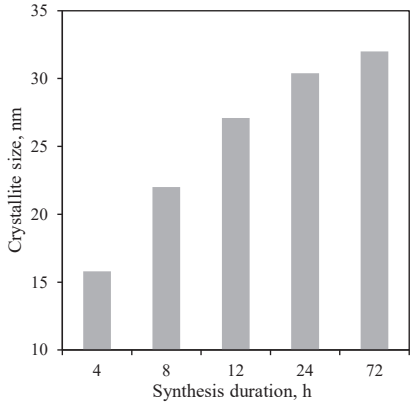

Fig. 3.62. Dependence of the crystallite size on the duration of synthesis from lime-opoka mixture

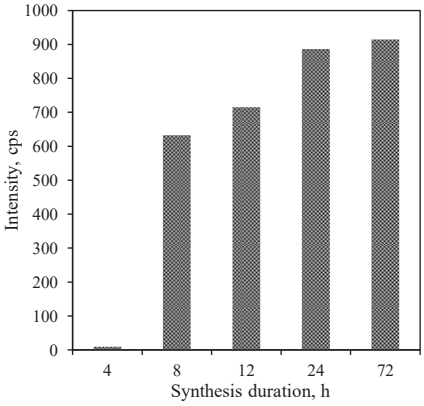

Fig. 3.63. Intensity of the tobermorite (d = 1.13 nm) peak obtained from lime-opoka mixture

The crystallite size after 8 h of synthesis is only 22 nm (Fig. 3.63). When comparing these results with the synthesis in an unstirred suspension, the size of the crystallites is 25% smaller. Furthermore, when prolonging the hydrothermal treatment, the size of crystallites increases, but, after 72 h of synthesis, it is still by ~25% (Fig. 3.63) smaller than for the crystallites obtained in unstirred suspensions (Table 3.2).

The data of simultaneous thermal analysis of hydrothermal synthesis by stirring at 50 rpm is shown in Figure 3.64. Its profile is very similar to the profile of the curves of the products synthesized in unstirred suspensions under the same conditions (Fig. 3.21). The only noticeable difference is that, in the stirred suspension, after 4 h of synthesis together with C-S-H(I), C-S-H(II) also coexists. This is evidenced by the effect of recrystallization into wollastonite – it is double, wide and blunt, shifted towards higher temperatures.

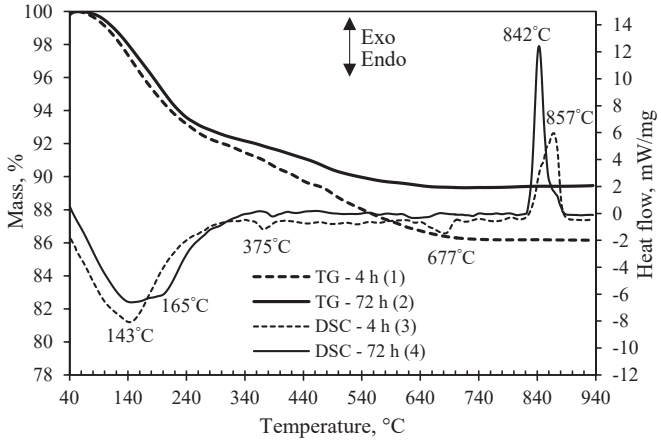

Fig. 3.64. TG (*1*, *2*) and DSC (*3*, *4*) curves of the synthesis products from lime-opoka mixture with CaO/SiO_2 = 0.83 at 180 °C under stirring at 50 rpm after 4 h (*1*, *3*) and 72 h (*2*, *4*)

However, oppositely, as it was stated in literature, the results under these conditions (when suspensions are stirred at 50 rpm) do not improve the formation of 1.13 nm tobermorite; the results are similar. It can be stated that the main reason for this phenomenon is the too low mixing intensity which results in the solid part of the suspension settling on the bottom of the autoclave (the planetary mixer does not sufficiently homogenize the suspension). Thus, we obtained the same system as in the case with the suspension without stirring.

To finally make sure, our syntheses were performed at 200 °C, while stirring the suspensions at the same speed. It was determined that 1.13 nm tobermorite is dominating in the synthesis product after 4 h of hydrothermal synthesis (Fig. 3.65, curve 1). Meanwhile, in the previous results, when hydrothermal synthesis was performed at 180 °C, the peak intensity of 1.13 nm tobermorite was significantly lower. Furthermore, the size of crystallites was smaller too.

XRD results show that, when prolonging the duration of hydrothermal synthesis, the peaks of 1.13 nm tobermorite slightly increased (Fig. 3.65, curves 4 and 5). However, the peaks of quartz continued to decrease, and, after 72 h of isothermal curing, only traces of the compound were left.

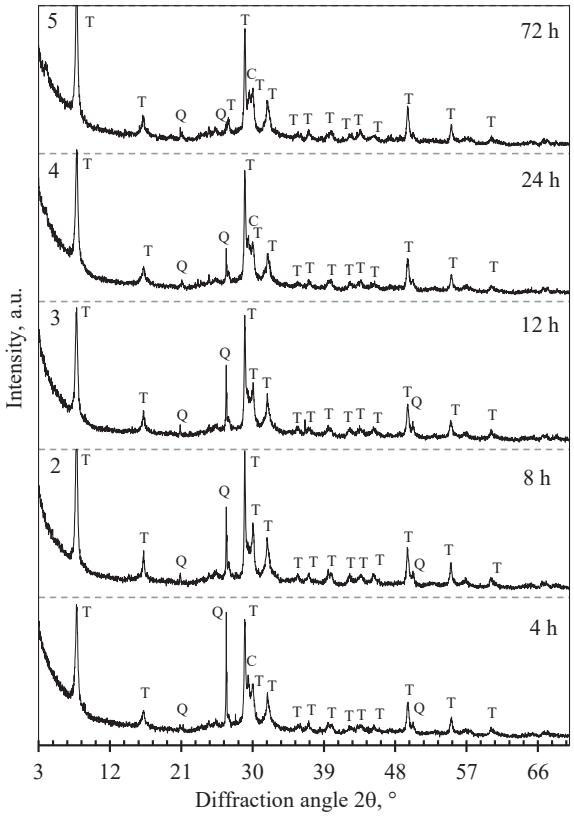

Fig. 3.65. XRD patterns of the hydrothermal synthesis from opoka-lime mixture with CaO/SiO_2 = 0.83 at 200 °C under 50 rpm stirring. Indexes: C – calcite, T – 1.13 nm tobermorite, Q – quartz

However, comparison of the results when the suspensions were mixed or were not mixed during hydrothermal treatment yielded conflicting data. The intensity of the 1.13 nm tobermorite peak after 4 h of hydrothermal synthesis is ~16% higher when the suspension is stirred (Fig. 3.65) than in a non-stirred system (Fig. 3.32). Moreover, this trend persists for up to 12 h of synthesis. However, with the further prolongation of the isothermal curing duration, the intensity of the 1.13 nm peak is higher when the suspensions are not stirred. On the other hand, the size of tobermorite crystallites was bigger by ~17% when the suspensions were stirred (Fig. 3.67 and Fig. 3.31). Moreover, the size of tobermorite crystallites after 8 h of hydrothermal synthesis at 200 °C was bigger by ~42% (Fig. 3.66) than for the case when the synthesis was carried out at 180 °C (Fig. 3.19). With further prolonging of hydrothermal synthesis duration, these tendencies persist, and the difference reaches as much as 2 times (at 200 °C – 88.7 nm, and at 180 °C – 44.4 nm). In general,

comparing with the previously obtained results (Figs. 3.19 and 3.31), the largest crystallites were obtained by stirring the suspension at 200 °C (Fig. 3.66). However, it can be concluded that the increase in the synthesis temperature rather than the moderate stirring intensity has a greater influence on the processes of 1.13 nm tobermorite formation.

Considering that autoclaves in which the suspension can be mixed are much more complex and expensive in construction, and the obtained added value is insignificant, it is recommended to synthesize 1.13 nm tobermorite from lime-calcined opoka mixtures without stirring.

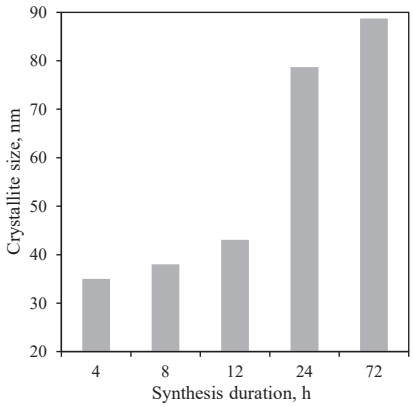

Fig. 3.66. Dependence of the tobermorite crystallite size on the duration of synthesis from lime-opoka mixture

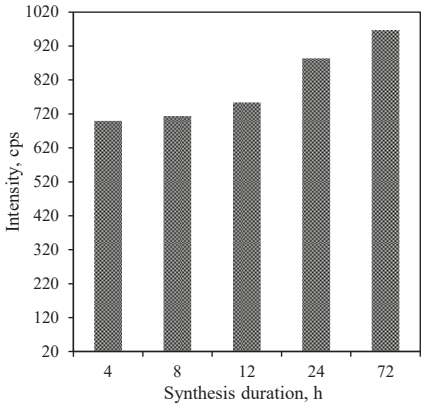

Fig. 3.67. The intensity of the tobermorite (d = 1.13 nm) peak obtained from lime-opoka mixture

The results of simultaneous thermal analysis of the product obtained after 4 h of hydrothermal synthesis by stirring at 50 rpm is presented in Figure 3.66. It was determined that the dehydration effect occurred in the temperature range between 100–250 °C; the mass loss was 6.32%; meanwhile, the overall mass loss was 11.3% (Fig. 3.68, curve 1). Comparing these results to the data obtained after 72 h of synthesis, TG analysis showed that the mass loss is 6.23%, but the overall mass loss is 12.1% (Fig. 3.68, curve 2). It can be assumed that the quantity of calcium silicate hydrates is similar, but a bigger quantity of 1.13 nm tobermorite was obtained after 72 h. It is in good agreement with the result where the size of 1.13 nm tobermorite crystallites increases significantly (Fig. 3.67). Moreover, after 72 h of synthesis, less C-S-H(I) and more tobermorite was obtained because the heat flow of the exothermic effect at 841 °C (C-S-H(I) recrystallization into wollastonite) decreased from 12.5 to 10 $mW \cdot mg^{-1}$ (Fig. 3.68, curve 4). The other thermal effect in the DSC curve was identified at a temperature of when 664 °C; it is related with the decomposition of calcite, and this endothermic effect is very weak – the data of TG analysis showed less than 0.5% mass loss (Fig. 3.68, curve 1).

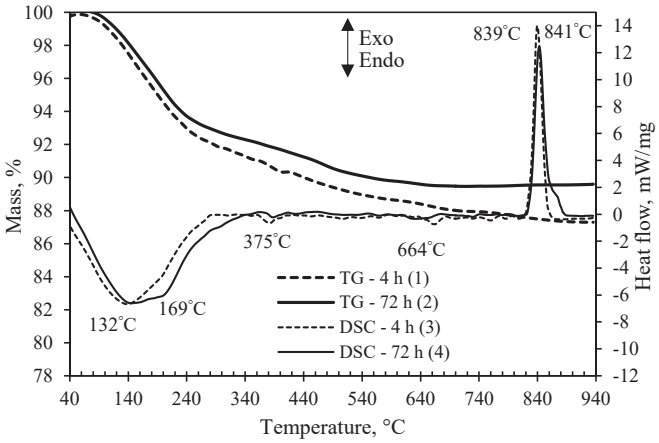

Fig. 3.68. TG (*1*, *2*) and DSC (*3*, *4*) curves of the synthesis products from lime-opoka mixture with CaO/SiO_2 = 0.83 at 200 °C under stirring at 50 rpm after 4 h (*1*, *3*) and 72 h (*2*, *4*)

The obtained results (Figs. 3.38 and 3.43) showed that the formation of tobermorite and xonotlite was improved when using mixtures with an increased content of calcium oxide. For this reason, the mixture with molar ratio 1.0 was examined (Fig. 3.69). It was determined that, in the XRD curve after 4 h of isothermal curing at 180 °C, only traces of 1.13 nm tobermorite are observed (Fig. 3.69, curve 1). Moreover, even after 8 h of hydrothermal synthesis, we identified very weak main peaks of the target compound (Fig. 3.69, curve 2). Compared to the previously obtained results, recrystallization of the target compound from C-S-H(I) was much quicker even using granite as a raw material (Fig. 3.6, curve 1). Moreover, the slower recrystallization also took place after 12 h of hydrothermal synthesis where intensive peaks of 1.13 nm tobermorite were identified (Fig. 3.69, curve 3). However, the intensity of diffraction peaks remains the same after 24 h of hydrothermal curing or even after 72 h of hydrothermal curing (Fig. 3.69, curve 5). Compared to the synthesis products obtained in the unstirred suspension, xonotlite was identified as early as after 4 h of hydrothermal synthesis (Fig. 3.59). This is one more result which shows that the rate of recrystallization decreases during stirring at 50 rpm.

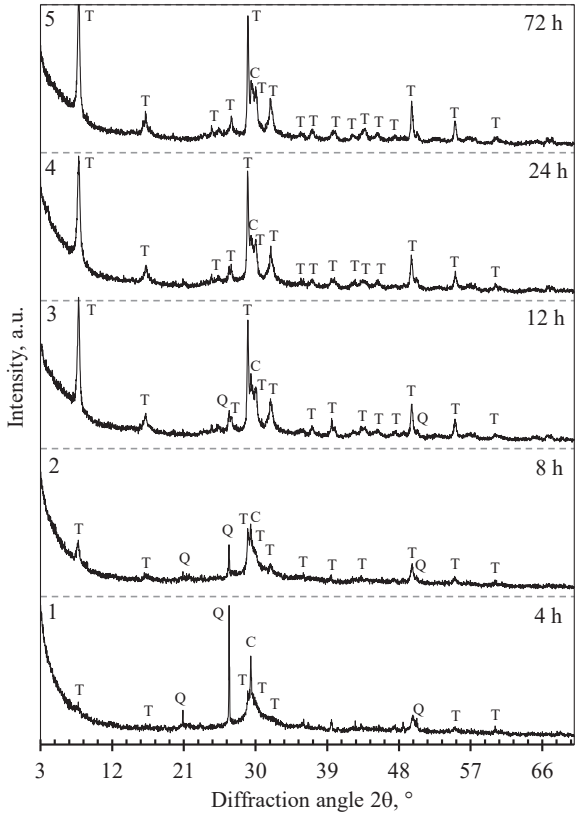

Fig. 3.69. XRD patterns of hydrothermal synthesis from opoka-lime mixture with CaO/SiO_2 = 1.0 at 180 °C under 50 rpm stirring. Indexes: C – calcite, T – 1.13 nm tobermorite, Q – quartz

The synthesis products obtained after hydrothermal curing at 180 °C when the molar ratio equals CaO/SiO_2 = 1.0 under stirring at 50 rpm was examined by simultaneous thermal analysis (Fig 3.70). Due to the reason that the intensity of the 1.13 nm tobermorite peak is low after 4 h of hydrothermal synthesis, the sample obtained after 12 h of synthesis was selected. It was determined that a strong exothermic effect at 836 °C was detected in the sample obtained after 12 h of hydrothermal synthesis (Fig 3.70, curve 3), and this effect is related to the recrystallization of C-S-H(I) into wollastonite. Meanwhile, in the DCS curve of the sample obtained after 72 h of synthesis, we identified an exothermal effect at 842 °C (Fig 3.70, curve 4). In comparison, the heat flow of these effects decreased from 24 mW/mg to 19 mW/mg when the duration of hydrothermal synthesis was extended. It is in good agreement with the previously obtained data, and we thus made an assumption that the quantity of C-S-H(I) can be reduced by prolonging the duration of hydrothermal treatment.

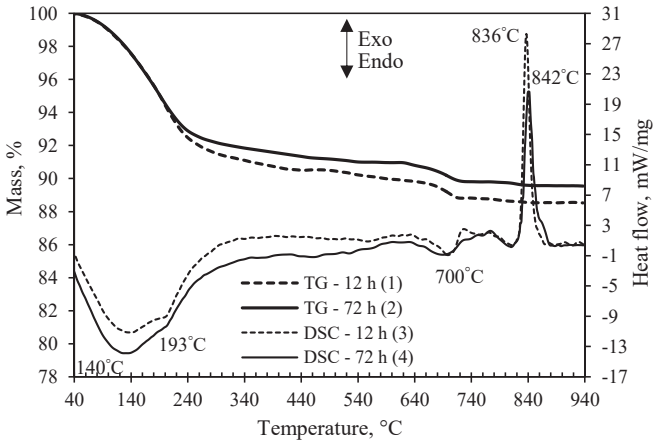

Fig. 3.68. TG (*1*, *2*) and DSC (*3*, *4*) curves of the synthesis products from lime-opoka mixture with CaO/SiO_2 = 1.0 at 180 °C under stirring at 50 rpm after 12 h (*1*, *3*) and 72 h (*2*, *4*)

It can be assumed that, when stirring at 50 rpm and using mixtures with the molar ratio equaling to CaO/SiO_2 = 1.0, xonotlite does not form. Due to this reason, in order to improve the formation of this compound, the synthesis temperature was raised to 200 °C. It was determined that, after 4 h of hydrothermal synthesis, we identified much higher intensity peaks of 1.13 nm tobermorite than in the synthesis product at 180 °C. Moreover, xonotlite was still not identified after synthesis of short duration (Fig. 3.71, curve 1). However, in the synthesis product after hydrothermal synthesis duration extended to 8 h together with 1.13 nm tobermorite, xonotlite was also identified (Fig. 3.71, curve 2). Furthermore, the intensity of the xonotlite peak significantly increased after hydrothermal synthesis prolonged up to 12 h (Fig. 3.73). Meanwhile, the intensity of the 1.13 nm tobermorite peak significantly increased as well (Fig. 3.73). Moreover, the intensity of the 1.13 nm tobermorite peak after 24 h of hydrothermal synthesis decreased. Further investigations showed that the intensity of 1.13 nm tobermorite continued to decrease even after 72 h of synthesis; meanwhile, the intensity of xonotlite was constantly increasing (Fig. 3.73). As literature indicates, xonotlite recrystallizes from tobermorite; due to this reason, with further prolonging of hydrothermal synthesis, the quantity of tobermorite was constantly decreasing. This leads to the highest intensity of the xonotlite peak after 72 h of hydrothermal synthesis and surpasses even the results obtained at 220 °C (Fig. 3.59) when the synthesis was performed under unstirred suspensions (Fig. 3.58, curve 1).

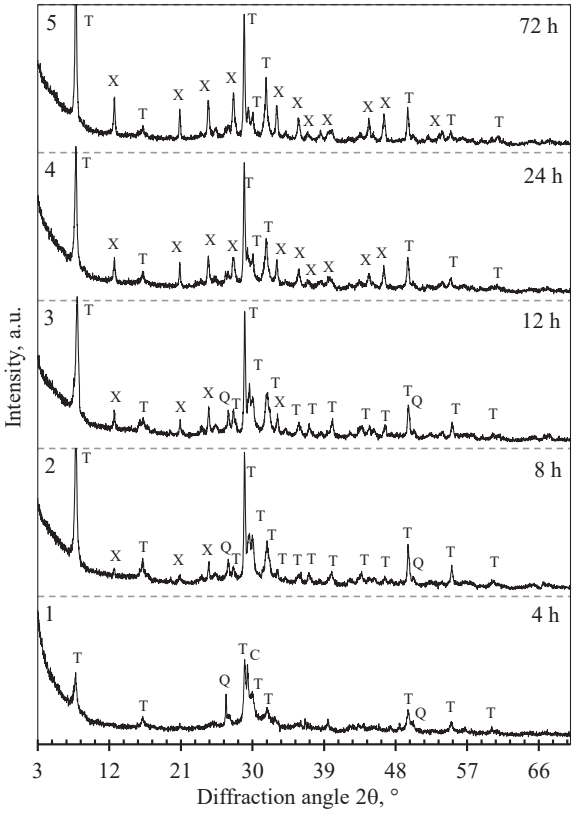

Fig. 3.69. XRD patterns of hydrothermal synthesis from opoka-lime mixture with CaO/SiO_2 = 1.0 at 200 °C under 50 rpm stirring. Indexes: C – calcite, T – 1.13 nm tobermorite, Q – quartz

The size of tobermorite crystallites from 33.1 nm increased up to 34.7 nm after 12 h of isothermal curing (Fig. 3.72). Meanwhile, the intensity of the 1.13 nm tobermorite peak increased 6 times (Fig. 3.73). By prolonging the duration of hydrothermal synthesis from 12 h to 24 h, the size of tobermorite crystallites remained unchanged. However, the size of xonotlite crystallites slightly increased (Fig. 3.72). Moreover, the size of the crystallites of this compound continues to increase by further extending the duration of hydrothermal synthesis up to 72 h.

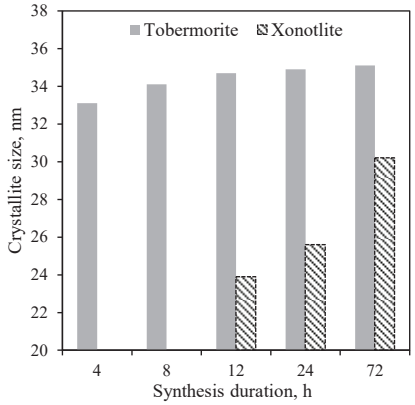

Fig. 3.70. Dependence of the tobermorite and xonotlite crystallite size on the duration of synthesis from lime-opoka mixture

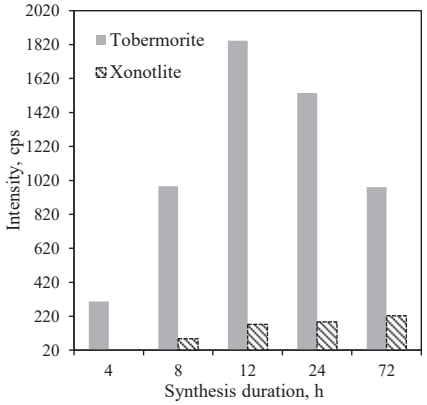

Fig. 3.71. Intensity of the tobermorite (d = 1.13 nm) peak and xonotlite (d = 0.702 nm) obtained from lime-opoka mixture

The STA data of products obtained after 12 h of synthesis at 200 °C under stirring at 50 rpm is presented in Figure 3.72. The endothermic effect at 204 °C indicates that 1.13 nm tobermorite is formed. The main exothermic effects were detected at 840 °C and 844 °C (Fig. 3.74, curves 3 and 4). Moreover, at this thermal effect (related to C-S-H(I) recrystallization into wollastonite), the heat flow from 20.63 mW/mg (Fig. 3.74, curve 3) decreased to 14.62 mW/mg (Fig. 3.74, curve 4). When summarizing these results, it can be stated that the amount of semi-amorphous C-S-H(I) compound was lower after a longer duration of synthesis. This result is in good agreement with our XRD data where we identified intensive peaks of xonotlite after 72 h of synthesis.

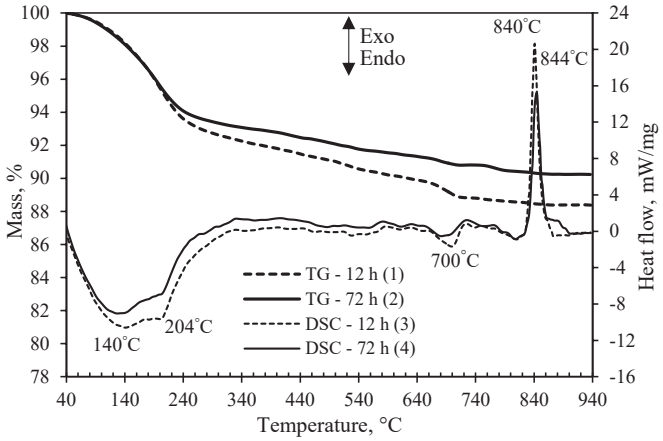

Fig. 3.72. TG (*1*, *2*) and DSC (*3*, *4*) curves of synthesis products from lime-opoka mixture with CaO/SiO_2 = 1.0 at 200 °C under stirring at 50 rpm after 12 h (*1*, *3*) and 72 h (*2*, *4*)

Therefore, by stirring the suspensions at an already low rate (50 rpm), the processes of xonotlite formation intensify. Some literature data suggests too that the

formation of this compound is accelerated by stirring the suspensions [91, 109, 180]. However, the literature data on the positive influence of mixing intensity on xonotlite synthesis is difficult to compare with each other because of the different raw materials, equipment, hydrothermal treatment parameters being used. For these reasons, it is worth investigating in detail the influence of the mixing intensity on the formation processes of the target compounds. Hydrothermal synthesis at 200 °C for 12 h by stirring at 120–300 rpm when CaO/SiO_2 = 1.0 was examined. It was determined that, under stirring at 120 rpm, in the synthesis products, 1.13 nm tobermorite of the highest crystallinity degree (according to Taylor) together with xonotlite is formed (Fig. 3.75, curve 1) [40, 46]. Further increase of stirring intensity had no effect as analogous products were obtained (Fig. 3.75, curves 2–5).

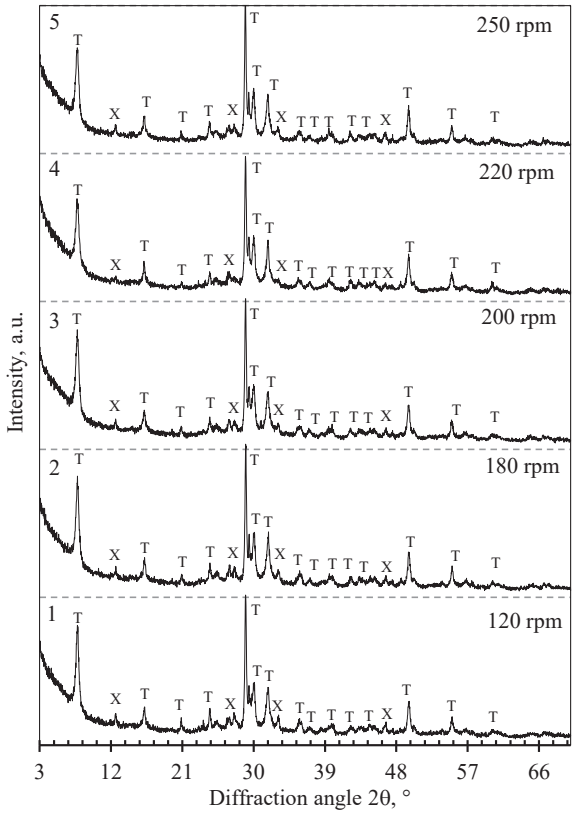

Fig. 3.73. XRD patterns of hydrothermal synthesis after 12 h under different stirring rate from lime-opoka mixture with CaO/SiO_2 = 1.0 at 200 °C. Indexes: C – calcite, T – 1.13 nm tobermorite, Q – quartz

It should be underlined that the stirring rate during hydrothermal synthesis has a significant impact on the consistency of the suspension. Moreover, the formed calcium silicate hydrates physically bind a large amount of water and acquire consistency which is thicker than water. The relative volume of the synthesis product is the ratio of the volume of the synthesis product after 24 hours of

sedimentation in a measuring cylinder and the mass of the product mixture. This relative volume increases steadily with the increasing stirring rate (Table 3.6).

Table 3.6. Ratio of volume and solid material mass after 24 h of sedimentation

Stirring rate, rpm	120	180	200	220	250	300
Relative volume after 24 h	7	7.5	10	11	13.5	15

It was determined that the higher is the relative volume of the suspension, the lower is the average density of thermal insulation products that can be formed [181]. For this reason, in order to obtain suspensions which are characterized by a higher relative volume, synthesis must be performed under 300 rpm stirring in further studies.

Summarizing the obtained results, we can state that stirring at 180 °C has virtually no effect on 1.13 nm tobermorite and xonotlite formation. A small positive effect was observed at a temperature of 200 °C as increasing the stirring intensity from 0 to 50 and 120 rpm increases the degree of crystallinity of the formed 1.13 nm tobermorite. In addition, compared to unstirred suspensions, the processes of xonotlite formation are slightly intensified. Further increasing the stirring intensity to 300 rpm no longer has a noticeable effect on the mineralogical composition of the product.

3.7. Formation of products in which the predominant compound is xonotlite

Many researchers suggest that, in order to obtain xonotlite via mixtures of hydrothermal synthesis, with a molar ratio equaling to $CaO/SiO_2 = 1.0$ have to be used [182]. However, according to our obtained results, the formation of the target compound is difficult under all experimental conditions. It was determined that, in all the cases, xonotlite was not detected when the granite sawing waste was used. Further studies showed that xonotlite was formed when using mixtures prepared form calcined opoka only when the temperature was set at 200 °C under unstirring hydrothermal synthesis after 8 h (Fig. 3.43, curve 2). Similar results were obtained in the stirred at 50 rpm suspensions (all other conditions were the same). Moreover, minor improvement on hydrothermal synthesis was observed during hydrothermal synthesis with mixtures being stirred at 250 rpm where the intensity of the target compounds slightly increased (Fig. 3.75, curve 5). Furthermore, significant acceleration of the formation of xonotlite was observed in the synthesis products obtained at 220 °C under unstirred suspension after 4 h of isothermal curing (Fig. 3.58, curve 1). Due to these reasons, we performed hydrothermal synthesis at 220 °C under stirring at 300 rpm while using a mixture from lime and calcined opoka when the molar ratio equals to $CaO/SiO_2 = 1.0$, and the obtained products were examined by XRD analysis. It was determined that the formation of xonotlite was increased two times when the synthesis temperature was increased from 200 °C to 220 °C. Due to this reason, we investigated the formation of the synthesis products at an elevated temperature (220 °C) while using mixtures from calcined opoka when the

molar ratio was $CaO/SiO_2 = 1.0$ under stirring at 300 rpm. It was found that xonotlite was detected in the synthesis product as early as after 4 hours of isothermal curing (Fig. 3.76, curve 1). However, this compound coexists together with 1.13 nm tobermorite.

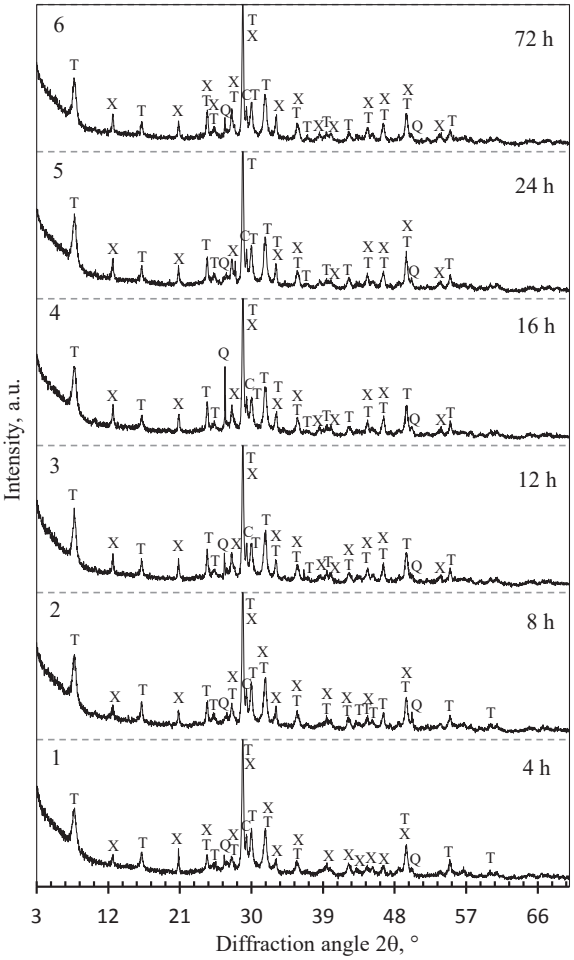

Fig. 3.76. XRD patterns of hydrothermal synthesis products from opoka-lime mixture with $CaO/SiO_2 = 1.0$ at 220 °C under 300 rpm stirring. Indexes: C – calcite, T – 1.13 nm tobermorite, Q – quartz, X – xonotlite

It was determined that xonotlite forms in a shorter time than in the previous cases (as early as after 8 h; see Fig. 3.71), and the intensity of this compound is ~2 times higher than in a non-stirred suspension (Fig. 3.59). By prolonging the duration of hydrothermal synthesis up to 8 h, the intensity of the xonotlite peak increased significantly (Fig. 3.77). Furthermore, investigations showed that the intensity of the xonotlite peak constantly increases (Fig. 3.77). Therefore, the intensity of this compound formed at 220 °C temperature is higher by ~35% than in the previous results where the mixture was not stirred at all (Fig. 3.45).

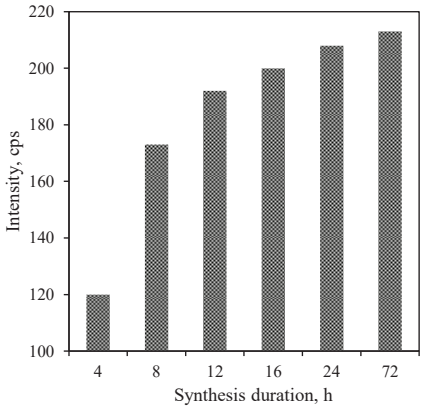

Fig. 3.77. Intensity of the xonotlite (d = 0.702 nm) peak obtained from lime-opoka mixture

Differential scanning calorimetry data within the 100–240 °C temperature range showed a very broad and vaguely expressed dehydration effect which is related to water removal from 1.13 nm tobermorite and semi-amorphous calcium silicate hydrate of the C-S-H(I) type without a clearly expressed crystal lattice (Fig. 3.78). As mentioned in *Introduction*, this compound forms when the synthesis duration is insufficient, or when the molar ratio of the mixture is disturbed. The endothermal effect at ~710 °C shows the decomposition of calcite. However, the exothermic process at 840–845 °C is clearly visible in the DSC curve. This effect is associated with the recrystallization of C-S-H(I) to wollastonite. It should be noted that the value of heat released during this process decreased from 13.0 mW (4 h) to 8.5 mW (12 h), and up to 7.5 mW (72 h) (Fig. 3.78, curves 1–3).

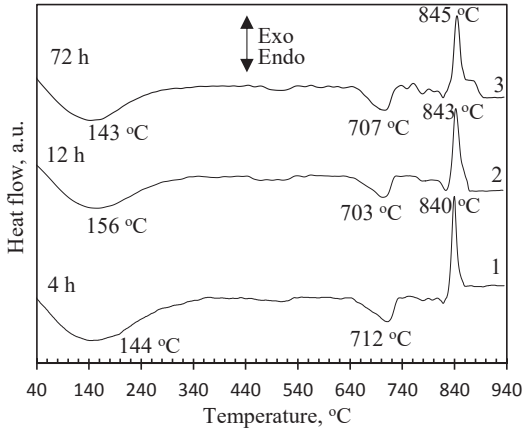

Fig. 3.78. DSC curves of hydrothermal synthesis products from opoka-lime mixture with CaO/SiO_2 = 1.0 at 220 °C under 300 rpm stirring. Indexes: C – calcite, T – 1.13 nm tobermorite, Q – quartz, X – xonotlite

It can be assumed that, when using mixtures with a molar ratio equaling to $CaO/SiO_2 = 1.0$, in all the cases, xonotlite was formed together with other low-base calcium silicate hydrates. This leads to the assumption that the molar ratio in opoka-lime mixtures is too low for pure xonotlite formation via hydrothermal synthesis. One of the reasons may be that not all CaO was involved in the formation of calcium silicate hydrates: part of it reacted with impurities in opoka and 2.95% of CaO was in the composition of $CaCO_3$ which was left after calcination of opoka at 775 °C. Increasing the calcination temperature is very problematic because, during the decomposition of carbonates, the obtained CaO is highly reactive, and, together with silica, wollastonite is formed. Due to this reason, the molar ratio of CaO/SiO_2 in the reactive media can be lower than 1.0. Moreover, as mentioned in *Introduction*, 1.13 nm tobermorite is closely related to xonotlite by its structure and synthesis mechanism. Therefore, the lower molar ratio is more favorable for 1.13 nm tobermorite formation than it is for xonotlite.

Due to this reason, it was decided to increase the molar ratio up to $CaO/SiO_2 = 1.2$ and investigate the formation of xonotlite (Fig. 3.79) in this particular case. It was determined that, under the same synthesis conditions, the reaction sequence in the products with this molar ratio changes significantly.

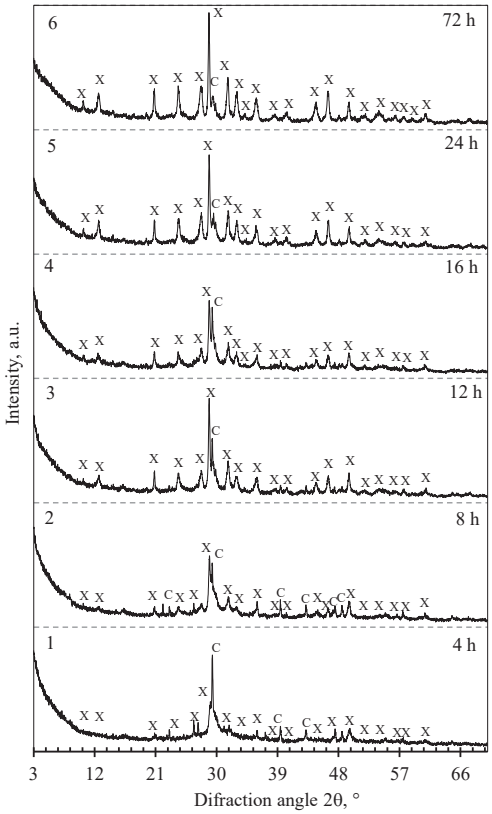

Fig. 3.79 XRD patterns of hydrothermal synthesis products from opoka-lime mixture with $CaO/SiO_2 = 1.2$ at 200 °C under 300 rpm stirring. Indexes: C – calcite, X – xonotlite

Therefore, even after 4 h of isothermal curing at 200 °C, only traces of xonotlite were identified (Fig. 3.79, curve 1). The main peaks of xonotlite after 8 h of hydrothermal synthesis began to dominate in the synthesis product (Fig. 3.79, curve 2). In addition to that, neither in the mixture with $CaO/SiO_2 = 1.2$ nor in 1.13 nm tobermorite or in any other crystalline calcium silicate hydrates were formed. Furthermore, calcite was identified together with xonotlite which originated from raw materials and partially from the carbonization of hydrothermal synthesis products during drying.

The main peak (d = 0.702 nm) intensity of xonotlite in the XRD curve gradually but constantly increases while prolonging the synthesis duration up to 16 h (Fig. 3.80). Moreover, the intensity of this compound after 24 h of isothermal curing increased significantly, and the value remained unchanged after 72 h. Nevertheless, the size of the crystallites of this compound even after 72 h is ~20% bigger than in the products obtained after 72 h of synthesis under stirring when the molar ratio is $CaO/SiO_2 = 1.0$.

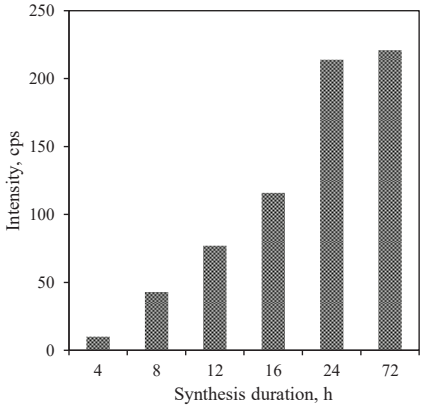

Fig. 3.80. Intensity of the xonotlite (d = 0.702 nm) peak obtained from lime-opoka mixture

In summary, in the mixtures with $CaO/SiO_2 = 1.2$, the formation of xonotlite at 200 °C is slow because, after 4 h of synthesis, only traces were identified. However, another important difference was observed that 1.13 nm tobemorite is no longer formed in this mixture. In order to improve the formation of xonotlite, it was decided to increase the synthesis temperature.

The results of the XRD analysis of hydrothermal synthesis at 220 °C when using mixtures with the molar ratio $CaO/SiO_2 = 1.2$ when stirring was carried out at 300 rpm is presented in Figure 3.81. It was determined that the formation of xonotlite is extremely rapid, and, as early as after 4 h of hydrothermal curing, it was identified as the main compound (Fig. 3.81, curve 1). It should be noted that in the synthesis product we could not identify even traces of quartz. Furthermore, and most importantly, no other crystalline calcium silicate hydrates were found.

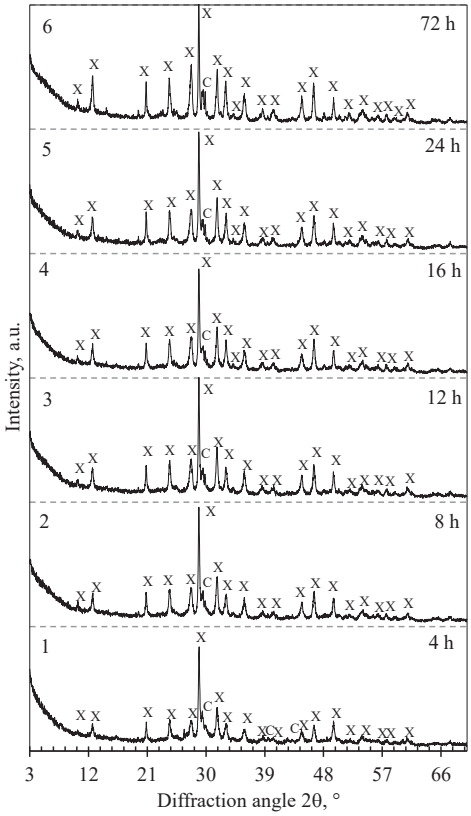

Fig. 3.81. XRD patterns of the hydrothermal synthesis products from opoka-lime mixture with CaO/SiO_2 = 1.2 at 220 °C under 300 rpm stirring. Indexes: C – calcite, X – xonotlite

It was determined that the size of crystallites significantly increased after prolonging hydrothermal synthesis (Fig. 3.83). Moreover, the size of xonotlite crystallites is bigger by ~1.5 times when the synthesis temperature was 20 °C lower (while all other conditions were the same). It should be noted that the crystallite size of this compound was also bigger compared to the previously obtained results. Furthermore, the intensity of the xonotlite peak after 8 h of isothermal curing increased, and, after 72 h of hydrothermal synthesis, the intensity increased significantly (Fig. 3.82). In addition, the intensity of this peak is ~2 times higher comparing with the obtained results when the temperature of hydrothermal synthesis was 200 °C (Fig. 3.77). Moreover, the intensity of the xonotlite peak is even higher than any other results which have been obtained previously (Figs. 3.34, 3.59, 3.80). In summary, indirectly, the results showed that the highest amount of xonotlite was obtained via hydrothermal synthesis at 220 °C when using mixtures with the molar ratio CaO/SiO_2 = 1.2 while stirring at 300 rpm.

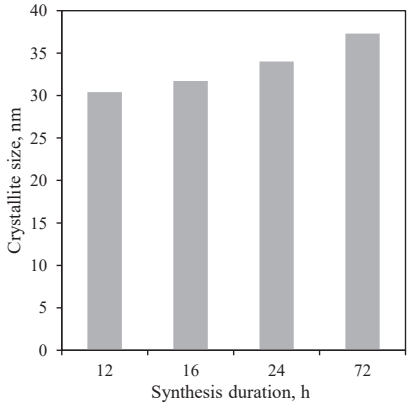

Fig. 3.82. Dependence of the xonotlite (d = 0.702 nm) crystallite **s**ize on the duration of synthesis from lime-opoka mixture

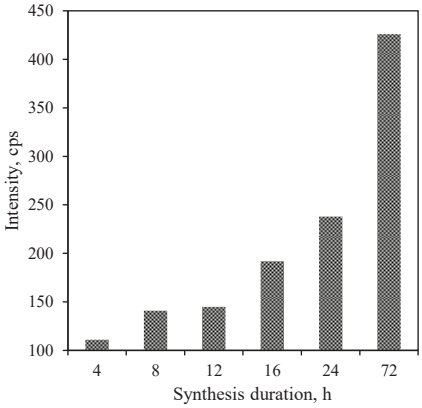

Fig. 3.83. Intensity of the xonotlite (d = 0.702 nm) peak obtained from lime-opoka mixture

The exothermic effect at 842 °C identified in the DSC curve suggests that, in the synthesis products obtained after 4 h of hydrothermal synthesis, there is some quantity of C-S-H(I) (Fig. 3.84, curve 1). However, this exothermic effect in the sample obtained after 12 h of synthesis decreased significantly, and only a blurred signal was captured (Fig. 3.84, curve 2). Comparing the exothermic effect of products after 4 h and 12 h curing, the heat flow decreased from 3.0 mW to 1.03 mW. Such results indicate that very small amounts of semi-amorphous compounds are formed under these conditions. It should be underlined that literature data shows that, when xonotlite recrystallizes into wollastonite, it does not produce any thermal effect (155). Hence, in this case, an exothermic effect occurs only when semi-amorphous C-S-H(I) recrystallizes. This is in good agreement with the XRD data as only intensive peaks of xonotlite were identified. In the DSC curve, we identified an exothermic effect at 845 °C, which suggests that xonotlite already dominates in products obtained after 12 h hydrothermal synthesis. In addition, in the DSC curve, we identified an endothermic effect at 723 °C (after 4h), which is related to the decomposition of calcite. Moreover, the same effects are identified after 12 h and 72 h of hydrothermal synthesis.

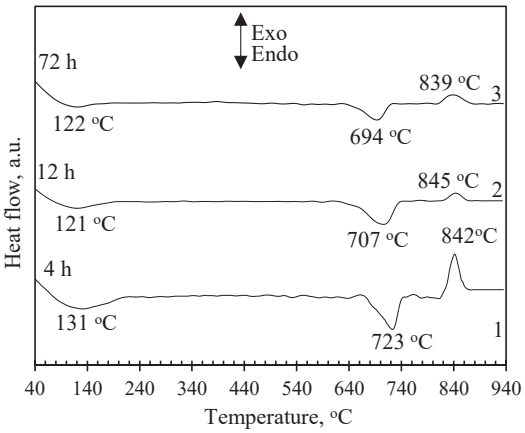

Fig. 3.84. DSC curves of hydrothermal synthesis at 220 °C of products from opoka-lime mixture with $CaO/SiO_2 = 1.2$

To summarize, the following technological parameters should be selected for the production of high temperature thermal insulating products with predominant xonotlite obtained from lime-opoka mixture: the molar ratio of the raw meal $CaO/SiO_2 = 1.2$; water/solid ratio W/S = 20.0; duration of hydrothermal treatment at 220 °C from 4 h to 12 h while stirring the suspension at 300 rpm.

3.8. Evaluation of the suitability of opoka for the production of heat-resistant thermal insulating materials from xonotlite

One of the essential requirements for thermal insulating products is their minimal shrinkage at a high temperature. Since semi-amorphous C-S-H(I) and C-S-H(II) type calcium silicate hydrates are not denoted by a clear crystalline structure, their shrinkage during recrystallization into wollastonite is very high. The structures of the crystal lattice of xonotlite and wollastonite are very similar; therefore, shrinkage during this recrystallization process is negligible. It means that the mineralogical composition of the products determines their working temperature. The change in the linear dimensions of the material and its ability to withstand the effects of a high temperature can be predetermined by the dilatometry analysis method. By using this method, 4 samples of synthesized powder were investigated to select the optimal conditions for the production of precursors for thermal insulating products.

The linear shrinkage in the temperature range of 300–1000 °C of the sample obtained at 200 °C under stirring at 300 rpm after 8 h was found to be very high at almost 15% (Fig. 3.85, curve 1). This result suggests that a particularly small quantity of crystalline compounds was formed under these conditions. By prolonging the duration of hydrothermal synthesis up to 24 h, the XRD curve of the obtained product shows that the peak intensities of the formed xonotlite are much higher (Fig. 3.79, curve 5, and Fig. 3.80). Due to this reason, the linear shrinkage of the sample decreases significantly up to 2.48% (Fig. 3.85, curve 2); however, it still

remains too high as it should not exceed 2% according to the requirements of the relevant standards.

For this reason, samples synthesized at 220 °C were analyzed. They are characterized by an even higher linear dimension stability – the shrinkage of the sample obtained after 4 h of synthesis was 1.68% (Fig. 3.85, curve 3). The obtained results support the presumption that the increased temperature improves the formation of xonotlite via hydrothermal synthesis, and the quantity of this compound increases. Moreover, the synthesis products obtained after 12 h of hydrothermal synthesis show an even lower linear shrinkage – only 0.86% (Fig. 3.85, curve 4). Furthermore, samples only shrink within the temperature range of 750–850 °C. These results are in good agreement with the data of the analysis of the mineralogical composition of the product. As it can be seen in the DSC curves, after 4 h of synthesis, there still remains a small amount of C-S-H(I) (Fig. 3.84, curve 1), while, after 12 h, this compound is no longer visible (Fig. 3.84, curve 2). These results confirm that the highest quantity of xonotlite from the lime-opoka mixture was obtained at 220 °C when the molar ratio was $CaO/SiO_2 = 1.2$. For this reason, all the precursors (suspensions) of thermal insulation products were further synthesized at 220 °C.

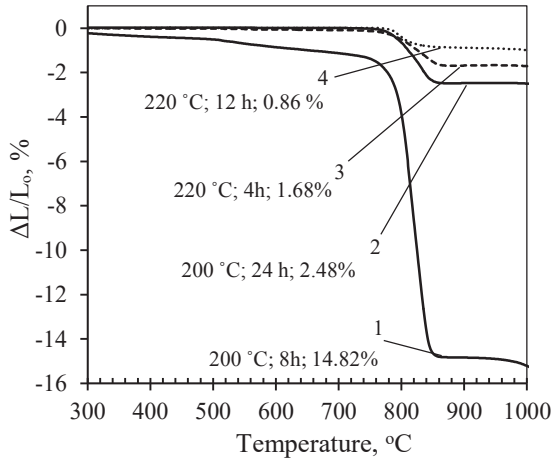

Fig. 3.85. Dilatometry analysis curves of the synthesis products at 200 °C and 220 °C, when $CaO/SiO_2 = 1.2$

Mixtures for hydrothermal synthesis were prepared from calcined opoka and lime until a molar ratio of $CaO/SiO_2 = 1.2$ was reached. After the preparation of the dry mixture, the test vessel was filled with water in such a ratio that the amount of the solids and water was equal to 20. Carbon wool was mixed into the obtained slurry, and its quantity was selected based on literature data (2 wt% of the initial mixture) [183]. Samples of thermal insulating materials were prepared from the suspension which was obtained via hydrothermal synthesis at 220 °C for 4–12 h. It should be noted that this suspension binds a high amount of water, and its relative density (the ratio of the suspension volume after 24 h of settling to the mass of the

initial mixture) was ~20. The samples (20×20×60 mm) were formed in a vacuum-press form while using simultaneous water suction and pressing at 1.6 MPa. Afterwards, they were reprocessed in an autoclave (220 °C, 12 h) and dried at 100±1 °C until constant weight.

The obtained samples were examined by X-ray diffraction analysis; the results are presented in Fig. 3.86. It was determined that carbon wool does not have any impact on the formation of the target compounds, and that specific peaks of xonotlite were identified as early as after 4 h of hydrothermal synthesis (Fig. 3.86, curve 1). By prolonging the duration of isothermal synthesis, the peaks of xonotlite constantly increased. It can be assumed that, during the second hydrothermal curing, the residue of C-S-H(I) converts to xonotlite, and the level of crystallinity increases. Due to this reason, sufficiently good mechanical properties are obtained.

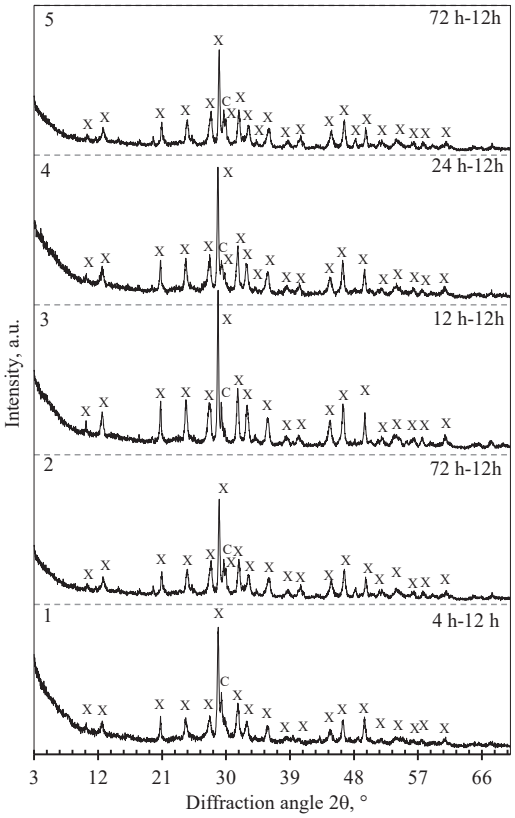

Fig. 3.86. XRD patterns of thermal insulating samples from opoka-lime mixture with CaO/SiO_2 = 1.2 at 220 °C in a stirred (300 rpm) suspension with second hydrothermal curing (220 °C, 12 h). Indexes: C – calcite, X – xonotlite

As it can be seen, the average density of the samples varies within a range of 173.8–214.2 kg/m^3 (Table 3.7). It was determined that thermal insulating samples obtained after 4–12 h of hydrothermal synthesis have the highest density. It is in good agreement with the XRD data where lower peaks of intensity of xonotlite were

identified. It can be assumed that a far lower amount of the compound was formed (which is a porous material). Due to this reason, semi-amorphous C-S-H(I) and unreacted quartz increased the density of the sample. Extending the duration of hydrothermal treatment to 12 h resulted in a significant decrease in density. The results were consistent with the XRD data where the intensity of the target compound peaks increased significantly, which resulted in a much higher quantity of xonotlite in the synthesis products. It can be assumed that the average density of the samples tends to decrease with the increasing duration of isothermal treatment. However, any further increase of the duration of synthesis does not have any significant impact, whereas the average density of the obtained samples even slightly increases.

Table 3.7. Sample density dependence on the duration of hydrothermal synthesis

Synthesis duration, h	4 h	8 h	12 h	24 h	72 h
Density of samples, kg/m^3	214.2	184	178	173.4	173.8

The thermal conductivity of the samples calculated according to the Japanese Standard JISA1413 was relatively low – 0.043–0.038 W/m·K. This is due to the fact that xonotlite density is 2700 kg/m^3, while the average density of the samples is 173.8–214.2 kg/m^3. This means that only 4.8% of the sample volume is occupied by the solid material, while the remaining 95.2% is air entrapped in very small pores.

The compressive strength of thermal insulation materials prepared from xonotlite is presented in Table 3.8. It was determined that, with the decreasing average density, the compressive strength of the samples increases. These results can be attributed to the quantity of xonotlite presented in the obtained samples. As XRD data suggests, by prolonging the duration of hydrothermal synthesis, the peak intensity of xonotlite increases. Duo to this reason, the produced matrix based on xonotlite increases the compressive strength of the final product. In addition, the obtained compressive strength for xonotlite-based thermal insulation materials is sufficient enough for product transportation and installation on site.

Table 3.8. Compressive strength dependence on the duration of hydrothermal synthesis

Synthesis duration, h	4 h	8 h	12 h	24 h	72 h
Compressive strength, MPa	1.40	1.44	1.84	1.79	2.93

3.9 Technological recommendations for the production of heat-resistant thermal insulating materials from xonotlite

According to the results of the current research, the following principal technological scheme for the production of heat-resistant thermal insulating materials based on synthetic xonotlite is presented in Figure 3.87. It was experimentally proven that calcined opoka and lime are the most suitable raw materials for the synthesis of xonotlite.

Opoka rock (pieces up to 300 mm in size) is delivered by a tipper truck (1) and poured into a receiving hopper (2), from which, it is transferred via a plate conveyor

(3) to a jaw crusher (4). The pieces are crushed into particles of a maximum size of 20 mm, and then the material is conveyed by a belt conveyor (5) to an elevator (6), where it is transported to a bunker (7) (1 week stocks). The crushed opoka is dosed by a plate feeder (8) on a belt conveyor (5) which transfers the material to a low-tonnage (capacity – up to 2 t/h) rotary kiln (9). The material stays for 1 hour in the combustion zone where the temperature is 775 °C. At the dust formation sites, air is sucked and cleaned in cyclones (10). The calcined opoka is cooled to 40 °C by ambient air in a grate cooler (11) and transported by an elevator (6) into the bunker (7). From the bunker (7) via the plate feeder (8), opoka is fed to a ball mill (12), where it is ground to a specific surface area of $S_{a.} \approx 1000$ m^2/kg. The prepared opoka powder is transported to a storage silo (13) by an elevator (6). Lime (CaO_{free} >92%) is transported by truck in closed bulk tanks (14) and fed by compressed air to the lime silo (15) (1 week stocks). Carbon wool is obtained from suppliers ready-made and stored in a dry room (16) (4 week stocks). Weight dispensers (17) are used to weigh the components to match the molar ratio of $CaO/SiO_2 = 1.2$, and the materials are supplied to the mixer (22) by screw conveyors (18). Carbon wool (2% by weight of dry matter) is weighed by using industry scales (19) and placed in a mixer. The required amount of water from a tank (20) (water/solid ratio = 20.0) is added by using a volumetric dispenser (21) into the mixer (22). Moreover, a tank (20) collects all the water generated in the process, and, if necessary, additional water is added from the water supply. The suspension is fed from the mixer (22) by a diaphragm pump (23) to an autoclave with a mixer (24), in which, hydrothermal synthesis is carried out at 220 °C under stirring at 300 rpm. After 4–12 h (it depends on what properties of product are required after completing production), the synthesis product is blown by a compressed air compressor (25) to a tank with a mixer (26). There, the synthesis product is stirred until it cools to a temperature of 30–40 °C; then, it is fed by a diaphragm pump (23) to a vacuum-pressing device (27) with simultaneous water suction. The material is formed under the following conditions: vacuum – ~90 kPa, pressing pressure – 1.6 MPa, forming time – ~2 min. The excess water is pumped out by centrifugal pumps (28) and returned to the tank (20) where the water formed in the technological process is collected. Pre-formed boards are conveyed by a roller conveyor (29) to a cutting device (30) which cuts blanks into semi-finished products of the required dimensions and shapes which are subsequently loaded on autoclave rail wagons (32). Cut-offs and other waste are returned to the process (31) and act as crystallization centers during the synthesis. Semi-finished products are hardened in an autoclave (33) for 12 h at 220 °C and then dried in a chamber dryer (34) at 100±1 °C. The finished heat-resistant thermal insulation materials are covered in a packaging machine (35) with a polyethylene film and dispatched to the customer (36).

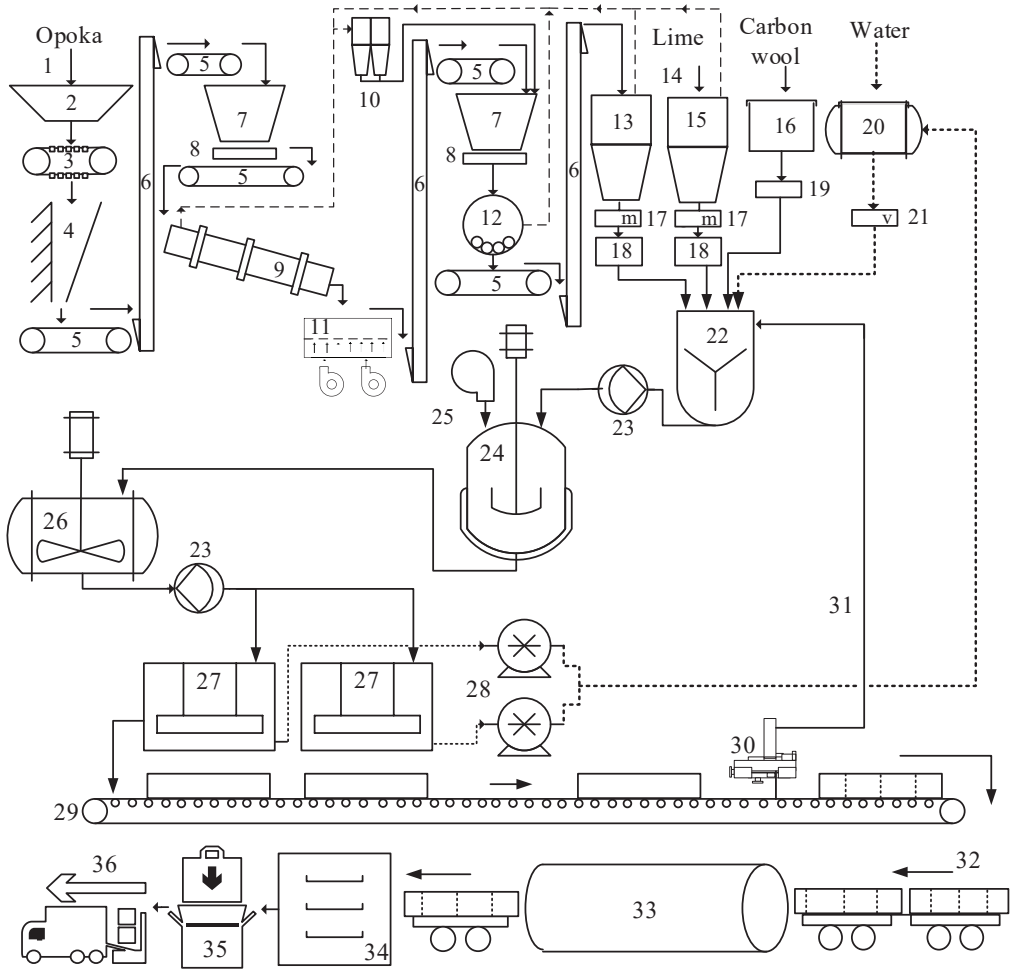

Fig. 3.87. Principal technological scheme of production of heat-resistant thermal insulation materials from xonotlite synthesized by using opoka-lime mixture. The solid line – solid flows; the dotted line – water flows; the dashed line represents gas flows. Indexes: 1 – tipper truck; 2 – receiving hopper; 3 – plate conveyor; 4 – jaw crusher; 5 – belt conveyors; 6 – elevators; 7 – bunkers; 8 – plate feeder; 9 – rotary kiln; 10 – cyclone dust extractor; 11 – gate cooler; 12 – ball mill; 13 – prepared opoka silo; 14 – bulk truck; 15 – prepared lime silo; 16 – carbon wool storage room; 17 – weight dispensers; 18 – screw feeders; 19 – industry scales; 20 – water tank; 21 – volume dispenser; 22 – mixer; 23 – diaphragm pumps; 24 – autoclave with a mixer; 25 – air compressor; 26 – tank with a mixer; 27 – vacuum-pressing equipment; 28 – centrifugal pumps; 29 – roller conveyor; 30 – cutting machine; 31 – waste after formation; 32 – autoclave rail wagons; 33 – curing autoclave; 34 – chamber dryer; 35 – packing machine; 36 – dispatching to user

4. Conclusions

1. It has been found that the granite sawing waste is a suitable material for the synthesis of 1.13 nm tobermorite. The size of the crystallites of this compound increases gradually but constantly by prolonging the duration of isothermal curing at 180 °C from 4 h to 72 h, but, only at the end of this interval, this mineral begins to predominate in the product. By increasing the synthesis temperature to 200 °C, 1.13 nm tobermorite formation processes take place much faster, and tobermorite becomes the main compound of the product after 8 h of hydrothermal treatment. Synthesis of xonotlite from this raw material is not recommended.
2. It has been determined that calcined at 775 °C opoka is an excellent raw material for the synthesis of 1.13 nm tobermorite. The optimum molar ratio is $CaO/SiO_2 = 0.83$, and the optimal hydrothermal curing temperature is 180 °C as this compound begins to dominate in the product as early as after 4 h. It is not worthwhile to prolong the synthesis duration or increase its temperature to 200 °C as the amount of formed 1.13 nm tobermorite and the crystallite size change only slightly.
3. 2.95% of the CaO in the opoka remains in the calcite thus reducing the CaO/SiO_2 molar ratio in the reacting medium to 0.93. It also contains 2.53% Al_2O_3. As Al^{3+} ions do not interfere in the crystal lattice of xonotlite (as opposed to 1.13 nm tobermorite), they can form calcium aluminates thus further reducing the basicity of the suspension. For these reasons, it is recommended to synthesize xonotlite not from the stoichiometric mixture ($CaO/SiO_2 = 1.0$), but rather to increase this ratio to 1.2 instead. The optimum temperature for the synthesis of xonotlite is 220 °C.
4. In lime-opoka/granite sawing waste suspensions, the formation of crystalline calcium silicate hydrates takes place much faster than in the reagent $CaO\text{-}SiO_2\cdot nH_2O$ system. The high reactivity of amorphous SiO_2 results in the rapid formation of intermediates (C-S-H, Z-phase, and $\alpha\text{-}C_2SH$) which are difficult to recrystallize to stable compounds under prolonged isothermal curing duration.
5. Al_2O_3 additive has been shown to affect the recrystallization of 1.13 nm tobermorite to other calcium silicate hydrates – after a long synthesis duration (72 h) or at a high temperature (200–220 °C), it can not only recrystallize to thermodynamically stable xonotlite, but also to decompose, and, together with the above mentioned mineral ultimately form a compound of lower basicity – gyrolite.
6. It has been found that, from the lime-opoka mixture at 200 °C for 12 h, the synthesized product features a specific surface area of ~68 m^2/g, a total pore volume of $245\cdot10^{-3}$ cm^3/g and has dominating 1–2.5 nm and 5–20 nm diameter pores. This porosity of the material should provide good thermal insulation properties for the products made from this material as no air convection occurs in the fine pores.
7. It has been shown that opoka is a suitable raw material for the production of heat-resistant products containing predominantly xonotlite. The technological

parameters are as follows: the molar ratio of the mixture CaO/SiO_2 = 1.2, hydrothermal synthesis – 220 °C, 12 h, W/S = 20; autoclaving – 220 °C, 8 h. The average density of the samples was ~180 kg/m^3, the compressive strength was 1.84 MPa, the operating temperature was 1000 °C, the linear shrinkage up to this temperature was 0.55%.

References

1. HONG, S-Y and GLASSER, F P. Phase relations in the $CaO–SiO_2–H_2O$ system to 200 C at saturated steam pressure. *Cement and Concrete Research*. 2004. Vol. 34, no. 9, p. 1529–1534.
2. RÍOS, Carlos A, WILLIAMS, Craig D and FULLEN, Michael A. Hydrothermal synthesis of hydrogarnet and tobermorite at 175 °C from kaolinite and metakaolinite in the $CaO–Al_2O_3–SiO_2–H_2O$ system: A comparative study. *Applied Clay Science*. 2009. Vol. 43, no. 2, p. 228–237.
3. THOMAS, Jeffrey J, JENNINGS, Hamlin M and ALLEN, Andrew J. Relationships between composition and density of tobermorite, jennite, and nanoscale $CaO−SiO_2−H_2O$. *The Journal of Physical Chemistry C*. 2010. Vol. 114, no. 17, p. 7594–7601.
4. TAYLOR, Harry F W. *Cement chemistry*. Thomas Telford, 1997. ISBN 0727725920.
5. TAYLOR, H F W and BESSEY, G E. Review of hydrothermal reactions in the system lime-silica-water. *Mag Concr Res*. 1950. Vol. 2, no. 4, p. 15.
6. SASAKI, Kaori, MASUDA, Tsuguya, ISHIDA, Hideki and MITSUDA, Takeshi. Synthesis of calcium silicate hydrate with Ca/Si=2 by mechanochemical treatment. *Journal of the American Ceramic Society*. 1997. Vol. 80, no. 2, p. 472–476.
7. FAUCON, P, DELAGRAVE, A, PETIT, J C, RICHET, C, MARCHAND, J M and ZANNI, H. Aluminum incorporation in calcium silicate hydrates (C−S−H) depending on their Ca/Si ratio. *The Journal of Physical Chemistry B*. 1999. Vol. 103, no. 37, p. 7796–7802.
8. SWANTON, S W, HEATH, T G and CLACHER, A. Leaching behaviour of low Ca:Si ratio $CaO–SiO_2–H_2O$ systems. *Cement and Concrete Research*. 2016. Vol. 88, p. 82–95.
9. WEISHI, Li, GUOYUAN, Lei, YA, Xu and QIFEI, Huang. The properties and formation mechanisms of eco-friendly brick building materials fabricated from low-silicon iron ore tailings. *Journal of Cleaner Production*. 2018. Vol. 204, p. 685–692.
10. CHEN, Tiefeng, GAO, Xiaojian and REN, Miao. Effects of autoclave curing and fly ash on mechanical properties of ultra-high performance concrete. *Construction and Building Materials*. 2018. Vol. 158, p. 864–872.
11. RICHARDSON, Ian G. The calcium silicate hydrates. *Cement and concrete research*. 2008. Vol. 38, no. 2, p. 137–158.
12. BROWN, P A. Xonotlite; a new occurrence at Rose Blanche, Newfoundland. *The Canadian Mineralogist*. 1978. Vol. 16, no. 4, p. 671–672.
13. GRANGEON, Sylvain, CLARET, Francis, LEROUGE, Catherine, WARMONT, Fabienne, SATO, Tsutomu, ANRAKU, Sohtaro, NUMAKO, Chiya, LINARD, Yannick and LANSON, Bruno. On the nature of structural disorder in calcium silicate hydrates with a calcium/silicon ratio similar to tobermorite. *Cement and Concrete Research*. 2013. Vol. 52, p. 31–37.
14. ASHRAF, Warda and OLEK, Jan. Carbonation behavior of hydraulic and

non-hydraulic calcium silicates: potential of utilizing low-lime calcium silicates in cement-based materials. *Journal of materials science*. 2016. Vol. 51, no. 13, p. 6173–6191.
15. SKINNER, L B, CHAE, S R, BENMORE, C J, WENK, H R and MONTEIRO, P J M. Nanostructure of calcium silicate hydrates in cements. *Physical review letters*. 2010. Vol. 104, no. 19, p. 195502.
16. HARTMANN, Andrea, SCHULENBERG, David and BUHL, Josef-Christian. Synthesis and Structural Characterization of CSH-Phases in the Range of C/S= 0.41-1.66 at Temperatures of the Tobermorite Xonotlite Crossover. *Journal of Materials Science and Chemical Engineering 3 (2015), Nr. 11*. 2015. Vol. 3, no. 11, p. 39–55.
17. BALTAKYS, K and SIAUCIUNAS, R. The influence of γ-Al_2O_3 and Na_2O on the formation of calcium silicate hydrates in the CaO–quartz–H_2O system. *Materials Science-Poland*. 2007. Vol. 25, no. 1, p. 185–198.
18. SIAUCIUNAS, Raimundas, HILBIG, Harald, PRICHOCKIENE, Edita, SMIGELSKYTE, Agne and TAKULINSKAS, Zilvinas. Accelerated carbonation of C2SH based dense concrete. *Ceramics International*. 2020.
19. VANDAMME, Matthieu and ULM, F-J. Nanoindentation investigation of creep properties of calcium silicate hydrates. *Cement and Concrete Research*. 2013. Vol. 52, p. 38–52.
20. PLASSARD, Cédric, LESNIEWSKA, Eric, POCHARD, Isabelle and NONAT, André. Investigation of the surface structure and elastic properties of calcium silicate hydrates at the nanoscale. *Ultramicroscopy*. 2004. Vol. 100, no. 3–4, p. 331–338.
21. GRANGEON, Sylvain, CLARET, Francis, LINARD, Yannick and CHIABERGE, Christophe. X-ray diffraction: a powerful tool to probe and understand the structure of nanocrystalline calcium silicate hydrates. *Acta Crystallographica Section B: Structural Science, Crystal Engineering and Materials*. 2013. Vol. 69, no. 5, p. 465–473.
22. MYERS, Rupert J, BERNAL, Susan A, SAN NICOLAS, Rackel and PROVIS, John L. Generalized structural description of calcium–sodium aluminosilicate hydrate gels: the cross-linked substituted tobermorite model. *Langmuir*. 2013. Vol. 29, no. 17, p. 5294–5306.
23. ZOU, Jingjing, GUO, Chunbin, JIANG, Yinshan, WEI, Cundi and LI, Fangfei. Structure, morphology and mechanism research on synthesizing xonotlite fiber from acid-extracting residues of coal fly ash and carbide slag. *Materials chemistry and Physics*. 2016. Vol. 172, p. 121–128.
24. LI, Jiaqi, ZHANG, Wenxin and MONTEIRO, Paulo J M. The structure and intrinsic mechanical properties of nanocrystalline calcium silicate hydrate. *ACS Sustainable Chemistry & Engineering*. 2020.
25. DU, Tao, LI, Hui, ZHOU, Qi, WANG, Zhe, SANT, Gaurav, RYAN, Joseph V and BAUCHY, Mathieu. Chemical composition of calcium-silicate-hydrate gels: Competition between kinetics and thermodynamics. *Physical Review Materials*. 2019. Vol. 3, no. 6, p. 65603.
26. WANG, Pan, QIAO, Gang, GUO, Yupeng, ZHANG, Yue, HOU, Dongshuai,

JIN, Zuquan, ZHANG, Jinrui, WANG, Muhan and HU, Xiaoxia. Molecular dynamics simulation of the interfacial bonding properties between graphene oxide and calcium silicate hydrate. *Construction and Building Materials*. 2020. Vol. 260, p. 119927.

27. KANCHANASON, V and PLANK, J. Role of pH on the structure, composition and morphology of CSH–PCE nanocomposites and their effect on early strength development of Portland cement. *Cement and Concrete Research*. 2017. Vol. 102, p. 90–98.
28. NONAT, André and LECOQ, Xavier. The Structure, Stoichiometry and Properties of CSH Prepared by C_3S Hydration Under Controlled Condition. In : *Nuclear magnetic resonance spectroscopy of cement-based materials*. Springer, 1998. p. 197–207.
29. RODRIGUEZ, Elena Tajuelo, GARBEV, Krassimir, MERZ, Daniela, BLACK, Leon and RICHARDSON, Ian G. Thermal stability of CSH phases and applicability of Richardson and Groves' and Richardson C-(A)-SH(I) models to synthetic CSH. *Cement and Concrete research*. 2017. Vol. 93, p. 45–56.
30. ZEHTAB, B and TARIGHAT, A. Molecular dynamics simulation to assess the effect of temperature on diffusion coefficients of different ions and water molecules in CSH. *Mechanics of Time-Dependent Materials*. 2018. Vol. 22, no. 4, p. 483–497.
31. WAGNER, Maximilian, DRESSLER, Christian, LOHMANN-RICHTERS, Felix P, HANUS, Kevin, SEBASTIANI, Daniel, VARGA, Aron and ABEL, Bernd. Mechanism of ion conductivity through polymer-stabilized CsH_2PO_4 nanoparticular layers from experiment and theory. *Journal of Materials Chemistry A*. 2019. Vol. 7, no. 48, p. 27367–27376.
32. HENRIQUES, J M, CAETANO, E W S, FREIRE, V N, DA COSTA, J A P and ALBUQUERQUE, E L. Structural and electronic properties of $CaSiO_3$ triclinic. *Chemical physics letters*. 2006. Vol. 427, no. 1–3, p. 113–116.
33. KOTSIS, Ildikó and BALOGH, Agnes. Synthesis of wollastonite. *Ceramics International*. 1989. Vol. 15, no. 2, p. 79–85.
34. JEFFERY, J W. Unusual X-ray diffraction effects from a crystal of wollastonite. *Acta Crystallographica*. 1953. Vol. 6, no. 11–12, p. 821–825.
35. WANG, Huanping, ZHANG, Qilong, YANG, Hui and SUN, Huiping. Synthesis and microwave dielectric properties of CaSiO3 nanopowder by the sol–gel process. *Ceramics International*. 2008. Vol. 34, no. 6, p. 1405–1408.
36. AKBAYRAK, Serdar and ÖZKAR, Saim. Ruthenium (0) nanoparticles supported on xonotlite nanowire: a long-lived catalyst for hydrolytic dehydrogenation of ammonia-borane. *Dalton Transactions*. 2014. Vol. 43, no. 4, p. 1797–1805.
37. LI, Sen, QIN, Haili, ZHANG, Tan, CONG, Huai-Ping and YU, Shu-Hong. Highly Tough Bioinspired Ternary Hydrogels Synergistically Reinforced by Graphene/Xonotlite Network. *Small*. 2018. Vol. 14, no. 22, p. 1800673.
38. LIU, Yang-Yi, CHANG, Fu-Jia, GAO, Huai-Ling, CHEN, Si-Ming, GAO, Min-Rui, ZHENG, Ya-Rong, CÖLFEN, Helmut, HE, Chuan-Xin and YU,

Shu-Hong. Bio-Inspired Synthesis of Hematite Mesocrystals by Using Xonotlite Nanowires as Growth Modifiers and Their Improved Oxygen Evolution Activity. *ChemSusChem*. 2019. Vol. 12, no. 16, p. 3747–3752.
39. VIEHLAND, Dwight, YUAN, Lijian J, XU, Z, CONG, Xian Dong and KIRKPATRICK, R James. Structural studies of jennite and 1.4 nm tobermorite: disordered layering along the [100] of jennite. *Journal of the American Ceramic Society*. 1997. Vol. 80, no. 12, p. 3021–3028.
40. TAYLOR, H F W. Tobermorite, jennite, and cement gel. *Zeitschrift für Kristallographie-Crystalline Materials*. 1992. Vol. 202, no. 1–2, p. 41–50.
41. BLACK, Leon, GARBEV, Krassimir, STEMMERMANN, Peter, HALLAM, Keith R and ALLEN, Geoffrey C. Characterisation of crystalline CSH phases by X-ray photoelectron spectroscopy. *Cement and concrete research*. 2003. Vol. 33, no. 6, p. 899–911.
42. GUTTERIDGE, W A and PARROTT, L J. A study of the changes in weight, length and interplanar spacing induced by drying and rewetting synthetic CSH (I). *Cement and Concrete research*. 1976. Vol. 6, no. 3, p. 357–366.
43. SMITH, R H, BAYLISS, P, GAMBLE, B R and MILLS, R H. Crystallographic investigation of CSH (1). *Cement and Concrete Research*. 1972. Vol. 2, no. 5, p. 559–566.
44. LI, Kai, SHUI, Zhonghe and DAI, Wei. A molecular dynamics study on the structure characteristic of calcium silicate hydrate (CSH) gels. In : *International Workshop on Computer Science for Environmental Engineering and EcoInformatics*. Springer, 2011. p. 33–39.
45. NONAT, André. The structure and stoichiometry of CSH. *Cement and concrete research*. 2004. Vol. 34, no. 9, p. 1521–1528.
46. TAYLOR, Harry F W. Proposed structure for calcium silicate hydrate gel. *Journal of the American Ceramic Society*. 1986. Vol. 69, no. 6, p. 464–467.
47. RICHARDSON, I G. Tobermorite/jennite-and tobermorite/calcium hydroxide-based models for the structure of CSH: applicability to hardened pastes of tricalcium silicate, β-dicalcium silicate, Portland cement, and blends of Portland cement with blast-furnace slag, metakaolin,. *Cement and Concrete Research*. 2004. Vol. 34, no. 9, p. 1733–1777.
48. HARA, N and INOUE, N. Formation of jennite from fumed silica. *Cement and Concrete Research*. 1980. Vol. 10, no. 5, p. 677–682.
49. JENNINGS, Hamlin M. A model for the microstructure of calcium silicate hydrate in cement paste. *Cement and concrete research*. 2000. Vol. 30, no. 1, p. 101–116.
50. STUMM, Andreas, GARBEV, Krassimir, BEUCHLE, Günter, BLACK, Leon, STEMMERMANN, Peter and NÜESCH, Rolf. Incorporation of zinc into calcium silicate hydrates, Part I: formation of CSH (I) with C/S= 2/3 and its isochemical counterpart gyrolite. *Cement and Concrete Research*. 2005. Vol. 35, no. 9, p. 1665–1675.
51. EL-KORASHY, S A. Cation exchange of alkali metal hydroxides with some hydrothermally synthesized calcium silicate compounds. *Journal of Ion Exchange*. 2004. Vol. 15, no. 1, p. 2–9.

52. MIYAKE, Michihiro, IWAYA, Masaki, SUZUKI, Takashi, KAKEHI, Hiroyuki and MITSUDA, Takeshi. Aluminum Substituted Gyrolite as Cation Exchanger. *Journal of the American Ceramic Society*. 1990. Vol. 73, no. 11, p. 3524–3527.
53. BANKAUSKAITE, Agne, EISINAS, Anatolijus, BALTAKYS, Kestutis and ZADAVICIUTE, Skirmante. A study on the intercalation of heavy metal ions in a wastewater by synthetic layered inorganic adsorbents. *Desalination and Water Treatment*. 2015. Vol. 56, no. 6, p. 1576–1586.
54. BALTAKYS, M, SIAUCIUNAS, R, JAUBERTHIE, R and BALTAKYS, K. The influence of Zn containing components on the synthesis of Z-phase. *Science of Sintering*. 2013. Vol. 45, no. 1, p. 49–60.
55. GARD, J A, MITSUDA, T and TAYLOR, H F W. Some observations on Assarsson's Z-phase and its structural relations to gyrolite, truscottite, and reyerite. *Mineralogical Magazine*. 1975. Vol. 40, no. 312, p. 325–333.
56. GUAN, Xuemao, LIU, Songhui, FENG, Chunhua and QIU, Man. The hardening behavior of γ-C2S binder using accelerated carbonation. *Construction and Building Materials*. 2016. Vol. 114, p. 204–207.
57. DAMBRAUSKAS, T, BALTAKYS, K, EISINAS, A and KITRYS, S. The specific surface area and porosity of synthetic and calcined α-C2SH, kilchoanite and hydroxyledgrewite. *Powder Technology*. 2019. Vol. 355, p. 504–513.
58. SIAUCIUNAS, Raimundas, BALTAKYS, Kestutis, GENDVILAS, Rokas and PRICHOCKIENE, Edita. Synthesis of low-energy cement based on α-C2SH. *Advances in Cement Research*. 2016. Vol. 28, no. 4, p. 241–250.
59. COLEMAN, Nichola J, BRASSINGTON, David S, RAZA, Atiya and MENDHAM, Andrew P. Sorption of Co^{2+} and Sr^{2+} by waste-derived 11 Å tobermorite. *Waste Management*. 2006. Vol. 26, no. 3, p. 260–267.
60. KOMARNENI, Sridhar and ROY, Della M. Tobermorites: a new family of cation exchangers. *Science*. 1983. Vol. 221, no. 4611, p. 647–648.
61. KOMARNENI, Sridhar and ROY, Della M. New tobermorite cation exchangers. *Journal of materials science*. 1985. Vol. 20, no. 8, p. 2930–2936.
62. PARADISO, P, SANTOS, R L, HORTA, R B, LOPES, J N C, FERREIRA, P J and COLAÇO, R. Formation of nanocrystalline tobermorite in calcium silicate binders with low C/S ratio. *Acta Materialia*. 2018. Vol. 152, p. 7–15.
63. GRANGEON, Sylvain, CLARET, Francis, ROOSZ, Cédric, SATO, Tsutomu, GABOREAU, Stéphane and LINARD, Yannick. Structure of nanocrystalline calcium silicate hydrates: insights from X-ray diffraction, synchrotron X-ray absorption and nuclear magnetic resonance. *Journal of applied crystallography*. 2016. Vol. 49, no. 3, p. 771–783.
64. MEGAW, Helen D and KELSEY, C H. Crystal structure of tobermorite. *Nature*. 1956. Vol. 177, no. 4504, p. 390–391.
65. BONACCORSI, Elena, MERLINO, Stefano and KAMPF, Anthony R. The crystal structure of tobermorite 14 Å (plombierite), a C–S–H phase. *Journal of the American Ceramic Society*. 2005. Vol. 88, no. 3, p. 505–512.
66. HAMID, S A. The crystal structure of the 11Å natural tobermorite $Ca_{2.25}$

$[Si_3O_{7.5}(OH)1.5]\cdot H_2O$. *Zeitschrift für Kristallographie-Crystalline Materials*. 1981. Vol. 154, no. 3–4, p. 189–198.
67. FROST, Ray L, MAHENDRAN, Mahen, POOLOGANATHAN, Keerthan and XI, Yunfei. Raman spectroscopic study of the mineral xonotlite $Ca_6Si_6O_{17}(OH)_2$ – A component of plaster boards. *Materials Research Bulletin*. 2012. Vol. 47, no. 11, p. 3644–3649.
68. LUKE, K, TAYLOR, H F W and KALOUSEK, G L. Some factors affecting formation of truscottite and xonotlite at 300–350 °C. *Cement and Concrete Research*. 1981. Vol. 11, no. 2, p. 197–203.
69. LIU, Fei, CAO, Jian Xin and ZHU, Bo. Effect of anion impurity on preparing xonotlite whiskers via hydrothermal synthesis. In : *Advanced Materials Research*. Trans Tech Publ, 2011. p. 1755–1758. ISBN 0878492011.
70. PUGOVKINA, Yulya, KUTUGIN, Viktor, OSTROUMOVA, Alina and RYMANOVA, Irina. High temperature and heat insulated calcium silicate materials. In : *Key Engineering Materials*. Trans Tech Publ, 2016. p. 209–214. ISBN 3038357294.
71. AKBAYRAK, Serdar and ÖZKAR, Saim. Inverse relation between the catalytic activity and catalyst concentration for the ruthenium (0) nanoparticles supported on xonotlite nanowire in hydrogen generation from the hydrolysis of sodium borohydride. *Journal of Molecular Catalysis A: Chemical*. 2016. Vol. 424, p. 254–260.
72. TASHIRO, Chuichi and KAWAGUCHI, K. Effects of the CaO/SiO_2 ratio and Cr_2O_3 on the hydrothermal synthesis of xonotlite. *Cement and Concrete Research*. 1977. Vol. 7, no. 1, p. 69–76.
73. LIU, F, CHEN, S, LIN, Q, WANG, X D and CAO, J X. Study on hydrothermal synthesis dynamics of nanoscale xonotlite fibers. In : *IOP Conference Series: Materials Science and Engineering*. IOP Publishing, 2018. p. 12021. ISBN 1757-899X.
74. DENT, L S and TAYLOR, H F W. The dehydration of xonotlite. *Acta Crystallographica*. 1956. Vol. 9, no. 12, p. 1002–1004.
75. BLACK, Leon, GARBEV, Krassimir and STUMM, Andreas. Structure, bonding and morphology of hydrothermally synthesised xonotlite. *Advances in Applied Ceramics*. 2009. Vol. 108, no. 3, p. 137–144.
76. BERNSTEIN, Saskia, THOMAS FEHR, Karl and HOCHLEITNER, Rupert. Crystal chemistry of Xonotlite $Ca_6Si_6O_{17}(OH)_2$. Part I: determination of polytypes using X-ray powder diffraction (XRPD). *Neues Jahrbuch für Mineralogie-Abhandlungen: Journal of Mineralogy and Geochemistry*. 2009. Vol. 186, no. 2, p. 153–162.
77. GARBEV, Krassimir, BLACK, Leon, BEUCHLE, Günter and STEMMERMANN, Peter. Inorganic polymers in cement based materials. *Wasser-und Geotechnologie*. 2002. Vol. 1, no. 2, p. 19–30.
78. GENDVILAS, Rokas and SIAUCIUNAS, Raimundas. The Influence of Temperature and Nature of CaO Component on the Formation of α-C_2SH. In : *Solid State Phenomena*. Trans Tech Publ, 2016. p. 12–18. ISBN 3038356328.

79. SHAW, S, CLARK, S M and HENDERSON, C M B. Hydrothermal formation of the calcium silicate hydrates, tobermorite ($Ca_5Si_6O_{16}(OH)_2 \cdot 4H_2O$) and xonotlite ($Ca_6Si_6O_{17}(OH)_2$): an in situ synchrotron study. *Chemical Geology*. 2000. Vol. 167, no. 1–2, p. 129–140.
80. BRINDLEY, G W. Crystallographic aspects of some decomposition and recrystallization reactions. *Progress in Ceramic Science vol. 3*. 1963.
81. KALOUSEK, G L, MITSUDA, T and TAYLOR, H F W. Xonotlite: cell parameters, thermogravimetry and analytical electron microscopy. *Cement and Concrete Research*. 1977. Vol. 7, no. 3, p. 305–312.
82. SUZUKI, Shigeru and SINN, Ekkehard. 1.4 nm Tobermorite-like calcium silicate hydrate prepared at room temperature from $Si(OH)_4$ and $CaCl_2$ solutions. *Journal of materials science letters*. 1993. Vol. 12, no. 8, p. 542–544.
83. DING, Jian, TANG, Zhenhua, MA, Shuhua, WANG, Yuejiao, ZHENG, Shili, ZHANG, Yi, SHEN, Shirley and XIE, Zongli. A novel process for synthesis of tobermorite fiber from high-alumina fly ash. *Cement and Concrete Composites*. 2016. Vol. 65, p. 11–18.
84. TAYLOR, H F W. The transformation of tobermorite into xonotlite. *Mineralogical Magazine and Journal of the Mineralogical Society*. 1959. Vol. 32, no. 245, p. 110–116.
85. GUO, Xiaolu, MENG, Fanjie and SHI, Huisheng. Microstructure and characterization of hydrothermal synthesis of Al-substituted tobermorite. *Construction and Building Materials*. 2017. Vol. 133, p. 253–260.
86. CHAN, Chien-Feng, SAKIYAMA, M and MITSUDA, T. Kinetics of the CaO-quartz-H_2O reaction at 120 to 180 °C in suspensions. *Cement and concrete research*. 1978. Vol. 8, no. 1, p. 1–5.
87. MCCONNELL, Ji D C. The hydrated calcium silicates riversideite, tobermorite, and plombierite. *Mineralogical Magazine and Journal of the Mineralogical Society*. 1954. Vol. 30, no. 224, p. 293–305.
88. YANAGISAWA, K, FENG, Q and YAMASAKI, N. Hydrothermal synthesis of xonotlite whiskers by ion diffusion. *Journal of materials science letters*. 1997. Vol. 16, no. 11, p. 889–891.
89. ISU, Norifumi, ISHIDA, Hideki and MITSUDA, Takeshi. Influence of quartz particle size on the chemical and mechanical properties of autoclaved aerated concrete (I) tobermorite formation. *Cement and concrete research*. 1995. Vol. 25, no. 2, p. 243–248.
90. ALUJEVIĆ, V, BEZJAK, A and GLASNOVIĆ, A. Kinetic study of the hydrothermal reaction in CaO-quartz system. *Cement and Concrete Research*. 1986. Vol. 16, no. 5, p. 695–699.
91. LI, Maoqiang and LIANG, Hongxun. Formation of micro-porous spherical particles of calcium silicate (xonotlite) in dynamic hydrothermal process. *China Particuology*. 2004. Vol. 2, no. 3, p. 124–127.
92. SPUDULIS, Edmundas, ŠAVAREIKA, Viktoras and ŠPOKAUSKAS, Algimantas. Influence of hydrothermal synthesis condition on xonotlite crystal morphology. *Materials science*. 2013. Vol. 19, no. 2, p. 190–196.

93. HARTMANN, A, KHAKHUTOV, M and BUHL, J-Ch. Hydrothermal synthesis of CSH-phases (tobermorite) under influence of Ca-formate. *Materials Research Bulletin*. 2014. Vol. 51, p. 389–396.
94. KIKUMA, Jun, TSUNASHIMA, Masamichi, ISHIKAWA, Tetsuji, MATSUNO, Shin Ya, OGAWA, Akihiro, MATSUI, Kunio and SATO, Masugu. In Situ Time Resolved X-Ray Diffraction of Tobermorite Formation Process Under Autoclave Condition. *Journal of the American Ceramic Society*. 2010. Vol. 93, no. 9, p. 2667–2674.
95. AITKEN, A and TAYLOR, H F W. Hydrothermal reactions in lime-quartz pastes. *Journal of Applied Chemistry*. 1960. Vol. 10, no. 1, p. 7–15.
96. Eℓ-HEMALY, S A S, MITSUDA, T and TAYLOR, H F W. Synthesis of normal and anomalous tobermorites. *Cement and Concrete Research*. 1977. Vol. 7, no. 4, p. 429–438.
97. CHAN, C F and MITSUDA, T. Formation of 11 Å tobermorite from mixtures of lime and colloidal silica with quartz. *Cement and Concrete Research*. 1978. Vol. 8, no. 2, p. 135–138.
98. GALVÁNKOVÁ, Lucie, MÁSILKO, Jiří, SOLNÝ, Tomáš and ŠTĚPÁNKOVÁ, Eva. Tobermorite synthesis under hydrothermal conditions. *Procedia Engineering*. 2016. Vol. 151, p. 100–107.
99. LIU, S K, HAN, C, LIU, J M and LI, H. Hydrothermal decomposition of potassium feldspar under alkaline conditions. *Rsc Advances*. 2015. Vol. 5, no. 113, p. 93301–93309.
100. YOUSSEF, H, IBRAHIM, D, KOMARNENI, Sridhar and MACKENZIE, K J D. Synthesis of 11 Å Al-substituted tobermorite from trachyte rock by hydrothermal treatment. *Ceramics International*. 2010. Vol. 36, no. 1, p. 203–209.
101. MAESHIMA, Takayuki, NOMA, Hiroaki, SAKIYAMA, Masato and MITSUDA, Takeshi. Natural 1.1 and 1.4 nm tobermorites from Fuka, Okayama, Japan: Chemical analysis, cell dimensions, 29Si NMR and thermal behavior. *Cement and Concrete Research*. 2003. Vol. 33, no. 10, p. 1515–1523.
102. SIAUCIUNAS, R, MIKALIUNAITE, J, URBONAS, L and BALTAKYS, K. Tribochemical and thermal activation of α-C_2S hydrate as precursor for cementitious binders. *Journal of Thermal Analysis and Calorimetry*. 2014. Vol. 118, no. 2, p. 817–823.
103. PANDA, Sandeep, BISWAL, Avijit, MISHRA, Srabani, PANDA, Prasanna Kumar, PRADHAN, Nilotpala, MOHAPATRA, Umaballava, SUKLA, Lala Behari, MISHRA, Barada Kanta and AKCIL, Ata. Reductive dissolution by waste newspaper for enhanced meso-acidophilic bioleaching of copper from low grade chalcopyrite: A new concept of biohydrometallurgy. *Hydrometallurgy*. 2015. Vol. 153, p. 98–105.
104. JIMÉNEZ, Ivelisse, PÉREZ, Gloria, GUERRERO, Ana and RUIZ, Begoña. Mineral phases synthesized by hydrothermal treatment from biomass ashes. *International Journal of Mineral Processing*. 2017. Vol. 158, p. 8–12.
105. TSUTSUMI, Takuma, NISHIMOTO, Shunsuke, KAMESHIMA, Yoshikazu

and MIYAKE, Michihiro. Hydrothermal preparation of tobermorite from blast furnace slag for Cs^{+} and Sr^{2+} sorption. *Journal of hazardous materials*. 2014. Vol. 266, p. 174–181.
106. WANG, Shuping, PENG, Xiaoqin, TANG, Luping, ZENG, Lu and LAN, Cong. Influence of inorganic admixtures on the 11 Å-tobermorite formation prepared from steel slags: XRD and FTIR analysis. *Construction and Building Materials*. 2014. Vol. 60, p. 42–47.
107. REINIK, Janek, HEINMAA, Ivo, MIKKOLA, Jyri-Pekka and KIRSO, Uuve. Synthesis and characterization of calcium–alumino-silicate hydrates from oil shale ash–Towards industrial applications. *Fuel*. 2008. Vol. 87, no. 10–11, p. 1998–2003.
108. COLEMAN, Nichola J. Synthesis, structure and ion exchange properties of 11 Å tobermorites from newsprint recycling residue. *Materials research bulletin*. 2005. Vol. 40, no. 11, p. 2000–2013.
109. CAO, Jianxin, LIU, Fei, LIN, Qian and ZHANG, Yu. Hydrothermal synthesis of xonotlite from carbide slag. *Progress in Natural Science*. 2008. Vol. 18, no. 9, p. 1147–1153.
110. NOCUÒ-WCZELIK, Wieslawa. Effect of Na and Al on the phase composition and morphology of autoclaved calcium silicate hydrates. *Cement and Concrete Research*. 1999. Vol. 29, no. 11, p. 1759–1767.
111. PEI, L Z, YANG, L J, YANG, Y, FAN, C G, YIN, W Y, CHEN, J and ZHANG, Q F. A green and facile route to synthesize calcium silicate nanowires. *Materials Characterization*. 2010. Vol. 61, no. 11, p. 1281–1285.
112. YAMAZAKI, Satoru and TORAYA, Hideo. Determination of positions of zeolitic calcium atoms and water molecules in hydrothermally formed aluminum substiqtuted tobermorite 1.1 nm using synchrotron radiation powder diffraction data. *Journal of the American Ceramic Society*. 2001. Vol. 84, no. 11, p. 2685–2690.
113. MANZANO, H, DOLADO, J S and AYUELA, A. Elastic properties of the main species present in Portland cement pastes. *Acta Materialia*. 2009. Vol. 57, no. 5, p. 1666–1674.
114. L'HÔPITAL, E, LOTHENBACH, B, LE SAOUT, G, KULIK, D and SCRIVENER, K. Incorporation of aluminium in calcium-silicate-hydrates. *Cement and Concrete Research*. 2015. Vol. 75, p. 91–103.
115. RICHARDSON, Ian G, BROUGH, Adrian R, BRYDSON, Rik, GROVES, Geoffrey W and DOBSON, Christopher M. Location of aluminum in substituted calcium silicate hydrate (C-S-H) gels as determined by 29Si and 27Al NMR and EELS. *Journal of the American Ceramic Society*. 1993. Vol. 76, no. 9, p. 2285–2288.
116. FAUCON, P, CHARPENTIER, T, BERTRANDIE, D, NONAT, A, VIRLET, J and PETIT, J C. Characterization of calcium aluminate hydrates and related hydrates of cement pastes by 27Al MQ-MAS NMR. *Inorganic chemistry*. 1998. Vol. 37, no. 15, p. 3726–3733.
117. PARDAL, Xiaolin, BRUNET, Francine, CHARPENTIER, Thibault, POCHARD, Isabelle and NONAT, André. 27Al and 29Si solid-state NMR

characterization of calcium-aluminosilicate-hydrate. *Inorganic chemistry*. 2012. Vol. 51, no. 3, p. 1827–1836.
118. SUN, G K, YOUNG, J Francis and KIRKPATRICK, R James. The role of Al in C–S–H: NMR, XRD, and compositional results for precipitated samples. *Cement and Concrete Research*. 2006. Vol. 36, no. 1, p. 18–29.
119. RICHARDSON, I G and GROVES, G W. The incorporation of minor and trace elements into calcium silicate hydrate (C-S-H) gel in hardened cement pastes. *Cement and Concrete Research*. 1993. Vol. 23, no. 1, p. 131–138.
120. MITSUDA, Takeshi. Synthesis of tobermorite from zeolite. *Mineralogical Journal*. 1970. Vol. 6, no. 3, p. 143–158.
121. COLEMAN, Nichola J and BRASSINGTON, David S. Synthesis of Al-substituted 11 Å tobermorite from newsprint recycling residue: a feasibility study. *Materials Research Bulletin*. 2003. Vol. 38, no. 3, p. 485–497.
122. XI, Yaozhong and GLASSER, L S Dent. Hydrothermal study in the system Na_2O-CaO-SiO_2-H_2O at 300 °C. *Cement and Concrete Research*. 1984. Vol. 14, no. 5, p. 741–748.
123. NELSON, Erik B and KALOUSEK, George L. Effects of Na_2O on calcium silicate hydrates at elevated temperatures. *Cement and Concrete Research*. 1977. Vol. 7, no. 6, p. 687–694.
124. LIU, Fei, WANG, Xiao-dan and CAO, Jian-xin. Effect of Na^+ on xonotlite crystals in hydrothermal synthesis. *International Journal of Minerals, Metallurgy, and Materials*. 2013. Vol. 20, no. 1, p. 88–93.
125. HAMMER, Vera M F, LIBOWITZKY, Eugen and ROSSMAN, George R. Single-crystal IR spectroscopy of very strong hydrogen bonds in pectolite, $NaCa_2[Si_3O_8(OH)]$, and serandite, $NaMn_2[Si_3O_8(OH)]$. *American Mineralogist*. 1998. Vol. 83, no. 5–6, p. 569–576.
126. PREWITT, C T. Refinement of the structure of pectolite, Ca2NaHSi3O9. *Zeitschrift für Kristallographie*. 1967. Vol. 125, p. 298–316.
127. MOSTAFA, N Y, SHALTOUT, A A, OMAR, H and ABO-EL-ENEIN, S A. Hydrothermal synthesis and characterization of aluminium and sulfate substituted 1.1 nm tobermorites. *Journal of Alloys and Compounds*. 2009. Vol. 467, no. 1–2, p. 332–337.
128. SCHAEDLER, Tobias A, JACOBSEN, Alan J, TORRENTS, Anna, SORENSEN, Adam E, LIAN, Jie, GREER, Julia R, VALDEVIT, Lorenzo and CARTER, Wiliam B. Ultralight metallic microlattices. *Science*. 2011. Vol. 334, no. 6058, p. 962–965.
129. KEARSLEY, E P and WAINWRIGHT, P J. Porosity and permeability of foamed concrete. *Cement and concrete research*. 2001. Vol. 31, no. 5, p. 805–812.
130. MAOQIANG, Li, YUFENG, Chen, SHUQIN, Xia, JIANHUI, Li and HONGXUN, Liang. Microstructure and Processing of Ultra-Light Calcium Silicate Insulation Material. *JOURNAL-CHINESE CERAMIC SOCIETY*. 2000. Vol. 28, no. 5, p. 401–406.
131. KORONTHALYOVA, Olga and MATIASOVSKY, Peter. Thermal conductivity of fibre reinforced porous calcium silicate hydrate-based

composites. *Journal of Thermal Envelope and Building Science*. 2003. Vol. 27, no. 1, p. 71–89.
132. ATAI, Mohammad, PAHLAVAN, Ayoub and MOIN, Niloofar. Nano-porous thermally sintered nano silica as novel fillers for dental composites. *Dental materials*. 2012. Vol. 28, no. 2, p. 133–145.
133. ZHANG, Bong June, KIM, Kwang Jin and YOON, Hyungkee. Enhanced heat transfer performance of alumina sponge-like nano-porous structures through surface wettability control in nucleate pool boiling. *International journal of heat and mass transfer*. 2012. Vol. 55, no. 25–26, p. 7487–7498.
134. LIU, Fei, CHEN, Sha, LIN, Qian, WANG, Xiao-dan and CAO, Jian-xin. Effect of anions from calcium sources on the synthesis of nano-sized xonotlite fibers. *Optoelectronics Letters*. 2017. Vol. 13, no. 2, p. 81–83.
135. GAO, Qing-fu, ZHANG, Chang-rui, FENG, Jian, FENG, Jun-zong, JIANG, Yong-gang and WU, Wei. Progress of silica aerogel insulation composites. *Journal of Materials Science and Engineering*. 2009. Vol. 2.
136. SHOU-GUO, Zhang, HONG-BO, Xie and GUO-ZHONG, Li. Research Advances in Calcium Silicate Insulation Material [J]. *Construction Conserves Energy*. 2006. Vol. 5.
137. REIM, M, KÖRNER, W, MANARA, J, KORDER, S, ARDUINI-SCHUSTER, M, EBERT, H-P and FRICKE, J. Silica aerogel granulate material for thermal insulation and daylighting. *Solar energy*. 2005. Vol. 79, no. 2, p. 131–139.
138. YUAN, Bo, DING, Shuqiang, WANG, Dongdong, WANG, Gang and LI, Hongxia. Heat insulation properties of silica aerogel/glass fiber composites fabricated by press forming. *Materials Letters*. 2012. Vol. 75, p. 204–206.
139. BAI, Jilin, LI, Yuanzhi, REN, Lu, MAO, Mingyang, ZENG, Min and ZHAO, Xiujian. Thermal insulation monolith of aluminum tobermorite nanosheets prepared from fly ash. *ACS Sustainable Chemistry & Engineering*. 2015. Vol. 3, no. 11, p. 2866–2873.
140. WEI, Gaosheng, LIU, Yusong, ZHANG, Xinxin, YU, Fan and DU, Xiaoze. Thermal conductivities study on silica aerogel and its composite insulation materials. *International Journal of Heat and Mass Transfer*. 2011. Vol. 54, no. 11–12, p. 2355–2366.
141. LIU, Fei, ZENG, Lingke, CAO, Jianxin and LI, Jing. Preparation of ultra-light xonotlite thermal insulation material using carbide slag. *Journal of Wuhan University of Technology-Mater. Sci. Ed.* 2010. Vol. 25, no. 2, p. 295–297.
142. WEI, Gaosheng, ZHANG, Xinxin and YU, Fan. Thermal conductivity of xonotlite insulation material. *International Journal of Thermophysics*. 2007. Vol. 28, no. 5, p. 1718–1729.
143. ZHENG, Qijun and WANG, Wei. Calcium silicate based high efficiency thermal insulation. *British ceramic transactions*. 2000. Vol. 99, no. 4, p. 187–190.
144. PUSCH, Walter G. *High density asbestos-free tobermorite thermal insulation containing wollastonite*. 5 December 1978. Google Patents.

145. HUANG, Xiang, JIANG, Dongliang and TAN, Shouhong. Novel hydrothermal synthesis method for tobermorite fibers and investigation on their thermal stability. *Materials research bulletin*. 2002. Vol. 37, no. 11, p. 1885–1892.
146. WEI, Gaosheng, ZHANG, Xinxin and YU, Fan. Thermal conductivity measurements on xonotlite-type calcium silicate by the transient hot-strip method. *Journal of University of Science and Technology Beijing, Mineral, Metallurgy, Material*. 2008. Vol. 15, no. 6, p. 791–795.
147. SHANNON, Richard F. *Method of producing structural insulation materials containing at least 50 percent xonotlite*. 18 December 1979. Google Patents.
148. SMALAKYS, G and SIAUCIUNAS, R. The synthesis of 1.13 nm tobermorite from carbonated opoka. *Journal of Thermal Analysis and Calorimetry*. 2018. Vol. 134, no. 1, p. 493–502.
149. MATSUSHITA, Fumiaki, AONO, Yoshimichi and SHIBATA, Sumio. Calcium silicate structure and carbonation shrinkage of a tobermorite-based material. *Cement and Concrete Research*. 2004. Vol. 34, no. 7, p. 1251–1257.
150. BAIRD, Thomas, CAIRNS-SMITH, A Graham and SNELL, Douglas S. Morphology and CO_2 uptake in tobermorite gel. *Journal of Colloid and Interface Science*. 1975. Vol. 50, no. 2, p. 387–391.
151. SAITO, Tsuyoshi, SAKAI, Etsuo, MORIOKA, Minoru and OTSUKI, Nobuaki. Carbonation of γ-Ca_2SiO_4 and the Mechanism of Vaterite Formation. *Journal of Advanced Concrete Technology*. 2010. Vol. 8, no. 3, p. 273–280.
152. BIAGIONI, Cristian, BONACCORSI, Elena, LEZZERINI, Marco and MERLINO, Stefano. Thermal behaviour of Al-rich tobermorite. *European Journal of Mineralogy*. 2016. Vol. 28, no. 1, p. 23–32.
153. JACKSON, Marie D, MOON, Juhyuk, GOTTI, Emanuele, TAYLOR, Rae, CHAE, Sejung R, KUNZ, Martin, EMWAS, Abdul-Hamid, MERAL, Cagla, GUTTMANN, Peter and LEVITZ, Pierre. Material and elastic properties of Al-tobermorite in ancient Roman seawater concrete. *Journal of the American Ceramic Society*. 2013. Vol. 96, no. 8, p. 2598–2606.
154. CONG, X and KIRKPATRICK, R J. H1-29Si CPMAS NMR study of the structure of calcium silicate hydrate. *Advances in cement research*. 1995. Vol. 7, no. 27, p. 103–111.
155. SHAW, S, HENDERSON, C M B and KOMANSCHEK, B U. Dehydration/recrystallization mechanisms, energetics, and kinetics of hydrated calcium silicate minerals: an in situ TGA/DSC and synchrotron radiation SAXS/WAXS study. *Chemical Geology*. 2000. Vol. 167, no. 1–2, p. 141–159.
156. YU, Ping, KIRKPATRICK, R James, POE, Brent, MCMILLAN, Paul F and CONG, Xiandong. Structure of calcium silicate hydrate (C-S-H): Near-, Mid-, and Far-infrared spectroscopy. *Journal of the American Ceramic Society*. 1999. Vol. 82, no. 3, p. 742–748.
157. WANG, Lei, GUO, Fanxing, LIN, Yuqiang, YANG, Huamei and TANG, S

W. Comparison between the effects of phosphorous slag and fly ash on the CSH structure, long-term hydration heat and volume deformation of cement-based materials. *Construction and Building Materials*. 2020. Vol. 250, p. 118807.
158. WANG, Lu, YANG, H Q, ZHOU, S H, CHEN, E and TANG, Shengwen W. Mechanical properties, long-term hydration heat, shinkage behavior and crack resistance of dam concrete designed with low heat Portland (LHP) cement and fly ash. *Construction and Building Materials*. 2018. Vol. 187, p. 1073–1091.
159. LIAO, Wei, LI, Wenqing, FANG, Zhenggang, LU, Chunhua and XU, Zhongzi. Effect of Different Aluminum Substitution Rates on the Structure of Tobermorite. *Materials*. 2019. Vol. 12, no. 22, p. 3765.
160. SIAUCIUNAS, R and BALTAKYS, K. Formation of gyrolite during hydrothermal synthesis in the mixtures of CaO and amorphous SiO_2 or quartz. *Cement and Concrete Research*. 2004. Vol. 34, no. 11, p. 2029–2036.
161. JASINA, L, SIAUCIUNAS, R and KITRYS, S. K. Baltakys, A. Eisinas, T. Dizhbite. *Mater Struct*. 2011. Vol. 44, p. 1687–1701.
162. RÓŻYCKA, Agnieszka, KOTWICA, Łukasz and MAŁOLEPSZY, Jan. Synthesis of single phase gyrolite in the CaO-quartz-Na2O-H2O system. *Materials letters*. 2014. Vol. 120, p. 166–169.
163. MERLINO, Stefano. Gyrolite: its crystal structure and crystal chemistry. *Mineralogical Magazine*. 1988. Vol. 52, no. 366, p. 377–387.
164. LUO, Feng, WEI, Cundi, XUE, Bing, WANG, Shujuan and JIANG, Yinshan. Dynamic hydrothermal synthesis of Al-substituted 11 Å tobermorite from solid waste fly ash residue-extracted Al 2 O 3. *Research on Chemical Intermediates*. 2013. Vol. 39, no. 2, p. 693–705.
165. SUZUKI, Kazutaka, NISHIKAWA, Tadahiro and ITO, Suketoshi. Formation and carbonation of CSH in water. *Cement and Concrete research*. 1985. Vol. 15, no. 2, p. 213–224.
166. BALTAKYS, Kestutis, ILJINA, Aliona and BANKAUSKAITE, Agne. Thermal properties and application of silica gel waste contaminated with F− ions for CSH synthesis. *Journal of Thermal Analysis and Calorimetry*. 2015. Vol. 121, no. 1, p. 145–154.
167. LI, Ming, JIANG, Hongyi and XU, Dong. Synthesis and characterization of a xonotlite fibers–silica aerogel composite by ambient pressure drying. *Journal of Porous Materials*. 2018. Vol. 25, no. 5, p. 1417–1425.
168. DIEZ-GARCIA, Marta, GAITERO, Juan J, SANTOS, Jose I, DOLADO, Jorge S and AYMONIER, Cyril. Supercritical hydrothermal flow synthesis of xonotlite nanofibers. *Journal of Flow Chemistry*. 2018. Vol. 8, no. 2, p. 89–95.
169. MATHIAS, Paul M, KUMAR, Ravi, MOYER, J Douglas, SCHORK, Joan M, SRINIVASAN, Sree R, AUVIL, Steven R and TALU, Orhan. Correlation of multicomponent gas adsorption by the dual-site Langmuir model. Application to nitrogen/oxygen adsorption on 5A-zeolite. *Industrial & engineering chemistry research*. 1996. Vol. 35, no. 7, p. 2477–2483.

170. BRAUNEUR, S, EMMET, P and TELLER, E. Adsorption of gases in multi molecular layer. *Journal of Am. Chemical. Soc*. 1938. Vol. 60, p. 309.
171. UNION, I and PURE, O F. Chemistry. *A., Divisions, PC, Working, I., For, P., Of, H., Assurance, Q., For, S., Laboratories, A., Thompson, M., Ellison, SLR and Wood*. 1985. P. 835–855.
172. CLARINGBULL, G F and HEY, M H. A re-examination of tobermorite. *Mineralogical Magazine and Journal of the Mineralogical Society*. 1952. Vol. 29, no. 218, p. 960–962.
173. KALOUSEK, George L. Tobermorite and related phases in the system CaO-SiO2-H2O. In : *Journal Proceedings*. 1955. p. 989–1011. ISBN 0002-8061.
174. VIRTUDAZO, Raymond V Rivera, WATANABE, Hideo, SHIRAI, Takashi and FUJI, Masayoshi. Simple preparation and initial characterization of semi-amorphous hollow calcium silicate hydrate nanoparticles by ammonia-hydrothermal-template techniques. *Journal of nanoparticle research*. 2013. Vol. 15, no. 5, p. 1604.
175. MARTINI, Francesca, TONELLI, Monica, GEPPI, Marco, RIDI, Francesca, BORSACCHI, Silvia and CALUCCI, Lucia. Hydration of MgO/SiO2 and Portland cement mixtures: A structural investigation of the hydrated phases by means of X-ray diffraction and solid state NMR spectroscopy. *Cement and Concrete Research*. 2017. Vol. 102, p. 60–67.
176. LODEIRO, I García, FERNÁNDEZ-JIMENEZ, Ana, PALOMO, A and MACPHEE, Donald E. Effect on fresh CSH gels of the simultaneous addition of alkali and aluminium. *Cement and Concrete Research*. 2010. Vol. 40, no. 1, p. 27–32.
177. KAPELUSZNA, Ewa, KOTWICA, Łukasz, RÓŻYCKA, Agnieszka and GOŁEK, Łukasz. Incorporation of Al in CASH gels with various Ca/Si and Al/Si ratio: Microstructural and structural characteristics with DTA/TG, XRD, FTIR and TEM analysis. *Construction and Building Materials*. 2017. Vol. 155, p. 643–653.
178. DYCZEK, J R L and TAYLOR, H F W. X-ray determination of tobermorite, quartz and α-dicalcium silicate hydrate in autoclaved calcium silicate materials. *Cement and Concrete Research*. 1971. Vol. 1, no. 6, p. 589–605.
179. HARA, N and MIDGLEY, H G. The determination of crystallinity of tobermorite in autoclaved products. *Cement and Concrete Research*. 1980. Vol. 10, no. 2, p. 213–221.
180. CAO, Jian Xin, ZHANG, Yu and ZENG, Ling Ke. Preparation of nanoporous super thermal insulation material compounded with xonotlite-SiO2-aerogel and characterization of the pore structure. In : *Key Engineering Materials*. Trans Tech Publ, 2007. p. 1505–1508. ISBN 0878494103.
181. ЛЕОНТЬЕВ, С В, ГОЛУБЕВ, В А, ШАМАНОВ, В А, КУРЗАНОВ, А Д, ЯКОВЛЕВ, Г И and ХАЗЕЕВ, Д Р. Модификация структуры теплоизоляционного автоклавного газобетона дисперсией многослойных углеродных нанотрубок. *Строительные материалы*. 2016. No. 1–2.
182. MILESTONE, N B and AHARI, Ghanbari K. Hydrothermal processing of

xonotlite based compositions. *Advances in Applied ceramics*. 2007. Vol. 106, no. 6, p. 302–308.
183. LEKŪNAITĖ, Lina. *Kalcio hidrosilikatų susidarymą intensyvinančių priedų poveikis autoklavinio akytojo betono formavimo mišinių ir produktų savybėms*. 2013. VGTU leidykla „TECHNIKA “. ISBN 609457494X.

List of Scientific Publications on the Theme of the Dissertation

Articles Published in Journals indexed in the Clarivate Analytics Web of Science with Impact Factor

1. Smalakys, G.; Siauciunas, R. Peculiarities of xonotlite synthesis from the raw materials with different SiO_2 activities // Journal of thermal analysis and calorimetry. Dordrecht: Springer. ISSN 1388-6150. 2020, Vol. 142, p. 1671-1679. DOI: 10.1007/s10973-020-09744-2. [IF: 2.731; AIF: 4.796; IF/AIF: 0.569; Q2 (2019)].
2. Smalakys, G.; Siauciunas, R. The hydrothermal synthesis of 1.13 nm tobermorite from granite sawing powder waste // Ceramics - Silikaty. Prague: Institute of Chemical Technology. ISSN 0862-5468. 2020, Vol. 64, iss. 3, p. 239-248. DOI: 10.13168/cs.2020.0013. [IF: 0.820; AIF: 3.004; IF/AIF: 0.272; Q4 (2019)].
3. Smalakys, G.; Siauciunas, R. The synthesis of 1.13 nm tobermorite from carbonated opoka // Journal of thermal analysis and calorimetry. Dordrecht: Springer. ISSN 1388-6150. 2018, vol. 134, iss. 1, p. 493-502. DOI: 10.1007/s10973-018-7418-1. [IF: 2.471; AIF: 4.295; IF/AIF: 0.575; Q2 (2018)].

Articles published in conference proceedings

1. Siauciunas, R.; Smalakys, G. Xonotlite synthesis from opoka and its application for thermal insulating materials // 15th international congress on the chemistry of cement: Prague, Czech Republic, September 16-20, 2019: papers and posters proceedings. Prague: CONFEA. ISSN 2523-935X. 2019, p. 233-241.

Publications of International Scientific Conferences

1. Šiaučiūnas, R.; Smalakys, G. Xonotlite synthesis from opoka and its application for thermal insulating materials // 15th International Congress on the Chemistry of Cement (ICCC 2019) September 16–20, 2019, Prague, Czech Republic.
2. Smalakys, G.; Šiaučiūnas, R. The impact of raw meal composition on low-base calcium silicate hydrates synthesis // Chemistry and chemical technology: Lithuanian chemists conference, 2019 May 16, Lithuanian Academy of Sciences, Vilnius: conference book. Vilnius: Vilnius University, 2019. eISBN 9786090701676. p. 118.
3. Siauciunas, R.; Smalakys, G. Impact of SiO_2 raw materials activity on xonotlite synthesis // 12th European symposium on thermal analysis and calorimetry, 27–30 August 2018, Brasov. Greifswald: Academica, 2018, PS1.052. ISBN 9783940237507. p. 236.
4. Smalakys, G.; Siauciunas, R. Thermal insulating materials from silica-calcite sedimentary rocks // BaltSilica 2018: book of abstracts of the 8th international conference on silicate materials, May 30–June 1, 2018, Riga, Latvia / Riga

Technical University. Riga: RTU publishing house. ISSN 2243-6057. 2018, P10, p. 40.
5. Siauciunas, R.; Smalakys, G. Peculiarities of 1.13 tobermorite and xonotlite synthesis from isomorphic Ca/Si rocks // Book of abstracts of the 4th Central and Eastern European conference on thermal analysis and calorimetry (CEEC-TAC4), 28–31 August 2017, Chisinau, Moldova. Rostock: Academica Greifswald, 2017, PS2.13. ISBN 9783940237477. p. 301.
6. Smalakys, G.; Šiaučiūnas, R. Formation of intermediate phases during 1.13 nm tobermorite synthesis // Chemistry and chemical technology 2017: proceedings of the international conference, April 28, 2017, Kaunas. Kaunas: KTU. ISSN 2538-7359. 2017, p. 71.

Appendices

Appendix 1

Table A1.1. Calculation of the total surface area of the synthesis product (200 °C, 12 h) from $SiO_2 \cdot H_2O$ when using the cylindrical pore model

Average K radius of the pores r_K (Å)	Average true pore radius, r_p (Å)	Change, Δt, Å	ΔV_{ad}, $cm^3 \cdot g^{-1}$	Change of vap. liquid ads. vol. ΔV^L, $10^3 m^3 \cdot g^{-1}$	$\Delta t\Sigma A$ ($\times 10^3 m^3 \cdot g^{-1}$)	True volume of the pores Vp ($\times 10^3$ $cm^3 \cdot g^{-1}$)	Surface of pore walls, A, $m^2 \cdot g^{-1}$	Total surface ΣA, $m^2 \cdot g^{-1}$
931.83	958.45	11.80	35.39	54.49	0.00	57.65	1.20	0.17
285.63	304.17	4.36	57.50	88.55	0.07	100.33	6.60	6.77
156.64	171.95	2.10	42.32	65.17	1.42	76.82	8.94	15.70
108.21	121.77	1.40	26.17	40.31	2.20	48.26	7.93	23.63
81.61	93.96	1.01	19.28	29.69	2.39	36.19	7.70	31.33
65.21	76.68	0.76	12.43	19.13	2.37	23.18	6.05	37.38
54.20	64.99	0.61	9.34	14.38	2.27	17.40	5.35	42.73
46.20	56.43	0.51	7.19	11.07	2.17	13.29	4.71	47.44
40.22	49.99	0.41	5.46	8.40	1.96	9.95	3.98	51.42
35.37	44.74	0.41	4.88	7.51	2.09	8.67	3.88	55.30
31.39	40.38	0.32	3.69	5.69	1.79	6.45	3.20	58.50
28.23	36.92	0.30	3.31	5.09	1.76	5.70	3.09	61.59
25.56	33.96	0.27	2.62	4.03	1.63	4.23	2.49	64.08
23.25	31.39	0.26	2.39	3.68	1.65	3.71	2.36	66.44
21.21	29.10	0.23	2.13	3.28	1.55	3.25	2.24	68.68
19.49	27.16	0.20	1.64	2.52	1.40	2.17	1.59	70.27
18.00	25.48	0.20	1.63	2.50	1.37	2.26	1.78	72.05
16.65	23.93	0.19	1.53	2.35	1.36	2.04	1.71	73.75
15.41	22.50	0.18	1.36	2.09	1.35	1.59	1.41	75.17
14.31	21.24	0.16	1.40	2.16	1.22	2.07	1.95	77.12
13.33	20.09	0.16	2.62	4.03	1.25	6.31	6.28	83.40
12.40	19.00	0.16	1.13	1.74	1.34	0.94	0.99	84.39
11.56	18.01	0.14	0.68	1.04	1.21	-0.41	-0.46	83.93

Table A1.2. Calculation of the total surface area of the synthesis product (200 °C, 72 h) from $SiO_2 \cdot H_2O$ when using the cylindrical pore model

Average K radius of the pores r_K (Å)	Average true pore radius, r_p (Å)	Change, Δt, Å	ΔV_{ad}, $cm^3 \cdot g^{-1}$	Change of vap. liquid ads. vol. ΔV^L, $10^3 m^3 \cdot g^{-1}$	$\Delta t\Sigma A$ ($\times 10^3 m^3 \cdot g^{-1}$)	True volume of the pores Vp ($\times 10^3$ $cm^3 \cdot g^{-1}$)	Surface of pore walls, A, $m^2 \cdot g^{-1}$	Total surface ΣA, $m^2 \cdot g^{-1}$
281.75	300.24	4.01	2.98	4.60	0.00	5.22	0.35	0.17
157.53	172.86	2.33	27.57	42.46	0.04	51.07	5.91	6.08
106.37	119.86	1.35	11.73	18.07	0.82	21.90	3.65	9.73
81.16	93.50	0.95	6.51	10.02	0.93	12.07	2.58	12.32
65.16	76.63	0.78	3.85	5.93	0.96	6.88	1.80	14.11
53.99	64.76	0.61	2.57	3.96	0.86	4.47	1.38	15.49
46.13	56.36	0.49	1.80	2.77	0.76	3.01	1.07	16.56
40.15	49.92	0.43	1.58	2.44	0.72	2.66	1.07	17.62
35.42	44.79	0.36	1.14	1.75	0.64	1.77	0.79	18.42
31.56	40.58	0.34	1.06	1.63	0.63	1.65	0.81	19.23
28.29	36.98	0.30	0.99	1.52	0.58	1.61	0.87	20.10
25.57	33.97	0.27	0.82	1.26	0.55	1.25	0.73	20.83
23.21	31.35	0.26	0.76	1.18	0.54	1.16	0.74	21.57
21.20	29.09	0.22	0.69	1.06	0.48	1.08	0.74	22.31
19.52	27.20	0.20	0.58	0.89	0.45	0.86	0.63	22.95
18.04	25.53	0.20	0.60	0.93	0.45	0.95	0.74	23.69
16.66	23.95	0.20	0.53	0.82	0.46	0.72	0.61	24.30
15.41	22.51	0.18	0.48	0.74	0.43	0.67	0.59	24.89
14.32	21.24	0.17	0.54	0.84	0.42	0.92	0.87	25.76
13.31	20.08	0.16	0.92	1.42	0.42	2.26	2.25	28.01
12.41	19.01	0.15	0.40	0.61	0.42	0.45	0.48	28.49
11.57	18.03	0.15	0.37	0.56	0.43	0.32	0.36	28.84
10.80	17.11	0.14	0.38	0.58	0.41	0.44	0.51	29.35
10.09	16.25	0.14	0.37	0.58	0.42	0.41	0.51	29.86
9.42	15.44	0.14	0.36	0.56	0.40	0.41	0.54	30.39
8.80	14.69	0.13	0.35	0.54	0.41	0.37	0.50	30.90
8.22	13.97	0.13	0.37	0.57	0.41	0.47	0.67	31.56
7.67	13.30	0.13	0.36	0.56	0.41	0.47	0.70	32.26
7.15	12.65	0.13	0.37	0.57	0.42	0.45	0.72	32.98
6.65	12.01	0.13	0.37	0.57	0.43	0.44	0.74	33.72
6.17	11.40	0.13	0.36	0.55	0.45	0.36	0.63	34.35
5.71	10.81	0.13	0.37	0.56	0.46	0.36	0.68	35.03
5.26	10.22	0.14	0.40	0.62	0.49	0.50	0.97	36.00
4.82	9.63	0.15	0.42	0.65	0.52	0.52	1.08	37.08
4.38	9.04	0.16	0.47	0.73	0.59	0.62	1.37	38.45
3.93	8.43	0.17	0.43	0.66	0.67	-0.07	-0.17	38.27

3.44	7.74	0.22	0.80	1.23	0.83	-	-	-
2.88	6.94	0.28	-	-	-	-	-	-

Table A1.3. Calculation of the total surface area of the synthesis product (200 °C, 12 h) from $SiO_2 \cdot H_2O$ when using the parallel plate pore model

Average K radius of the pores r_K (Å)	Average true pore radius, r_p (Å)	Change, Δt, Å	ΔV_{ad}, $cm^3 \cdot g^{-1}$	Change of vap. liquid ads. vol. ΔV^L, $10^3 m^3 \cdot g^{-1}$	$\Delta t\Sigma A$ ($\times 10^3 m^3 \cdot g^{-1}$)	True volume of the pores Vp ($\times 10^3$ $cm^3 \cdot g^{-1}$)	Surface of pore walls, A, $m^2 \cdot g^{-1}$	Total surface ΣA, $m^2 \cdot g^{-1}$
931.83	985.07	11.80	35.39	54.49	0.00	57.61	1.17	0.17
285.63	322.71	4.36	57.50	88.55	0.07	99.88	6.19	6.36
156.64	187.25	2.10	42.32	65.17	1.33	74.72	7.98	14.34
108.21	135.33	1.40	26.17	40.31	2.01	45.39	6.71	21.05
81.61	106.32	1.01	19.28	29.69	2.13	33.14	6.23	27.28
65.21	88.16	0.76	12.43	19.13	2.07	20.28	4.60	31.88
54.20	75.78	0.61	9.34	14.38	1.94	14.68	3.87	35.76
46.20	66.66	0.51	7.19	11.07	1.81	10.74	3.22	38.98
40.22	59.76	0.41	5.46	8.40	1.61	7.70	2.58	41.56
35.37	54.10	0.41	4.88	7.51	1.69	6.33	2.34	43.90
31.39	49.38	0.32	3.69	5.69	1.42	4.48	1.82	45.71
28.23	45.60	0.30	3.31	5.09	1.37	3.79	1.66	47.37
25.56	42.37	0.27	2.62	4.03	1.26	2.51	1.19	48.56
23.25	39.53	0.26	2.39	3.68	1.25	2.01	1.02	49.58
21.21	37.00	0.23	2.13	3.28	1.16	1.68	0.91	50.48
19.49	34.84	0.20	1.64	2.52	1.03	0.81	0.47	50.95
18.00	32.96	0.20	1.63	2.50	1.00	0.94	0.57	51.52
16.65	31.22	0.19	1.53	2.35	0.98	0.75	0.48	52.00
15.41	29.60	0.18	1.36	2.09	0.95	0.37	0.25	52.25
14.31	28.16	0.16	1.40	2.16	0.85	0.92	0.65	52.91
13.33	26.86	0.16	2.62	4.03	0.86	4.66	3.47	56.38
12.40	25.60	0.16	1.13	1.74	0.91	-0.15	-0.12	56.26
11.56	24.46	0.14	0.68	1.04	0.81	-	-	-
10.82	23.43	0.14	-	-	-	-	-	-

Table A1.4. Calculation of the total surface area of the synthesis product (200 °C, 72 h) from $SiO_2 \cdot H_2O$ when using the parallel plate pore model

Average K radius of the pores r_K (Å)	Average true pore radius, r_p (Å)	Change, Δt, Å	ΔV_{ad}, $cm^3 \cdot g^{-1}$	Change of vap. liquid ads. vol. ΔV^L, $10^3 m^3 \cdot g^{-1}$	$\Delta t\Sigma A$ ($\times 10^3 m^3 \cdot g^{-1}$)	True volume of the pores Vp ($\times 10^3$ $cm^3 \cdot g^{-1}$)	Surface of pore walls, A, $m^2 \cdot g^{-1}$	Total surface ΣA, $m^2 \cdot g^{-1}$
281.75	318.73	4.01	2.98	4.60	0.00	5.20	0.33	0.17
157.53	188.18	2.33	27.57	42.46	0.04	50.63	5.38	5.55
106.37	133.34	1.35	11.73	18.07	0.75	20.77	3.12	8.67
81.16	105.83	0.95	6.51	10.02	0.83	10.91	2.06	10.73
65.16	88.09	0.78	3.85	5.93	0.84	5.76	1.31	12.04
53.99	75.54	0.61	2.57	3.96	0.73	3.50	0.93	12.96
46.13	66.59	0.49	1.80	2.77	0.63	2.17	0.65	13.62
40.15	59.68	0.43	1.58	2.44	0.59	1.87	0.63	14.24
35.42	54.16	0.36	1.14	1.75	0.52	1.09	0.40	14.64
31.56	49.59	0.34	1.06	1.63	0.50	0.98	0.40	15.04
28.29	45.67	0.30	0.99	1.52	0.45	0.99	0.43	15.47
25.57	42.38	0.27	0.82	1.26	0.42	0.68	0.32	15.79
23.21	39.49	0.26	0.76	1.18	0.41	0.61	0.31	16.10
21.20	36.99	0.22	0.69	1.06	0.36	0.58	0.32	16.42
19.52	34.89	0.20	0.58	0.89	0.33	0.41	0.24	16.65
18.04	33.01	0.20	0.60	0.93	0.33	0.50	0.30	16.95
16.66	31.23	0.20	0.53	0.82	0.33	0.28	0.18	17.13
15.41	29.61	0.18	0.48	0.74	0.30	0.26	0.18	17.31
14.32	28.17	0.17	0.54	0.84	0.29	0.51	0.36	17.67
13.31	26.84	0.16	0.92	1.42	0.29	1.69	1.26	18.93
12.41	25.62	0.15	0.40	0.61	0.28	0.09	0.07	19.00
11.57	24.48	0.15	0.37	0.56	0.29	-0.03	-0.02	18.98
10.80	23.41	0.14	0.38	0.58	0.27	-	-	-

Table A1.5. Calculation of the total surface area of the synthesis product (200 °C, 12 h) from granite when using the cylindrical pore model

Average K radius of the pores r_K (Å)	Average true pore radius, r_p (Å)	Change, Δt, Å	ΔV_{ad}, $cm^3 \cdot g^{-1}$	Change of vap. liquid ads. vol. ΔV^L, $10^3 m^3 \cdot g^{-1}$	$\Delta t\Sigma A$ ($\times 10^3 m^3 \cdot g^{-1}$)	True volume of the pores Vp ($\times 10^3$ $cm^3 \cdot g^{-1}$)	Surface of pore walls, A, $m^2 \cdot g^{-1}$	Total surface ΣA, $m^2 \cdot g^{-1}$
283.78	302.26	4.49	8.71	13.41	0.00	15.22	1.01	0.17
153.31	168.51	2.08	10.86	16.73	0.04	20.16	2.39	2.56
106.02	119.49	1.38	4.96	7.64	0.35	9.26	1.55	4.11
80.76	93.08	0.92	2.62	4.03	0.38	4.85	1.04	5.16

65.03	76.49	0.79	1.77	2.73	0.41	3.21	0.84	5.99
53.68	64.43	0.62	1.51	2.32	0.37	2.80	0.87	6.86
45.96	56.18	0.46	0.91	1.39	0.31	1.62	0.58	7.44
40.26	50.03	0.43	0.85	1.31	0.32	1.53	0.61	8.05
35.37	44.73	0.40	0.92	1.42	0.32	1.76	0.79	8.84
31.34	40.33	0.34	0.66	1.02	0.30	1.19	0.59	9.43
28.16	36.84	0.29	0.65	0.99	0.27	1.24	0.67	10.10
25.52	33.91	0.28	0.57	0.88	0.28	1.07	0.63	10.73
23.18	31.32	0.25	0.55	0.85	0.27	1.05	0.67	11.40
21.18	29.07	0.23	0.53	0.82	0.26	1.05	0.72	12.13
19.44	27.12	0.21	0.45	0.70	0.26	0.86	0.63	12.76
17.92	25.39	0.20	0.44	0.67	0.25	0.84	0.67	13.42
16.55	23.83	0.19	0.35	0.54	0.26	0.59	0.50	13.92
15.34	22.43	0.17	0.36	0.55	0.24	0.66	0.59	14.51
14.26	21.17	0.17	0.32	0.49	0.25	0.53	0.50	15.01
13.26	20.01	0.16	0.48	0.74	0.24	1.13	1.13	16.14
12.35	18.95	0.15	0.37	0.57	0.25	0.76	0.80	16.94
11.53	17.97	0.15	0.32	0.50	0.25	0.61	0.68	17.61
10.76	17.06	0.14	0.32	0.50	0.25	0.61	0.71	18.32
10.05	16.21	0.14	0.33	0.51	0.26	0.65	0.80	19.13
9.39	15.40	0.14	0.36	0.55	0.26	0.76	0.99	20.12
8.76	14.65	0.13	0.33	0.51	0.27	0.66	0.90	21.02
8.19	13.94	0.13	0.33	0.51	0.28	0.68	0.98	22.00
7.64	13.26	0.13	0.29	0.45	0.29	0.48	0.73	22.73
7.12	12.61	0.13	0.31	0.48	0.30	0.59	0.93	23.66
6.62	11.98	0.13	0.32	0.50	0.31	0.63	1.05	24.70
6.15	11.37	0.13	0.34	0.52	0.33	0.66	1.16	25.86
5.68	10.77	0.13	0.35	0.54	0.35	0.70	1.30	27.16
5.24	10.19	0.14	0.35	0.54	0.38	0.61	1.19	28.35
4.79	9.60	0.15	0.37	0.56	0.42	0.56	1.16	29.51
4.35	9.00	0.16	0.41	0.63	0.47	0.70	1.55	31.07
3.90	8.39	0.18	0.35	0.54	0.55	-0.04	-0.10	30.96
3.42	7.72	0.21	0.65	0.99	0.65	-	-	-
2.85	6.89	0.31	-	-	-	-	-	-

Table A1.6. Calculation of the total surface area of the synthesis product (200 °C, 12 h) from granite when using the parallel plate pore model

Average K radius of the pores r_K (Å)	Average true pore radius, r_p (Å)	Change, Δt, Å	ΔV_{ad}, $cm^3 \cdot g^{-1}$	Change of vap. liquid ads. vol. ΔV^L, $10^3 m^3 \cdot g^{-1}$	$\Delta t\Sigma A$ ($\times 10^3 m^3 \cdot g^{-1}$)	True volume of the pores Vp ($\times 10^3$ $cm^3 \cdot g^{-1}$)	Surface of pore walls, A, $m^2 \cdot g^{-1}$	Total surface ΣA, $m^2 \cdot g^{-1}$
283.78	320.75	4.49	8.71	13.41	0.00	15.16	0.95	0.17
153.31	183.71	2.08	10.86	16.73	0.04	19.96	2.17	2.34
106.02	132.96	1.38	4.96	7.64	0.32	8.77	1.32	3.66
80.76	105.39	0.92	2.62	4.03	0.34	4.38	0.83	4.49
65.03	87.95	0.79	1.77	2.73	0.35	2.73	0.62	5.11
53.68	75.19	0.62	1.51	2.32	0.32	2.36	0.63	5.74
45.96	66.39	0.46	0.91	1.39	0.26	1.26	0.38	6.12
40.26	59.81	0.43	0.85	1.31	0.26	1.17	0.39	6.51
35.37	54.09	0.40	0.92	1.42	0.26	1.38	0.51	7.02
31.34	49.32	0.34	0.66	1.02	0.24	0.85	0.34	7.37
28.16	45.52	0.29	0.65	0.99	0.21	0.92	0.41	7.77
25.52	42.31	0.28	0.57	0.88	0.21	0.75	0.36	8.13
23.18	39.45	0.25	0.55	0.85	0.20	0.74	0.38	8.50
21.18	36.96	0.23	0.53	0.82	0.20	0.75	0.41	8.91
19.44	34.79	0.21	0.45	0.70	0.19	0.57	0.33	9.24
17.92	32.85	0.20	0.44	0.67	0.18	0.56	0.34	9.58
16.55	31.10	0.19	0.35	0.54	0.18	0.33	0.21	9.79
15.34	29.52	0.17	0.36	0.55	0.17	0.41	0.28	10.07
14.26	28.09	0.17	0.32	0.49	0.17	0.28	0.20	10.27
13.26	26.76	0.16	0.48	0.74	0.17	0.83	0.62	10.89
12.35	25.54	0.15	0.37	0.57	0.17	0.49	0.38	11.27
11.53	24.42	0.15	0.32	0.50	0.17	0.36	0.29	11.56
10.76	23.36	0.14	0.32	0.50	0.17	0.35	0.30	11.86
10.05	22.36	0.14	0.33	0.51	0.17	0.39	0.35	12.21
9.39	21.42	0.14	0.36	0.55	0.17	0.48	0.45	12.66
8.76	20.53	0.13	0.33	0.51	0.17	0.39	0.38	13.04
8.19	19.68	0.13	0.33	0.51	0.17	0.41	0.41	13.45
7.64	18.88	0.13	0.29	0.45	0.18	0.24	0.25	13.70
7.12	18.10	0.13	0.31	0.48	0.18	0.32	0.35	14.05
6.62	17.34	0.13	0.32	0.50	0.18	0.35	0.40	14.46
6.15	16.60	0.13	0.34	0.52	0.19	0.36	0.44	14.90
5.68	15.87	0.13	0.35	0.54	0.20	0.40	0.50	15.40
5.24	15.15	0.14	0.35	0.54	0.21	0.32	0.42	15.82
4.79	14.41	0.15	0.37	0.56	0.24	0.27	0.38	16.19
4.35	13.66	0.16	0.41	0.63	0.26	0.37	0.54	16.73
3.90	12.88	0.18	0.35	0.54	0.29	-0.17	-0.26	16.47

3.42	12.01	0.21	0.65	0.99	0.34	-	-	-
2.85	10.92	0.31	-	-	-	-	-	-

Table A1.7. Calculation of the total surface area of the synthesis product (200 °C, 12 h) from opoka when using the cylindrical pore model

Average K radius of the pores r_K (Å)	Average true pore radius, r_p (Å)	Change, Δt, Å	ΔV_{ad}, $cm^3 \cdot g^{-1}$	Change of vap. liquid ads. vol. ΔV^L, $10^3 m^3 \cdot g^{-1}$	$\Delta t\Sigma A$ ($\times 10^3 m^3 \cdot g^{-1}$)	True volume of the pores Vp ($\times 10^3$ $cm^3 \cdot g^{-1}$)	Surface of pore walls, A, $m^2 \cdot g^{-1}$	Total surface ΣA, $m^2 \cdot g^{-1}$
278.79	297.20	4.10	10.99	16.92	0.00	19.23	1.29	0.17
156.23	171.53	2.14	35.23	54.26	0.04	65.35	7.62	7.79
107.36	120.88	1.40	25.45	39.20	1.09	48.31	7.99	15.78
81.42	93.77	0.96	15.88	24.45	1.51	30.43	6.49	22.28
65.35	76.83	0.78	9.95	15.33	1.74	18.78	4.89	27.16
54.06	64.84	0.62	6.41	9.87	1.68	11.79	3.64	30.80
46.25	56.49	0.47	3.93	6.06	1.44	6.88	2.44	33.24
40.34	50.12	0.44	3.60	5.55	1.48	6.29	2.51	35.74
35.50	44.87	0.37	2.56	3.95	1.32	4.19	1.87	37.61
31.57	40.58	0.35	2.34	3.60	1.31	3.78	1.86	39.47
28.27	36.96	0.30	1.86	2.86	1.18	2.86	1.55	41.02
25.53	33.93	0.28	1.74	2.67	1.15	2.69	1.59	42.61
23.21	31.35	0.25	1.51	2.32	1.05	2.32	1.48	44.09
21.22	29.12	0.23	1.32	2.03	1.03	1.89	1.30	45.39
19.46	27.14	0.21	1.27	1.96	0.97	1.91	1.41	46.80
17.92	25.38	0.20	1.12	1.72	0.95	1.56	1.23	48.03
16.60	23.87	0.17	0.97	1.49	0.83	1.35	1.13	49.16
15.43	22.53	0.18	0.89	1.37	0.86	1.07	0.95	50.11
14.33	21.26	0.17	1.03	1.59	0.86	1.60	1.51	51.62
13.33	20.10	0.16	1.01	1.56	0.80	1.71	1.70	53.32
12.42	19.03	0.16	0.87	1.34	0.85	1.14	1.20	54.52
11.57	18.02	0.15	0.82	1.26	0.82	1.07	1.19	55.71
10.80	17.11	0.14	0.79	1.22	0.79	1.09	1.27	56.98
10.09	16.25	0.14	0.77	1.19	0.81	1.00	1.22	58.20
9.42	15.45	0.14	0.74	1.14	0.79	0.94	1.22	59.42
8.80	14.69	0.13	0.73	1.12	0.79	0.91	1.23	60.65
8.22	13.98	0.13	0.65	1.00	0.81	0.54	0.78	61.43
7.67	13.29	0.13	0.61	0.94	0.80	0.42	0.63	62.06
7.15	12.64	0.13	0.70	1.07	0.81	0.84	1.33	63.38
6.65	12.02	0.13	0.75	1.16	0.82	1.08	1.80	65.19
6.17	11.41	0.13	0.74	1.14	0.87	0.92	1.62	66.81
5.71	10.81	0.14	0.80	1.22	0.90	1.15	2.13	68.93
5.26	10.22	0.14	0.57	0.87	0.97	-0.35	-0.68	68.25

4.82	9.64	0.15	1.06	1.64	1.00	-	-	-
4.38	9.04	0.16	-	-	-	-	-	-

Table A1.8. Calculation of the total surface area of the synthesis product (200 °C, 72 h) from opoka when using the cylindrical pore model

Average K radius of the pores r_K (Å)	Average true pore radius, r_p (Å)	Change, Δt, Å	ΔV_{ad}, $cm^3 \cdot g^{-1}$	Change of vap. liquid ads. vol. ΔV^L, $10^3 m^3 \cdot g^{-1}$	$\Delta t\Sigma A$ ($\times 10^3 m^3 \cdot g^{-1}$)	True volume of the pores Vp ($\times 10^3$ $cm^3 \cdot g^{-1}$)	Surface of pore walls, A, $m^2 \cdot g^{-1}$	Total surface ΣA, $m^2 \cdot g^{-1}$
277.11	295.49	4.08	5.64	8.69	0.00	9.88	0.67	0.17
155.60	170.87	2.13	22.29	34.33	0.04	41.36	4.84	5.01
106.49	119.98	1.44	10.46	16.11	0.72	19.53	3.26	8.27
80.50	92.80	0.92	5.60	8.63	0.76	10.45	2.25	10.52
65.25	76.72	0.73	4.09	6.30	0.77	7.64	1.99	12.51
54.43	65.24	0.61	2.95	4.55	0.76	5.44	1.67	14.18
46.32	56.56	0.52	2.62	4.03	0.74	4.90	1.73	15.91
40.20	49.97	0.42	1.88	2.90	0.66	3.46	1.38	17.30
35.44	44.81	0.39	1.65	2.54	0.67	2.99	1.33	18.63
31.50	40.51	0.34	1.43	2.21	0.62	2.62	1.29	19.92
28.23	36.92	0.31	1.28	1.98	0.62	2.33	1.26	21.18
25.48	33.87	0.27	1.13	1.74	0.58	2.05	1.21	22.39
23.16	31.30	0.25	0.98	1.51	0.56	1.75	1.12	23.51
21.24	29.14	0.21	0.81	1.25	0.50	1.41	0.97	24.48
19.57	27.25	0.21	0.80	1.23	0.52	1.38	1.01	25.49
18.03	25.51	0.20	0.74	1.15	0.51	1.28	1.00	26.49
16.65	23.94	0.19	0.72	1.12	0.50	1.26	1.06	27.55
15.43	22.53	0.18	0.71	1.10	0.48	1.31	1.16	28.71
14.33	21.26	0.17	0.71	1.10	0.49	1.34	1.26	29.97
13.30	20.06	0.17	1.04	1.61	0.51	2.50	2.50	32.46
12.39	18.99	0.15	0.57	0.89	0.47	0.97	1.02	33.49
11.58	18.03	0.15	0.57	0.88	0.51	0.92	1.02	34.51
10.80	17.11	0.14	0.50	0.77	0.50	0.68	0.80	35.31
10.08	16.25	0.14	0.52	0.81	0.50	0.80	0.98	36.29
9.42	15.44	0.14	0.45	0.70	0.49	0.55	0.71	37.00
8.80	14.69	0.13	0.48	0.73	0.50	0.65	0.89	37.89
8.21	13.97	0.13	0.50	0.77	0.50	0.78	1.11	39.00
7.67	13.29	0.13	0.48	0.74	0.51	0.69	1.04	40.04
7.14	12.64	0.13	0.49	0.76	0.52	0.75	1.18	41.22
6.65	12.01	0.13	0.50	0.78	0.54	0.78	1.30	42.52
6.17	11.40	0.13	0.51	0.79	0.56	0.77	1.35	43.86
5.71	10.81	0.14	0.52	0.80	0.60	0.73	1.35	45.22

5.26	10.22	0.14	0.52	0.81	0.63	0.67	1.30	46.52
4.81	9.63	0.15	0.56	0.86	0.69	0.69	1.44	47.96
4.41	9.09	0.13	0.59	0.91	0.63	1.21	2.67	50.63
3.96	8.47	0.20	0.66	1.01	1.02	-0.06	-0.13	50.50
3.43	7.73	0.22	0.83	1.27	1.09	-	-	-
2.88	6.93	0.28	-	-	-	-	-	-

Table A1.9. Calculation of the total surface area of the synthesis product (200 °C, 12 h) from opoka when using the parallel plate pore model

Average K radius of the pores r_K (Å)	Average true pore radius, r_p (Å)	Change, Δt, Å	ΔV_{ad}, $cm^3 \cdot g^{-1}$	Change of vap. liquid ads. vol. ΔV^L, $10^3 m^3 \cdot g^{-1}$	$\Delta t\Sigma A$ ($\times 10^3 m^3 \cdot g^{-1}$)	True volume of the pores Vp ($\times 10^3$ $cm^3 \cdot g^{-1}$)	Surface of pore walls, A, $m^2 \cdot g^{-1}$	Total surface ΣA, $m^2 \cdot g^{-1}$
278.79	315.62	4.10	10.99	16.92	0.00	19.16	1.21	0.17
156.23	186.82	2.14	35.23	54.26	0.04	64.79	6.94	7.11
107.36	134.41	1.40	25.45	39.20	0.99	46.59	6.93	14.04
81.42	106.12	0.96	15.88	24.45	1.34	28.37	5.35	19.39
65.35	88.31	0.78	9.95	15.33	1.52	16.62	3.76	23.15
54.06	75.62	0.62	6.41	9.87	1.43	9.81	2.59	25.74
46.25	66.73	0.47	3.93	6.06	1.21	5.26	1.58	27.32
40.34	59.90	0.44	3.60	5.55	1.21	4.64	1.55	28.87
35.50	54.25	0.37	2.56	3.95	1.07	2.77	1.02	29.89
31.57	49.59	0.35	2.34	3.60	1.04	2.38	0.96	30.84
28.27	45.65	0.30	1.86	2.86	0.92	1.63	0.71	31.56
25.53	42.33	0.28	1.74	2.67	0.88	1.50	0.71	32.27
23.21	39.48	0.25	1.51	2.32	0.79	1.25	0.63	32.90
21.22	37.01	0.23	1.32	2.03	0.77	0.87	0.47	33.37
19.46	34.81	0.21	1.27	1.96	0.72	0.94	0.54	33.91
17.92	32.85	0.20	1.12	1.72	0.69	0.64	0.39	34.30
16.60	31.15	0.17	0.97	1.49	0.60	0.55	0.36	34.66
15.43	29.64	0.18	0.89	1.37	0.61	0.29	0.19	34.85
14.33	28.18	0.17	1.03	1.59	0.60	0.77	0.55	35.39
13.33	26.86	0.16	1.01	1.56	0.55	0.92	0.68	36.08
12.42	25.64	0.16	0.87	1.34	0.58	0.38	0.30	36.38
11.57	24.47	0.15	0.82	1.26	0.55	0.36	0.29	36.67
10.80	23.41	0.14	0.79	1.22	0.52	0.40	0.34	37.01
10.09	22.42	0.14	0.77	1.19	0.52	0.32	0.28	37.29
9.42	21.47	0.14	0.74	1.14	0.51	0.29	0.27	37.56
8.80	20.59	0.13	0.73	1.12	0.50	0.27	0.26	37.82
8.22	19.73	0.13	0.65	1.00	0.51	-0.03	-0.03	37.79
7.67	18.92	0.13	0.61	0.94	0.49	-	-	-
7.15	18.14	0.13	-	-	-	-	-	-

Table A1.10. Calculation of the total surface area of the synthesis product (200 °C, 72 h) from opoka when using the parallel plate pore model

Average K radius of the pores r_K (Å)	Average true pore radius, r_p (Å)	Change, Δt, Å	ΔV_{ad}, $cm^3 \cdot g^{-1}$	Change of vap. liquid ads. vol. ΔV^L, $10^3 m^3 \cdot g^{-1}$	$\Delta t \Sigma A$ ($\times 10^3 m^3 \cdot g^{-1}$)	True volume of the pores Vp ($\times 10^3$ $cm^3 \cdot g^{-1}$)	Surface of pore walls, A, $m^2 \cdot g^{-1}$	Total surface ΣA, $m^2 \cdot g^{-1}$
277.11	313.86	4.08	5.64	8.69	0.00	9.84	0.63	0.17
155.60	186.14	2.13	22.29	34.33	0.04	40.98	4.40	4.57
106.49	133.47	1.44	10.46	16.11	0.66	18.53	2.78	7.35
80.50	105.11	0.92	5.60	8.63	0.68	9.49	1.81	9.16
65.25	88.20	0.73	4.09	6.30	0.67	6.70	1.52	10.68
54.43	76.05	0.61	2.95	4.55	0.65	4.54	1.19	11.87
46.32	66.80	0.52	2.62	4.03	0.62	4.02	1.20	13.07
40.20	59.75	0.42	1.88	2.90	0.55	2.69	0.90	13.98
35.44	54.18	0.39	1.65	2.54	0.54	2.23	0.82	14.80
31.50	49.51	0.34	1.43	2.21	0.50	1.91	0.77	15.57
28.23	45.60	0.31	1.28	1.98	0.48	1.64	0.72	16.29
25.48	42.26	0.27	1.13	1.74	0.45	1.41	0.67	16.95
23.16	39.43	0.25	0.98	1.51	0.42	1.14	0.58	17.53
21.24	37.04	0.21	0.81	1.25	0.37	0.88	0.47	18.01
19.57	34.94	0.21	0.80	1.23	0.39	0.83	0.47	18.48
18.03	32.99	0.20	0.74	1.15	0.37	0.75	0.45	18.93
16.65	31.22	0.19	0.72	1.12	0.36	0.74	0.48	19.41
15.43	29.63	0.18	0.71	1.10	0.34	0.80	0.54	19.95
14.33	28.18	0.17	0.71	1.10	0.34	0.82	0.58	20.53
13.30	26.82	0.17	1.04	1.61	0.35	1.84	1.37	21.90
12.39	25.59	0.15	0.57	0.89	0.32	0.51	0.40	22.30
11.58	24.48	0.15	0.57	0.88	0.34	0.45	0.36	22.67
10.80	23.41	0.14	0.50	0.77	0.33	0.25	0.22	22.88
10.08	22.41	0.14	0.52	0.81	0.32	0.35	0.31	23.20
9.42	21.47	0.14	0.45	0.70	0.31	0.15	0.14	23.34
8.80	20.58	0.13	0.48	0.73	0.31	0.24	0.24	23.58
8.21	19.73	0.13	0.50	0.77	0.31	0.35	0.35	23.93
7.67	18.92	0.13	0.48	0.74	0.31	0.28	0.30	24.23
7.14	18.13	0.13	0.49	0.76	0.32	0.33	0.36	24.59
6.65	17.38	0.13	0.50	0.78	0.32	0.36	0.41	25.00
6.17	16.64	0.13	0.51	0.79	0.33	0.34	0.41	25.40
5.71	15.90	0.14	0.52	0.80	0.35	0.30	0.38	25.79
5.26	15.18	0.14	0.52	0.81	0.36	0.25	0.33	26.12
4.81	14.45	0.15	0.56	0.86	0.38	0.27	0.37	26.49

4.39	13.73	0.14	0.59	0.91	0.38	0.47	0.69	27.18
3.94	12.95	0.19	0.66	1.01	0.51	-0.05	-0.08	27.09
3.43	12.04	0.22	0.83	1.27	-	-	-	-
2.88	10.98	0.28	-	-	-	-	-	-

SL344. 2021-04-19, 17,25 leidyb. apsk. l. Tiražas 12 egz. Užsakymas 103.
Išleido Kauno technologijos universitetas, K. Donelaičio g. 73, 44249 Kaunas
Spausdino leidyklos „Technologija“ spaustuvė, Studentų g. 54, 51424 Kaunas